Bayesian Population PBPK Approach for Support of Drug Development

Bayesscher Populations-PBPK Ansatz zur Unterstützung der Medikamentenentwicklung

Von der Fakultät für Maschinenwesen der Rheinisch-Westfälischen Technischen Hochschule Aachen zur Erlangung des akademischen Grades eines Doktors der Ingenieurwissenschaften genehmigte Dissertation

vorgelegt von

Markus Krauß

Berichter:	Univ.-Prof. Dr.rer.nat. Andreas Schuppert
	Univ.-Prof. Alexander Mitsos, Ph.D.
Tag der mündlichen Prüfung:	29.08.2016

„Diese Dissertation ist auf den Internetseiten der Universitätsbibliothek online verfügbar."

Abstract

Low likelihood-of-approval rates of new drugs constitute a major problem in clinical development. Only one out of ten development programs entering the first clinical phase succeeds in being approved by the U.S. Food and Drug Administration (FDA) [1]. A main challenge is thereby an insufficient understanding and prediction of drug safety and efficacy, leading to the withdrawal of new drug candidates [2,3]. Here, model-based assessment of drug exposure and response can support the development process at all stages, starting from early preclinical to late clinical phases [4,5]. Thus, the quantification of interindividual variability in clinical outcomes and the identification of related sources of such variability are of utmost importance e.g. for individualized dosing strategies [6–8]. Furthermore, of particular interest are translational approaches that transfer and integrate knowledge of recent study programs or earlier steps of drug development in order to make improved conclusions about drug behavior in clinically-relevant populations [3,9].

In this thesis, we present a Bayesian population physiologically-based pharmacokinetic (PBPK) approach for assessment of interindividual variability and clinical translation. Therein, we combine large-scale mechanistic PBPK models describing the behavior of drugs within the body with a Bayesian statistical framework for efficient estimation of the parameter space. The parameter space consists of clearly deconvoluted physiological- and drug-specific parameters, which facilitates the use of large amounts of prior information about the parameters. Such prior knowledge is updated with information extracted from experimental data by considering the Bayesian theorem and in particular performing a Markov chain Monte Carlo (MCMC) approach. This allows to solve the inverse and strongly ill-posed parameter estimation problem and at the same time preserve the extrapolation capabilities of PBPK models.

Our Bayesian population PBPK approach represents a specifically-designed workflow for whole-body PBPK models to take into account the distinct properties of such models and guarantee a generic form for broad applicability and to support translation of knowledge. The overall framework contains i.a. an hierarchical model to separate individual uncertainty about the parameters from population variability, and a covariate model to cope for systematic relationships of model parameters to age, gender and body height. We further provide a method for estimation of the *a posteriori* parameter dependency structure at the population level. A blockwise MCMC sampling structure reduces complexity and accounts for the different types of parameters that are estimated. Additionally, we present an adaptive sampling method that combines gradient-based sampling with continuous adaptation of the proposal scaling for a strongly improved performance of the MCMC approach

compared to standard methods. Moreover, we establish a translational learning workflow, where our Bayesian population PBPK approach is iteratively conducted in several learning steps to finally predict an unsupervised scenario, e.g. the pharmacokinetic behavior of a diseased population after administration of a new drug candidate.

Subsequently, three application examples represent how to support different phases of drug development by the developed workflow. In the first example we successfully identify clinically-relevant subgroups in a cohort of individuals. These findings can improve safety and efficacy assessment in a clinical phase I study. In the second example we determine the interindividual variability in the pharmacokinetic behavior and the underlying physiological parameters, and improve population simulations by adding estimated information about parameter dependencies. We further reveal the performance of our new adaptive MCMC approach. In the third example we predict the pharmacokinetic behavior in a cohort of patients after accumulation of available study data in three iterations of our Bayesian population PBPK approach. We here successfully demonstrate the concept of translational learning from a phase I to a phase II study, taking into account the derived pathophysiology of the population.

Overall, these examples indicate the capabilities of our approach in accumulation of knowledge and extrapolation of drug behavior. Applied to drug development programs, our method could improve clinical trial design to increase the benefit/risk ratio of new compounds. Our model-based concept could hence give significant support to raise approval rates of new drugs in the future.

Zusammenfassung

Niedrige Zulassungsraten neuer Medikamente stellen ein großes Problem in der klinischen Entwicklung dar. Nur eines von zehn Entwicklungsprogrammen aus der klinischen Phase I wird erfolgreich durch die U.S. Food and Drug Administration (FDA) zugelassen [1]. Ein Hauptproblem sind ein unzureichendes Verständnis und die unzureichende Vorhersage der Sicherheit und Effizienz von Medikamenten, was zum Abbruch der Entwicklung neuer Medikamentenkandidaten führt [2,3]. Hier kann die Beurteilung der Exposition und des Effekts von Medikamenten auf Basis von Modellen entlang des Medikamentenentwicklungsprozesses, von der präklinischen Entwicklung bis zu späten klinischen Phasen, helfen [4,5]. Dabei sind vor allem die Quantifizierung der interindividuellen Variabilität des klinischen Ergebnisses und die Identifikation der zugehörigen Auslöser der Variabilität von immenser Bedeutung, zum Beispiel um individuelle Dosierungen zu entwickeln [6–8]. Von weiterem Interesse sind translationale Ansätze, die Information aus vorhergegangen klinischen Studien oder früheren Phasen der klinischen Entwicklung integrieren und transferieren und so verbesserte Schlussfolgerungen über das Verhalten von Medikamenten in klinisch-relevanten Populationen ermöglichen [3,9].

In dieser Arbeit stellen wir einen Bayesschen Populations- und Physiologiebasierten Pharmakokinetik (PBPK) Ansatz vor, der die Abschätzung interindividueller Variabilität erlaubt und die klinische Translation ermöglicht. Dabei werden große mechanistische PBPK Modelle, welche das Verhalten von Medikamenten im Körper beschreiben, mit einem Ansatz der Bayesschen Statistik kombiniert, um den Parameterraum effizient identifizieren zu können. Dieser Parameterraum enthält klar voneinander abgegrenzte physiologische und Medikamenten-spezifische Parameter, was die Integration einer großen Menge an Vorinformation über diese Parameter erleichtert. Dieses initiale Wissen über die Parameter wird dann mit neuer Information aktualisiert, welche aus experimentellen Daten durch Anwendung des Bayesschen Theorems und vor allem der Anwendung von Markov Ketten Monte Carlo (MCMC) Methoden, extrahiert werden kann. Dieser Ansatz erlaubt dabei das entstehende inverse schlecht gestellte Problem zu lösen und dabei trotzdem die Extrapolationsfähigkeit von PBPK Modellen zu erhalten.

Unser Ansatz repräsentiert einen spezifisch-angepassten Workflow für Ganzkörper PBPK Modelle, der die ausgeprägten Eigenschaften dieser Modelle mit berücksichtigt und dabei durch seine generische Form für breite Anwendbarkeit sorgt sowie den Transfer von erhaltener klinischer Information unterstützt. Die zugrundeliegende Struktur beinhaltet unter anderem ein hierarchisches Modell, um Parameterunsicherheit auf Ebene der Individuen von Parametervariabilität auf Ebene der Population voneinander zu trennen. Außerdem beinhaltet sie ein Kovariationsmodell, um

systematische Abhängigkeiten von Modellparametern zu Eigenschaften wie Alter, Geschlecht oder Körpergröße mit einzubeziehen. Weiterhin stellen wir eine Methode bereit, mit der sich die *a posteriori* Abhängigkeiten der Parameter auf Populationsebene abschätzen lassen. Ein blockweises Sampling der Parameter im MCMC Lauf reduziert die Komplexität und berücksichtigt die verschiedenen Parametertypen, die identifiziert werden sollen. Zusätzlich stellen wir eine adaptive Sampling Methode vor, welche Gradienten-basierte Ansätze mit Ansätzen kombiniert, die kontinuierlich die Vorschlagsdichte eines MCMC Laufs anpassen. Dies führt zu einer starken Verbesserung der Performance der MCMC Läufe im Vergleich zu Standardmethoden. Weiterhin etablieren wir einen Workflow für translationales Lernen, innerhalb dessen der hier entwickelte Bayessche Populations-PBPK Ansatz iterativ angewendet wird, um schlussendlich ein bisher nicht bekanntes Szenario, zum Beispiel das pharmakokinetische Verhalten einer kranken Population nach Gabe eines neuen Medikaments, vorherzusagen.

Anschließend präsentieren wir in drei Anwendungsbeispielen, wie der vorgestellte Workflow verschiedene Phasen des Medikamentenentwicklungsprozesses unterstützen kann. Im ersten Beispiel identifizieren wir erfolgreich klinisch-relevante Untergruppen in einer Kohorte von gesunden Individuen. Solche Ergebnisse könnten die Bewertung von Sicherheit und Effizienz in einer klinischen Phase I Studie verbessern. Im zweiten Beispiel quantifizieren wir die interindividuelle Variabilität des pharmakokinetischen Verhaltens und der zugrundeliegenden physiologischen Parameter und können durch die Abschätzung von Abhängigkeiten zwischen Parametern die Simulation der Pharmakokinetik in Populationen verbessern. Außerdem evaluieren wir die Leistungsfähigkeit unseres neuen adaptiven MCMC Ansatzes. Im dritten Beispiel machen wir eine Vorhersage des pharmakokinetischen Verhaltens einer Gruppe von Patienten nach erfolgter Akkumulation von vorhandenen Studiendaten in drei Iterationen unseres Bayesschen Populations-PBPK Workflows. Dabei demonstrieren wir erfolgreich das Konzept des translationalen Lernens ausgehend von einer Phase I Studie zu einer Phase II Studie, wobei wir die abgeleitete Pathophysiologie der Population mit einbeziehen.

Zusammenfassend zeigen diese drei Beispiele die Anwendungsmöglichkeiten unseres Ansatzes bezüglich Akkumulation von Information und Extrapolation des Verhaltens von Medikamenten im Körper auf. Angewendet auf Medikamentenentwicklungsprogramme könnte unsere Methode das Design klinischer Studien verbessern um das Nutzen/Risiko Verhältnis neuer Medikamente zu erhöhen. In der Zukunft könnte unser Modell-basiertes Konzept daher die Verbesserung der Akkzeptanzraten neuer Medikamente signifikant unterstützen.

Danksagung

Die vorliegende Arbeit entstand aus einer Kooperation der RWTH Aachen und der Bayer AG. Daher gilt mein herzlicher Dank zunächst meinem Betreuer Prof. Andreas Schuppert, ohne den die Kooperation und damit auch diese Arbeit nicht möglich gewesen wären. Zusätzlich auch vielen Dank für die hervorragende Betreuung mit vielen wertvollen Diskussionen während der zurückliegenden Jahre. Weiterhin geht auf Seiten der RWTH ein herzliches Dankeschön an meinen Zweitgutachter Prof. Alexander Mitsos für sein großes Engagement und die aufgewandte Zeit in seiner Bereitschaft, diese Arbeit mit zu betreuen. Zudem danke ich dem ganzen Team des AICES für die tolle Unterstützung in allen organisatorischen Fragen.

Auf Seiten der Bayer AG danke ich vor allem Dr. Linus Görlitz und Dr. Lars Küpfer für ihre Unterstützung und Fachkompetenz: unendliche Stunden der Diskussionen, der klaren Worte, fairen Kritik und wertvollen Tipps. All das zudem in wunderbar entspannter und freundschaftlich-kollegialer Atmosphäre. Weiter möchte ich im Besonderen Dr. Kai Tappe und Christian Müller danken, die ebenfalls tolle Unterstützung und hilfreiche Tipps während der Erstellung der Arbeit geliefert haben. Und auch wenn ich nicht alle Namen aufzählen kann, möchte ich der gesamten Abteilung der Computational Systems Pharmacology/Applied Mathematics meinen Dank sagen für ganz viele offene Ohren, Hilfe, Tipps und ein immer herzliches und wirklich sehr kollegiales Umfeld.

Als nächstes geht ein riesiges Dankeschön an Dr. Stephan Schaller und Jan Schlender sowie Dr. Kristin Dickschen und auch an alle anderen Doktoranden und Praktikanten, die mich in dieser Zeit begleitet haben. Die Zeit im Doktoranden Büro mit all unseren Gesprächen möchte ich nicht missen.

Sowieso danke ich allen Freunden aus Köln, Kassel und meinem Lieblingsverein 1. CfB Köln, auch wenn hier ohne Namen genannt dürft ihr euch alle angesprochen fühlen: Danke für entspannte Stunden in Kneipe, Sporthalle oder Wohnzimmer, ihr habt immer wieder für die richtige Ablenkung gesorgt. Speziell zu nennen sind hier trotzdem Axel, Stephan und Jan, die mir immer wieder den Kopf gewaschen und die Lockerheit zurück gebracht haben, um den Blick auf die wirklich wichtigen Dinge im Leben zu schärfen.

Zuletzt und gleichzeitig am allerwichtigsten: Allergrößten Dank für den großen Rückhalt und das große Verständnis sowie jede vorstellbare Unterstützung meiner Familie, vor allem meiner Eltern und meines Bruders sowie meiner Freundin Anne. Vom ersten bis zum letzten Tag habt ihr mehr Geduld, Unterstützung und Verständnis aufgebracht als ich mir vorstellen konnte und könnt euch klar als essentielle Mitwirkende dieser Arbeit sehen.

Contents

List of Figures

List of Tables

List of Abbreviations

ADME	absorption, distribution, metabolization and excretion
AM	adaptive Metropolis
AUC	area under curve
BH	body height
BMI	body mass index
BW	body weight
CI	confidence interval
C_{max}	maximum concentration
CV	coefficient of variation
CYP2C8	cytochrome P450 2C8
CYP2C9	cytochrome P450 2C9
CYP3A4	cytochrome P450 3A4
CYP3A5	cytochrome P450 3A5
fu	unbound protein fraction
GET	gastric emptying time
HMC	Hamiltonian Monte Carlo methods
HMG-CoA	3-hydroxy-3-methyl-glutaryl-Coenzyme A
$intP$	intestinal permeability
ITT	intestinal transit time
k_{cat}	catalytic rate constant
LBW	lean body weight
LLOQ	lower limit of quantification
$logP$	logarithmic of the partition coefficient between octanol and water
MALA	Metropolis-adjusted Langevin algorithm
MCMC	Markov chain Monte Carlo
MH	Metropolis-Hastings
MLE	maximum likelihood estimation
mMALA	manifold Metropolis-adjusted Langevin algorithm
MALA	Metropolis-adjusted Langevin algorithm
MRP2	multidrug resistance-associated protein 2
NASH	nonalcoholic steatohepatitis
nESS	time-normalized effective sampling size
NLME	nonlinear mixed-effects modeling
NRMSE	normalized root-mean-square-error
OAT3	organic anion transporter 3
OATP1B1	organic anion transporting polypeptide 1B1
ODE	ordinary differential equation

PBPK	physiologically-based pharmacokinetic
PBTK	physiologically-based toxicokinetic
PD	pharmacodynamic
Pgp	P-glycoprotein
PK	pharmacokinetic
PopPK	population pharmacokinetics approaches
$\hat{R}$	Gelman and Rubin convergence criterion
RMSE	root-mean-square-error
SCAM	single-component adaptive Metropolis
SLCO1B1	solute carrier organic anion transporter family member 1B1
t_{max}	time point, where maximum concentration is reached
TK	toxicokinetic
UGT1A4	uridine diphosphate glucuronosyltransferase 1A4
VPC	visual predictive check

List of Original Publications

This thesis is based on the following publications [10–12]:

- Chapters 2 and 3: **Krauss M**, Burghaus R, Lippert J, Niemi M, Neuvonen P, Schuppert A, Willmann S, Kuepfer L, Görlitz L (2013) Using Bayesian-PBPK modeling for assessment of inter-individual variability and subgroup stratification. *In Silico Pharmacol*, 1: 1-11.

- Chapters 2 and 4: **Krauss M**, Tappe K, Schuppert A, Kuepfer L, Goerlitz L (2015) Bayesian Population Physiologically-Based Pharmacokinetic (PBPK) Approach for a Physiologically Realistic Characterization of Interindividual Variability in Clinically Relevant Populations. *PLoS One*, 10: e0139423.

- Chapters 2 and 5: **Krauss M**, Hofmann U, von Schoenfels W, Igel S, Schafmayer C, Schlender J, et al. Translational learning from clinical studies predicts drug pharmacokinetics across patient populations. in internal revision.

The following publication has been created in addition during the time of creating the presented thesis and had minor influence on the results of the thesis [13]:

- Chapter 2: Schlender JF, Meyer M, Thelen K, **Krauss M**, Willmann S, Eissing T, Jaede U (2016) Development of a Whole-Body Physiologically Based Pharmacokinetic Approach to Assess the Pharmacokinetics of Drugs in Elderly Individuals. *Clin Pharmacokinet*, 1-17.

The following master thesis related to the topic of my thesis has been developed under my supervision [14]:

- Chapters 2 and 5: Baier V (2015) Investigation of Extrapolation within the Bayesian Population PBPK Modelling on the Example of Erythromycin and Midazolam. Master Thesis, Institute of Computer Science, Johann-Wolfgang-Goethe-University, Frankfurt

The following publications have been created in addition during the time of creating the presented thesis but had no influence on the results of the thesis:

- **Krauss M**, Schaller S, Borchers S, Findeisen R, Lippert J, Kuepfer L (2012) Integrating Cellular Metabolism into a Multiscale Whole-Body Model. *PLoS Comput Biol*, 8: e1002750.
- Schwen LO, **Krauss M**, Niederalt C, Gremse F, Kiessling F, Schenk A, Preusser T, Kuepfer L (2014) Spatio-temporal simulation of first pass drug perfusion in the liver. *PLoS Comput Biol*, 10: e1003499.
- Thiel C, Schneckener S, **Krauss M**, Ghallab A, Hofmann U, Kanacher T, Zellmer S, Gebhardt R, Hengstler JG, Kuepfer L (2015) A Systematic Evaluation of the Use of Physiologically Based Pharmacokinetic Modeling for Cross-Species Extrapolation. *J Pharm Sci*, 104: 191-206.

Chapter 1

Introduction

1.1 Motivation

Translational pharmacology approaches aim for an integration of data generated from diverse research platforms during pharmaceutical development programs [3,9]. They are designed for the support of drug development, for example to increase safety and efficacy of new drugs and to help to reduce the continuously high drug attrition rate [1,2,15]. Thus, of particular importance is the understanding of drug pharmacokinetics (PK), which describes the behavior of a drug characterized by its specific absorption, distribution, metabolization and excretion (ADME) processes. An important example for translation is to assign research findings from preclinical research to clinical development, which could improve the design of such clinical research programs. Thereby, a mechanistic translation, organization and continuous re-evaluation of knowledge along the development path of novel drugs is promised to overcome many of the current limitations in the pharmaceutical research process. These are among others translation strategies between healthy volunteers and patients or the setting of objectives on the basis of previous studies and data [3]. In addition, a better understanding of the interindividual variability of the PK outcome in specific patient cohorts is necessary, aiming for explanation of lack of efficacy in potential subgroups of non-responders or the occurrence of adverse events in high-risk subgroups of patients [5,6,16]. Altogether, a clear need is formulated for possible translation along the drug development pathway, across species or clinically-relevant patient cohorts [17].

Generally, vast amounts of data are generated along the whole drug development process. This and the complexity of especially the preclinical and clinical data represents a big challenge when trying to generate an in-depth mechanistic understanding of the processes driving ADME of drugs. Here, *in silico* approaches provide a rational way to describe and analyze data determining a drugs PK [4,18]. After their validation, computational models are able to assess the effect of different dosing schemes or a varying anthropometry or physiology in detail [10,19,20].

In recent years, systems approaches provided important mechanistic insights in various areas of life sciences such as biology, pharmacology or medicine. Mechanistic computational models were used to describe biological processes at a high level of physiological detail. With regard to medicine and pharmacology, physiologically-

based pharmacokinetic (PBPK) modeling can be expected to support translational approaches, because the highly physiological PK description in these models fosters a mechanistic understanding of the underlying processes. PBPK models include specific information about the (patho-) physiology of a certain population as well as the physicochemistry of the drug. In particular, the mechanistic formulation and the separation of drug-specific knowledge and physiological information suits PBPK models to extrapolate the PK behavior of new drugs in well-known patient cohorts or in turn to forecast the PK of known drugs in new populations. These particular properties allow to translate available knowledge about key processes governing drug ADME [18,21–23].

PBPK models are large ordinary differential equation (ODE)-based compartmental models. Especially whole-body PBPK models contain more than one hundred ODEs and several hundreds of parameters. Moreover, available PK data is sparse and usually consists of only few samples of venous blood plasma. Therefore, parameter estimation of PBPK models represents an ill-posed inverse problem and the use of standard methods for parameter estimation is strongly limited. However, a big advantage of PBPK models is their mechanistic consideration such that each parameter has a foundation based on a biological or pharmacological function. A lot of prior information is hence available, for example about organ volumes or blood flow rates, that can be used to inform a lot of the parameters within PBPK models. Current use of such models often aims for the description of a single time-concentration profile in a mean individual. Many physiological parameters are considered as fixed and known values and only few key parameters are estimated. This obviously neglects potentially relevant individual properties and undermines the possibility of PBPK models to create highly personalized models for individuals by integration of the individual's physiology [24–26]. Therefore, the assessment of individualized PBPK models and interindividual variability in the PK behavior is of particular interest.

A possible way to deal with the above stated issues and the ill-posedness of the problem is to model the parameters as random values that are assigned probability distributions. This transforms the inverse problem into a problem of statistical inference [27]. A Bayesian formulation can be considered to integrate the large amounts of prior information and to update such information about model parameters by including new observations in the so-called posterior distribution. Even if not all physiological parameters are informed by a new set of experimental data, they may be necessary for extrapolation to new scenarios. The integration of prior information about such parameters into the estimation ensures that they are informed and allows to include large numbers of parameters into the analyses [17]. The acquired posterior probability distributions then contain the uncertainty of each parameter as an additional and desired result. Since large numbers of individuals and patients are integrated into clinical studies, one can interpret the experimental setting as a large number of parallel situations [28]. This calls for the combination of the Bayesian approach with a hierarchical model and nonlinear mixed-effects modeling (NLME) since it allows the estimation of the underlying population distribution of each parameter, thereby separating the assessment of parameter uncertainty and interindividual variability [17,29]. All in all, such an overall framework of generic

PBPK models and a Bayesian statistical model may be well suited for the translational idea.

1.2 State of the Art

One of the first approaches where physiological modeling and Bayesian statistical approaches were merged was published already in 1996 by Gelman and coworkers [30]. Here, informative prior distributions of physiological parameters were integrated into an hierarchical model approach in combination with a compartmental PK model that described the distribution and metabolism of an environmental chemical in humans [31,32]. This work addressed the importance of quantifying the uncertainty of model parameters and also of quantities of interest when applying the results to risk analyses. The applied model consisted of 4 compartments representing a semi-physiological level of detail. Beside the population parameters, six individuals were analyzed and 17 parameters were estimated per individual. To determine the posterior distribution, a Markov chain Monte Carlo (MCMC) approach was performed, in particular the Metropolis algorithm [33].

The work from Gelman et al. [30] can be seen as a starting point for a number of publications in the field of physiologically-based toxicokinetic (PBTK) modeling and the risk assessment of environmental chemicals [34–37]. All these publications focused on identification of the interindividual variability of the toxicokinetics (TK) of chemicals in different species. A good example was published by Chui and coworkers [38], who established their model in rats, mice and humans and integrated several studies in one Bayesian population approach. The objective was an improved quantification of the variability and uncertainty in the TK of an environmental chemical. Chui et al. demonstrated how Bayesian approaches can summarize the knowledge of several studies to achieve such issues in the field of TK, where a decrease of uncertainty for a high quality risk assessment is of utmost importance.

One of the first applications of a Bayesian population PBPK model approach was then published in 2006 by Gueorguieva et al. [39]. Here, a PBPK model was used to estimate physiological parameters in rats. The posterior parameter values of the Bayesian analysis in rats were then considered as informative priors for the estimation of the same parameters in humans, which can be seen as the first translation of knowledge to a different species using such approaches. Data of 24 rats and 11 humans were used for this investigation. The PBPK model itself was much more detailed than the one from Gelman et al [30]. It consisted of 14 compartments representing the most important organs, but the organs themselves were not separated into substructures.

Only few other approaches have been published addressing Bayesian population modeling using mechanistic physiological models. Leil et al. [17] emphasized the advantages of the combined use of complex PK/pharmacodynamic (PD) models with Bayesian approaches and population approaches. In [40], Leil et al. presented an investigation using a semi-mechanistic PK/PD model to evaluate the utility of a possible biomarker for interactions of a metabolizing enzyme with drugs. A Bayesian approach was shown to serve as a tool for identification of new interactions with the enzyme and the optimization of clinical trials.

Two very recent approaches presented applications of a Bayesian population approach within a pharmacological issue [41,42]. Both applications focused on model building of highly specific PBPK models to address a specific issue with the created models. In Zurlinden et al. [41], a model for acetaminophen and its metabolites was created. Zurlinden et al. simulated the concentrations of two metabolites which were assumed to provide additional information for dose extrapolation studies or the impact of co-administration of other drugs. The overall objective was to assess model parameter uncertainty and variability for subsequent predictions of relevant pharmacological outcomes such as cofactor depletion or dose response of PK endpoints. In Tsamandouras et al. [42], an established model of simvastatin was used e.g. to describe PK effects of a genetic polymorphism, which is important in the risk evaluation of possible adverse events. The model consisted of 16 differential equations. 14 model parameters were assessed, whereby informative prior distributions were defined for 10 parameters. A covariate model was also integrated *a priori*, in particular two covariates, body weight and body surface area were defined. Of further importance was a second application with the constructed model and the Bayesian approach, where drug-drug interaction effects were successfully predicted. They further discussed the advantages and also disadvantages of a full Bayesian analysis of highly-detailed mechanistic models and highlighted the possibility of using assessed posterior knowledge as prior knowledge in future investigations with the created model and new study data.

So far, the MCMC algorithms considered for estimation of the posterior distribution have not been in focus in PBPK modeling applications. In most applications, a standard Metropolis-Hastings (MH) algorithm was used, although there are a lot of sophisticated MCMC methods available that largely improve the performance of the analyses [43–47]. Such methods were, however, only applied and developed in other large biological models such as cell signaling models [47–49]. Few publications considered a comparison or combined use of MCMC and classical, frequentist methods such as maximum likelihood estimation (MLE) [48–50]. In [50], the problems of MLE in the context of PBPK modeling were highlighted. Furthermore, [51] performed a simulation-based comparison between parametric and nonparametric estimation methods in PBPK models.

For more information about the developments in the field of PBPK modeling and clinical applications, please refer to [52]. Information about population approaches can be found in [29,53,54]. For detailed information about MCMC approaches and their development, please refer to [55].

1.3 Objectives

As described in Section 1.2, recent work regarding combined approaches of physiological modeling and Bayesian statistics was performed using specifically-defined models for a certain case study. This allows reduction of such models for purpose, such that final models consist of few compartments and describe the behavior of a compound of interest with few model parameters. However, it limits the translational idea as formulated in Section 1.1. If model structures differ from one application to another or models are even created for a specific purpose only, transfer

of information is strongly perturbed. Moreover, lumped parameters that contain mixed information of physiology and a drugs physicochemistry cannot be translated to another population or another drug. For efficient translation of information about a drug or a populations physiology, a generic mechanistic model would be necessary which does not contain lumped parameters and describes organs and tissues in a great level of detail. By the consideration of parameters representing an underlying biological function such as organ volumes or blood flow rates, large amounts of prior information would be available. Such models would then be suited to integrate data from a lot of different clinical studies iteratively. All information gained could be transferred to the next analysis and at the same time be collected in a physiological database for later use, since the overall model structure does not change.

Furthermore, recent Bayesian analyses with physiological models did not focus on the technical aspects, in particular the set up of MCMC algorithms. However, standard approaches such as the MH algorithm are ineffective when dealing with high dimensional parameter spaces and models with large numbers of ODEs. This would be another advantage of a generic workflow: The MCMC algorithm could be adapted to consider the specific properties of the model structure and thereby increase the speed and efficacy of the parameter estimation.

The objective of this thesis is therefore the development of a Bayesian population PBPK approach that is applicable for assessment of interindividual variability and translational learning. An overall workflow needs to be developed that incorporates a generic, mechanistic and highly-detailed PBPK model and takes into account the specific properties of such models, for example existing covariate relationships or a priori independence between model parameters due to their biological interpretability. The derived Bayesian population PBPK approach should facilitate and support translational learning. Furthermore, advanced MCMC algorithms should be considered for improved performance and efficient use of the developed workflow.

The Bayesian population PBPK approach should be then qualified in application examples that cover different scenarios for parameter identification and translation along the drug development process.

1.4 Outline

Chapter 2 presents the development of the Bayesian population PBPK approach. The chapter is separated into several sections that describe the different parts of the overall approach. These include the overall model structure, the Bayesian framework, MCMC sampling and a concept for translational learning.

We apply the approach to several scenarios to demonstrate its usability. Chapters 3, 4 and 5 present application examples of the Bayesian population PBPK workflow. Pros and cons of the approach are discussed per application example, since they arise in the application of the developed framework. Chapter 6 gives a conclusion of the derived results.

Chapter 2

Bayesian population PBPK approach

In this chapter, the development of a Bayesian population physiologically-based pharmacokinetic (PBPK) approach is described [10–12]. The approach shall be able to efficiently estimate the high-dimensional distribution of unknown model parameters of a generic mechanistic PBPK model. The resulting parameter distribution then allows assessment of interindividual variability in clinically-relevant patient populations and the quantification of the physiological and absorption, distribution, metabolization and excretion (ADME)-related sources.

In brief, the overall approach is established by the consideration of several modeling concepts: A generic, highly detailed whole-body PBPK model constitutes the model kernel and provides a mechanistic representation of human physiology [52,56]. This allows for a separated consideration of physiological parameters and substance-specific parameters. A Bayesian framework is chosen to provide a statistical basis for efficient use of prior information about the different types of parameters in a PBPK model. Furthermore, the Bayesian paradigm supports a computationally intensive, but straightforward way to estimate the parameter distributions, in particular by Markov chain Monte Carlo (MCMC) methods [55] (Figure 2.1). Within the Bayesian framework, a nonlinear mixed-effects model is incorporated to establish a two level approach for the identification of population characteristics and the identification of the underlying individual parameters [29]. A block-wise MCMC approach is used to identify the high-dimensional parameter distribution. For an improved performance of the MCMC runs, an adaptive method is presented that uses and tunes a combination of previously established MCMC samplers [43,57,58]. In addition, a covariate model accounts for systematic variability that can be explained by the covariates age, gender and body height. For population simulations using the inferred distributions, we present a framework for estimating the posterior dependency structure and identify significant correlations of physiological parameters within the population. Subsequently, a translational learning workflow is presented, where the developed Bayesian population PBPK approach is iteratively used for a continuous generation of knowledge about the physiology of a diseased population and the characteristics of a new candidate drug to finally predict the pharmacokinetic (PK) behavior of the candidate drug in the diseased population.

Section 2.1 introduces the various types of parameters and indices as well as

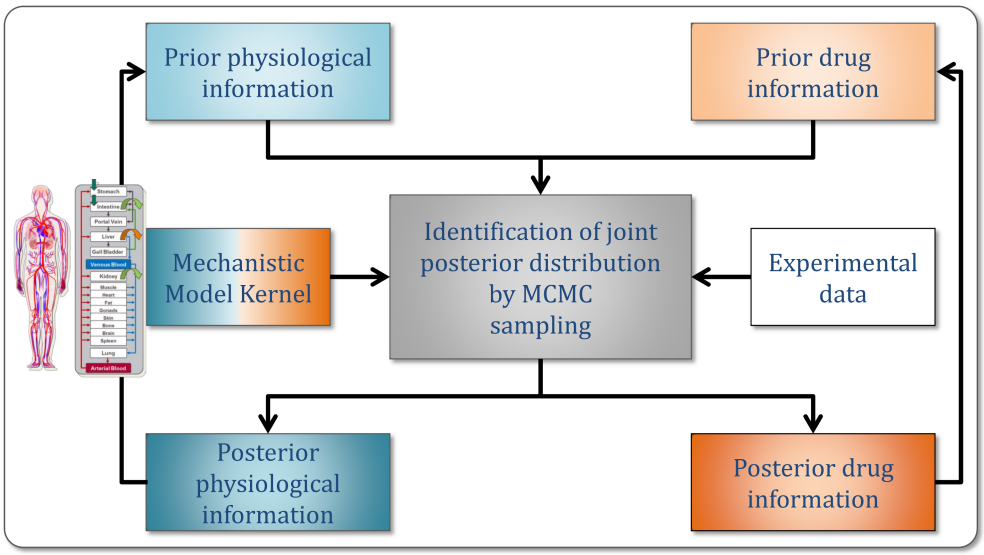

Figure 2.1: The combination of MCMC sampling with the deconvoluted model structure of a mechanistic PBPK model allows to identify the personalized physiology of individuals on the one hand and global compound parameters on the other hand in the joint posterior distribution. Such possible attribution of obtained knowledge enables the separated transfer of physiological or drug-specific information to new scenarios, e.g. in a drug development process.

basic functions that are used in several parts of this work. Section 2.2 defines the PBPK- and the hierarchical model and introduces covariate relationships to link the population level and the individual level and explain systematic variability of model parameters. Section 2.3 introduces the Bayesian framework, where the full Bayesian theorem is defined and the likelihood as well as the prior distributions are specified. In Section 2.4, the sampling structure is presented that is used to account for the specific types of parameters during MCMC sampling for increased performance of the approach. The specific sampling of organ volumes due to a sum constraint is explained further. The establishment of a specific adaptive MCMC sampling method is introduced in Section 2.5. Section 2.6 deals with the simulation of the derived results on the PK level. Thereby, the estimation of an *a posteriori* dependency structure is explained. The development of a translational learning concept is then illustrated in Section 2.7. Finally, the implementation of the approach is briefly explained in Section 2.8.

2.1 Preliminaries

In this section, we define and list important parameters, indices and functions that are used in the following sections describing the development of the Bayesian population PBPK approach.

Table 2.1: List of parameters and symbols used to define the Bayesian population PBPK model framework

parameter	**symbol**
age	A
dose	D
gender	G
height	H
identity matrix	$\mathcal{I}$
population mean value	M
population standard deviation	S
truncated normal distribution function	$\mathcal{T}$
acceptance probability	p_{Ac}
allometric scaling constant	α
experimental data	y
fix model parameter	ν
fixed effects	ψ
full parameter set of all variable parameters	ω
Hastings ratio	r_H
individual characteristics	ξ
intraindividual variation	e
measurement error	σ_M
PBPK model function	f
population model function	g
proposal density function	q
random effects	η
scaling variable (a,b for age-scaling, c for height-scaling)	sv
simulation output	$\tilde{y}$
standard deviation of proposal density	σ_P
time point	t
variable model parameter	θ

Parameters and indices

Generally, lower-case and upper-case letters in normal font denote single parameters, while lower-case and upper-case letters in bold font denote parameter vectors. The form of experimental data being available is often diverse, as for example the experimental data for one individual can contain more data points than that for another individual. The same is for different observed species such as urinary excretion or venous plasma. This is why matrices are not considered. Such a structure can be better specified in a vector notation.

For a better overview and for referencing, we here further list the most important parameters and indices: Table 2.1 lists the parameters that are needed for the description of the following approach, while Table 2.2 lists the considered indices to describe e.g. a certain parameter or individual.

Table 2.2: List of indices and symbols used to define the Bayesian population PBPK model framework

index	**symbol**
individual parameter	I
global parameter	G
number of individuals	$i = 1 \dots N$
number of observed species (e.g. venous plasma)	$o = 1 \dots O_i$
number of time points	$j = 1 \dots T_{i,o}$
number of individual parameters	$k = 1 \dots K$
number of global parameters	$l = 1 \dots L$
number of fix parameters	$m = 1 \dots M$
number of grid points related to age	$p = 1 \dots P$
number of grid points related to gender	$q = 1 \dots Q$
number of sampling blocks	$b = 1 \dots B$
number of organ volumes	$v = 1 \dots V$

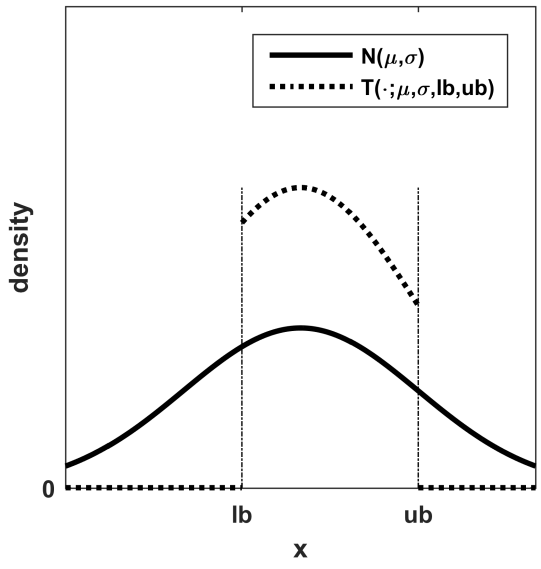

Figure 2.2: Example for the use of truncated normal distributions. In case of known lower (lb) and upper bounds (ub) for a random variable $x \sim \mathcal{N}(\mu, \sigma)$ based on physiological constraints, the symmetric normal distribution with mean value μ and standard deviation σ needs to be defined as truncated normal distribution T (Equation 2.1).

Supporting functions

For physiological parameters often physiological constraints are known, which limit the possible parameter space for these parameters. In such cases, the probability density for an arbitrary random variable, that is for example normally distributed with $x \sim \mathcal{N}(\mu, \sigma)$, needs to be defined as truncated distribution to account for imbalances of the underlying distribution (Figure 2.2).

In this work, we need a formulation for a truncated normal distribution to define truncated normal and lognormal distributions (due to the transformation from a lognormally distributed variable x to a normally distributed variable y: $y = \ln(x)$) that represent the prior distributions of physiological parameters. We here define the probability density of the truncated normal distribution as

$$\mathcal{T}(x; \mu, \sigma, lb, ub) = \frac{\frac{1}{\sigma} \cdot \phi\left(\frac{x-\mu}{\sigma}\right)}{\Phi\left(\frac{ub-\mu}{\sigma}\right) - \Phi\left(\frac{lb-\mu}{\sigma}\right)},\ lb \leq x \leq ub,\ lb \neq ub \tag{2.1}$$

and $\mathcal{T} = 0$ *elsewhere*. ϕ and Φ denote the probability density and cumulative distribution function, respectively, of the standard normal distribution, with mean value μ and standard deviation σ. lb and ub are the lower and upper bound of the random variable x. Notably, the truncated normal distribution is a probability density function as it integrates to one.

In later sections, we will just refer to Equation 2.1 to simplify the representation of some equations.

Remark. *To further simplify the representation of some equations, we state: If a function f is only defined for a specific range of values (such as $a < x < b$), this will implicit automatically that for all other values of x: $f(x) = 0$.*

2.2 The model framework

In this section, the specific model framework is presented. The approach to describe the population PBPK model consists of: (i) the PBPK model itself to describe the concentration-time curve of a drug in single individuals, (ii) a proportional error model to account for measurement uncertainty, (iii) a covariate model to integrate known systematic relations between PK parameters and individual characteristics and (iv) a population model to be able to describe remaining interindividual variability of the PK parameters in a population.

2.2.1 Definition of the PBPK model

Whole-body PBPK models aim for a mechanistic description of the PK behavior of endogenous and exogenous substances in the body. Such mechanistic consideration allows a detailed representation of all important ADME processes and the individual physiology based on a large amount of prior information [18,22,59]. The basic idea is to set up a compartmental structure which includes all relevant organs and tissues as containers (Figure 2.3a). All compartments are further subdivided into smaller

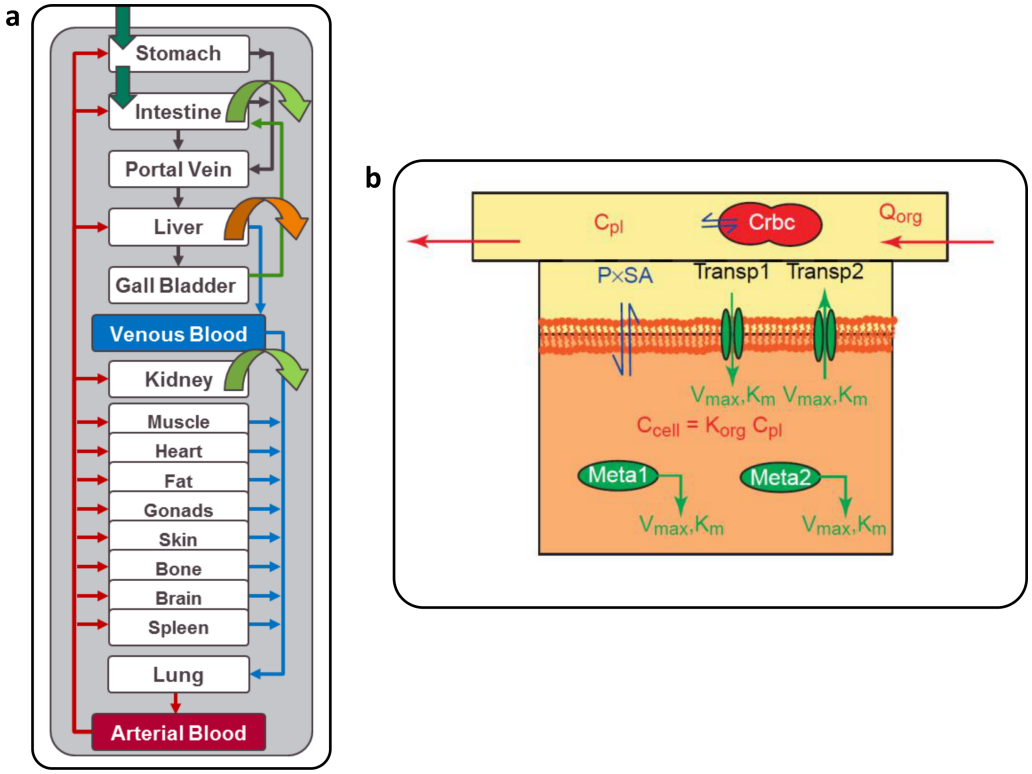

Figure 2.3: Illustrations of the mechanistic PBPK model structures. (**a**) Generic compartmental structure of a whole-body PBPK model, from [60]. (**b**) Schematic illustration of organ representation in PK-Sim from [56], where C are concentrations, Q flow rates, $P \cdot SA$ permeability - surface area products, pl plasma, org organ, rbc red blood cells, K partition coefficients, $Meta$ metabolization reactions represented by e.g. Michaelis-Menten kinetics, V_{max}, K_m Michaelis-Menten kinetic parameters.

well-stirred units which describe e.g. intracellular space and extracellular space in

more detail (Figure 2.3b). An underlying distribution model connects all compartments via mass balance equations representing physiological transport such as blood flow (between the organ compartments) or passive diffusion through cell membranes (between for example intracellular and interstitial space) [61–63]. The assumption of well-stirred compartments is key in the PBPK model. It allows to describe the model as a system of linear ODEs or also nonlinear ODEs (in case that nonlinear equations such as Michael-Menten kinetics are used to describe active processes, for example transport across membranes) [18].

The originating system of ODEs can be solved numerically for example with CVODE [64], which results in concentration-time curves of a certain substance in each considered compartment and subcompartment. That allows to predict concentration profiles directly at the mode of action of a certain xenobiotic, e.g. in the intracellular space of the liver [63].

Prior anatomical and physiological information is used to parameterize PBPK models, since all parameters are related to explicit biological functions. The physiology of an individual is determined by its anthropometry, such as age, gender, ethnicity, body height (BH) and body weight (BW). Based on these values, organ volumes and blood flow rates are extracted from physiological databases. The distribution model is parameterized by only few substance-specific parameters such as molecular weight, lipophilicity and protein binding. Notably, lipophilicity is often expressed as logarithmic of the partition coefficient between octanol and water ($logP$) and protein binding is often expressed as unbound protein fraction (fu). These parameters are used to determine permeabilities across membranes and partition coefficients between compartments [61,62,65–67]. In addition to such passive processes, active transport-, metabolization-, and excretion processes are integrated into the model based on the specific PK behavior of a substance. These processes can be represented as first or second order rate kinetics, such that also nonlinearities are considered if needed.

Beside the physiological parameters and the substance-specific parameters, important model parameters that need to be determined are ADME-related parameters such as catalytic constants of active transport and metabolization or excretion processes. Further absorption-related parameters are the intestinal permeability or gastric emptying and intestinal transit times. For a detailed review of PBPK modeling and its applications, please refer to [18,52].

The current state of the dynamical system 'PBPK model' can be defined as:

$$\tilde{\boldsymbol{y}}_i = f(\boldsymbol{\theta}_i^I, \boldsymbol{\theta}^G, \boldsymbol{\nu}_i, \boldsymbol{t}_i, D_i), \tag{2.2}$$

where for individual i, $\tilde{\boldsymbol{y}}_i = \left(\tilde{y}_{i,1,1}, \ldots, \tilde{y}_{i,1,T_{i,1}}, \tilde{y}_{i,2,1}, \ldots, \tilde{y}_{i,2,T_{i,2}}, \ldots, \tilde{y}_{i,O,1}, \ldots, \tilde{y}_{i,O,T_{i,O}}\right)$ is the vector of all model outputs $\tilde{y}_{i,o,j}$ of a certain simulation for the observed species $o = 1, \ldots, O$ and time points $j = 1, \ldots, T_{i,o}$. When necessary, $\tilde{\boldsymbol{y}}$ denotes the concatenated vectors $\tilde{\boldsymbol{y}}_i$ for all individuals $i = 1, \ldots, N$. The underlying PBPK model is formalized by a function f taking the following arguments:

- the individual parameters $\boldsymbol{\theta}_i^I = \left(\theta_{i,1}^I, \ldots, \theta_{i,K}^I\right)$, where $\theta_{i,k}^I$ with $k = 1, \ldots, K$ is the kth individual parameter for individual i and when necessary, $\boldsymbol{\theta}^I$ denotes the concatenated vectors $\boldsymbol{\theta}_i^I$ for all individuals $i = 1, \ldots, N$,

- the global, substance-specific parameters $\boldsymbol{\theta}^G = \left(\theta_1^G, \ldots, \theta_L^G\right)$ where θ_l^G with $l = 1, \ldots, L$ is the lth substance-specific parameter for individual i,
- remaining model parameters $\boldsymbol{\nu}_i = (\nu_1, \ldots, \nu_M)$ where ν_m with $m = 1, \ldots, M$ is the mth parameter for individual i,
- time points $\boldsymbol{t}_i$, where $\boldsymbol{t}_i$ and $t_{i,o,j}$ are similarly defined as $\tilde{\boldsymbol{y}}_i$,
- dose D_i, which denotes the administered dose for individual i.

Thereby, individual parameters define the physiology of the individual such as organ volumes or blood flow rates as well as individual ADME properties. Substance-specific parameters, e.g. the lipophilicity or *fu* remain the same for all individuals. Therefore, they are also called global parameters. Both, individual- and global parameters need to be identified. In contrast, the remaining model parameters $\boldsymbol{\nu}_i$ are considered as fixed parameters and are not included into the identification process. Experimental data is often obtained for several species, e.g. venous blood plasma and urinary excretion or the concentration in plasma of the parent drug and its metabolite(s), which requires the observation of several species in the PBPK model.

2.2.2 Definition of the hierarchical model

Experimental data, such as e.g. concentration-time curves obtained during clinical investigations, are described with individual-specific PBPK models. However, interindividual variability in the PK outcome needs to be identified for a thorough description of a population and the extrapolation of the derived results to other investigations. To assess the interindividual variability of the population, the description of the individuals alone is not sufficient. Especially in early clinical phases, only a small number of individuals are integrated into the investigations, such that a thorough extrapolation of population characteristics and the identification of sources of variability are not well founded. Furthermore, an independent consideration of the individuals would not account for similarities between them. Similarities are, however, expected, since clinical studies usually are conducted in homogeneous groups of healthy volunteers or patients to identify the PK behavior of a drug in a controlled environment. For that, a second hierarchical level is needed in the model which describes the relations between the individual parameters in a functional form. Furthermore, prior information about model parameters is often provided at a population level.

We therefore consider a hierarchical model approach (Figure 2.4) which is defined as [11,29]:

$$\boldsymbol{\theta}_i^I = g(\boldsymbol{\xi}_i, \boldsymbol{\psi}, \boldsymbol{\eta}_i),\ \boldsymbol{\eta}_i \sim \mathcal{N}(\boldsymbol{0}, \boldsymbol{R}), \tag{2.3}$$

$$\begin{aligned} \boldsymbol{y}_i &= f(\boldsymbol{\theta}_i^I, \boldsymbol{\theta}^G, \boldsymbol{\nu}_i, \boldsymbol{t}_i, D_i) \cdot (\boldsymbol{1} + \boldsymbol{e}_i), \\ &= \tilde{\boldsymbol{y}}_i \cdot (\boldsymbol{1} + \boldsymbol{e}_i), \\ \boldsymbol{e}_i &\sim \mathcal{N}(\boldsymbol{0}, \boldsymbol{\sigma}_M^2). \end{aligned} \tag{2.4}$$

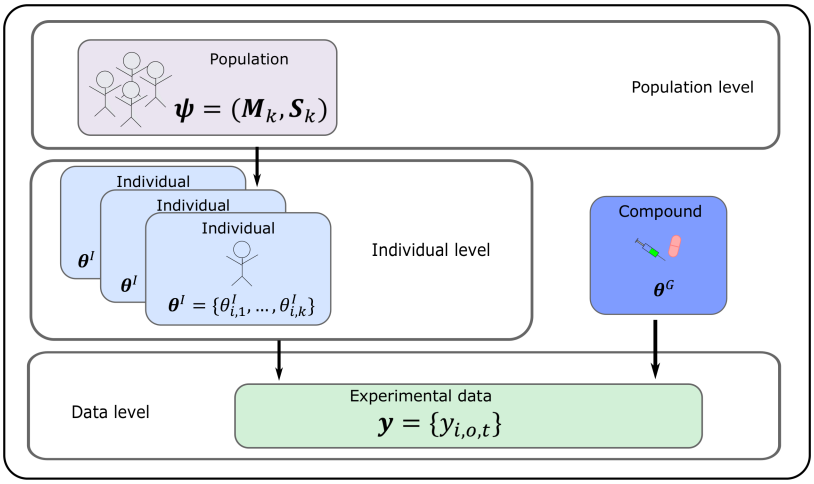

Figure 2.4: Schematic illustration of the hierarchical model concept (adapted from [14]) Experimental data $\boldsymbol{y}$ is provided specifically for an individual i, observed species (such as venous plasma) o and time points t. Such data can be described on an individual level with individual-specific physiological parameters $\boldsymbol{\theta}^I$ and global substance-specific parameters $\boldsymbol{\theta}^G$. All individuals are linked at a population level, which is specified by population parameters $\boldsymbol{\psi}$. In the here presented approach, population parameters are defined as mean values $\boldsymbol{M}_k$ and standard deviations $\boldsymbol{S}_k$ for parameter k.

Equation 2.3 represents the population level, where interindividual variability of the individual parameters is described by function g taking the following arguments: individual characteristics $\boldsymbol{\xi}_i$ such as e.g. age or BW, fixed effects $\boldsymbol{\psi}$ in the following referred to as population parameters and individual-specific random effects $\boldsymbol{\eta}_i$, which are assumed to be multivariate normal distributed with covariance matrix $\boldsymbol{R}$.

Equation 2.4 represents the individual level, where specific for individual i, $\boldsymbol{y}_i$ is the vector of all experimental data $y_{i,o,j}$ for the observed species o and time points j. $\boldsymbol{y}_i$ and also the intraindividual variation $\boldsymbol{e}_i$ are similarly described as $\tilde{\boldsymbol{y}}_i$, which was already defined in Section 2.2.1. When necessary, $\boldsymbol{y}$ denotes the concatenated vectors $\boldsymbol{y}_i$ for all individuals $i = 1, \ldots, N$. The error model was chosen as proportional error model, thereby taking into account only the measurement uncertainty $\boldsymbol{\sigma}^2_M$. This is a common assumption as for PK applications the measurement error is usually much larger than the true intraindividual variation and the measurement error becomes larger when the to be measured concentration value increases [29,68]. Measurement uncertainty $\boldsymbol{\sigma}^2_M = \left(\sigma^2_{M_1}, \ldots \sigma^2_{M_O}\right)$ is assumed to be normally distributed with mean equal to zero and specific for observed species o but not for individual i.

With the hierarchical model, it is now possible to describe interindividual variability. All individuals are linked within a population model, which is specified by the population parameters $\boldsymbol{\psi}$. The population parameters are unknown and need to be identified. Within the population, interindividual variability can be described by systematic variation according to physiological covariates $\boldsymbol{\xi}_i$. A distribution assumption is needed to further specify remaining variation $\boldsymbol{\eta}_i$, which cannot be assigned to a specific covariate and which is referred to as unexplained variability in the following.

Generally, there is no specific form of g and several functions can be used to de-

scribe the relationship between a specific individual parameter $\theta_{i,k}$ and covariates like age, gender or BW in PBPK models. Organ volumes and blood flow rates represent typical parameters that can be derived by covariate scaling. Several approaches exist where different types of scaling functions are considered. In particular, Willmann et al. [8] used age, gender and BH, while Price et al. [69] employed several regression equations to generate parameters dependent on the anthropometry of a respective individual. In an approach by Huisinga et al. [70] scaling was presented dependent on the lean body weight (LBW), which is defined as $LBW = BW - OW_{adi}$, whereby OW_{adi} represents the organ weight of the adipose tissue. In this thesis, the model from Willmann et al. is considered for the definition of the covariate model of Equation 2.3. The integration is described in detail in the following.

2.2.3 Definition of the covariate model

As mentioned above, we here describe systematic interindividual variability by covariate scaling with age, gender and body height (BH) from Willmann et al. [8]. For covariate scaling, we use the information from the physiological data base of the considered PBPK modeling software tool (see Section 2.8).

Structure of the physiological database

Age- and gender-specific population distributions of individual parameters are defined on a grid where the number of grid points is $P{\cdot}Q$ and $p = 1, \ldots, P,\ q = 1, \ldots, Q$ [13,63]. The grid is spanned in ten year age bins from 20 to 100 years and specific for gender [8,13,56], with $\boldsymbol{A} = (A_1, \ldots, A_P)$, $\boldsymbol{G} = (G_1, \ldots, G_Q)$ and A_p, G_q representing the age and gender at grid point $[p, q]$. The population distribution is defined by distribution type (normal and lognormal, respectively) and the associated mean value and standard deviation, such that for a parameter k:

$$\begin{aligned} \boldsymbol{M}_k &= \left(M^k_{A_1,G_1}, \ldots, M^k_{A_P,G_1}, M^k_{A_1,G_Q}, \ldots, M^k_{A_P,G_Q}\right), \\ \boldsymbol{S}_k &= \left(S^k_{A_1,G_1}, \ldots, S^k_{A_P,G_1}, S^k_{A_1,G_Q}, \ldots, S^k_{A_P,G_Q}\right), \end{aligned} \tag{2.5}$$

where $\boldsymbol{M}_k$ is the vector of all population mean values $M^k_{A_p,G_q}$ for age A_p and gender G_q and $\boldsymbol{S}_k$ is the vector of all population standard deviations $S^k_{A_p,G_q}$ for age A_p and gender G_q. Notably, gender is a categorical covariate and $Q = (1, 2)$, however, we write an index q for formal reasons. $\boldsymbol{M}$ and $\boldsymbol{S}$ are the concatenated vectors of all $\boldsymbol{M}_k$ and $\boldsymbol{S}_k$ with $k = 1, \ldots, K$, respectively.

Information about BH is also available, such that a reference height H_{ref} can be defined for each grid point as:

$$\boldsymbol{H}_{ref} = \left(H^{ref}_{A_1,G_1}, \ldots, H^{ref}_{A_P,G_1}, H^{ref}_{A_1,G_Q}, \ldots, H^{ref}_{A_P,G_Q}\right). \tag{2.6}$$

Figure 2.5 depicts the age dependent distribution of liver volume for male individuals as an example. Such information was generated by accumulation of several autopsy studies where each study was weighted with the number of individuals studied in the respective investigation [13].

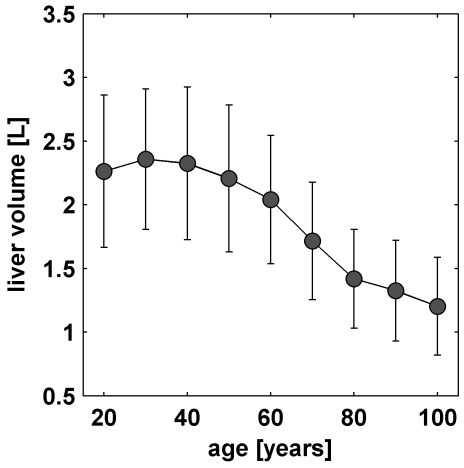

Figure 2.5: The covariance information for age is depicted exemplarily for liver volume in male individuals. The mean values $\boldsymbol{M}_k$ (grey dots) and the standard deviations $\boldsymbol{S}_k$ (black errorbars) are illustrated for each age bin (see also Equation 2.5 for comparison).

Taking the described covariance information into account, the population model (Equation 2.3) is parameterized with:

$$\begin{aligned} \boldsymbol{\xi}_i &= (A_i, G_i, H_i)\,, \\ \boldsymbol{\psi} &= (\boldsymbol{M}, \boldsymbol{S})\,, \end{aligned} \tag{2.7}$$

where A_i, G_i and H_i represent the age, gender and BH of individual i, respectively.

The random effects model is simplified by assuming *a priori* independence between the individual paramters, such that

$$\eta_{i,k} \sim \mathcal{N}(0, 1). \tag{2.8}$$

Scaling by age

For a specific individual i, age dependent scaling for a parameter k is then performed by linear interpolation, such that

$$\begin{aligned} m\left(A_i, G_i, \boldsymbol{M}_k\right) &= M^k_{A_a,G_i} \cdot sv_a + M^k_{A_b,G_i} \cdot sv_b, \\ s\left(A_i, G_i, \boldsymbol{S}_k\right) &= S^k_{A_a,G_i} \cdot sv_a + S^k_{A_b,G_i} \cdot sv_b, \end{aligned} \tag{2.9}$$

where $m\left(A_i, G_i, \boldsymbol{M}_k\right)$ is the age-scaled population parameter M and $s\left(A_i, G_i, \boldsymbol{S}_k\right)$ is the age-scaled population parameter S. Thereby, the two scaling variables sv_a and sv_b are defined as

$$sv_a = \frac{A_b - A_i}{A_b - A_a}, \qquad sv_b = \frac{A_i - A_a}{A_b - A_a}, \tag{2.10}$$

where A_b represents the age of the nearest upper grid point where $A_b > A_i$ and A_a represents the age of the nearest lower grid point where $A_a < A_i$.

Scaling by body height

Scaling of the population parameters based on the individual body height BH_i is performed continuously using an allometric scaling function. Thereby, a reference

Table 2.3: Values for the height scaling parameter α [8].

parameter	$\boldsymbol{\alpha}$
bone volume	2
brain volume	0
fat volume	2
muscle volume	2
skin volume	1.6
$\forall$ other volumes	0.75
$\forall$ non-volumes	0

body height for individual i is determined by linear interpolation again. For linear interpolation, the reference body heights of the age bins are considered (see Equation 2.6).

$$sv_c\left(A_i, G_i, BH_i, \boldsymbol{H}_{ref}, \alpha_k\right) = \left(\frac{BH_i}{H^{ref}_{A_a,G_i} \cdot sv_a + H^{ref}_{A_b,G_i} \cdot sv_b}\right)^{\alpha_k}. \tag{2.11}$$

$sv_c\left(A_i, G_i, BH_i, \boldsymbol{H}_{ref}, \alpha_k\right)$ is then the scaling variable for the population parameters $\boldsymbol{M}$ and $\boldsymbol{S}$ based on body height. The allometric scaling constants α_k are shown in Table 2.3. They are specific for parameter k and in particular considered for organ volumes. For all parameters not representing an organ volume scaling by body weight is not performed, such that $\alpha = 0$ for convenience [8].

Composing the population model

Finally, the different assumptions of the probability distribution of a physiological parameter needs to be taken into account. For example, in the physiological database liver volume is assumed to be normally distributed in a population , while fat volume is assumed to be lognormally distributed [63].

The population model of Equation 2.3 is hence defined for a normally distributed individual parameter $\theta^I_{i,k}$ as:

$$\begin{aligned}\theta^I_{i,k} &= g_k\left(\left[A_i, G_i, H_i\right], \left[\boldsymbol{M}_k, \boldsymbol{S}_k\right], \eta_{i,k}\right)\\ &= m\left(A_i, G_i, \boldsymbol{M}_k\right) \cdot sv_c\left(A_i, G_i, H_i, \boldsymbol{H}_{ref}, \alpha_k\right)\\ &\quad + s\left(A_i, G_i, \boldsymbol{S}_k\right) \cdot sv_c\left(A_i, G_i, H_i, \boldsymbol{H}_{ref}, \alpha_k\right) \cdot \eta_{i,k},\end{aligned} \tag{2.12}$$

and for a log normally distributed individual parameter as:

$$\begin{aligned}\theta^I_{i,k} &= g_k\left(\left[A_i, G_i, H_i\right], \left[\boldsymbol{M}_k, \boldsymbol{S}_k\right], \eta_{i,k}\right)\\ &= \exp(m\left(A_i, G_i, \boldsymbol{M}_k\right) + log\left(sv_c\left(A_i, G_i, H_i, \boldsymbol{H}_{ref}, \alpha_k\right)\right)\\ &\quad + s\left(A_i, G_i, \boldsymbol{S}_k\right) \cdot \eta_{i,k}),\end{aligned} \tag{2.13}$$

By using Equations 2.12 and 2.13, the population model becomes linear and is described by age-, gender- and height-scaled mean values and standard deviations. Furthermore, independence is assumed *a priori* in the random effects $\boldsymbol{\eta}_i$, since no

information about dependencies between parameters is available. This will be helpful for the consideration of the population model as a prior distribution for θ_i^I, as described below in Section 2.3.3.

In summary, $\boldsymbol{\theta}^I$, $\boldsymbol{\theta}^G$, $\boldsymbol{M}$, $\boldsymbol{S}$ and $\boldsymbol{\sigma}_M^2$ are the parameter vectors which now need to be identified in the presented model framework to be able to describe individual-specific experimental data and assess the interindividual variability in the population.

2.3 The Bayesian framework

The whole model approach of Section 2.2.1 is formulated within a Bayesian framework which allows for efficient integration of prior knowledge about the parameters. Furthermore, the Bayesian model approach defines an unknown parameter as random variable and assigns it a probability distribution such that uncertainty about each parameter is automatically derived with the approach.

In Section 2.3.1, the full Bayesian theorem is defined given the previously described model framework. In sections 2.3.2 and 2.3.3, the specific considerations of the likelihood and the prior distributions according our Bayesian-PBPK approach are presented, respectively.

2.3.1 Specification of the Bayesian theorem

The central idea in Bayesian statistics is to define a parameter as a random variable with a probability distribution. This is in contrast to the general definition in frequentist statistics where a parameter is considered as a fixed but unknown value [71]. Bayesian statistics is based on Bayes' theorem [72]

$$p(\boldsymbol{\omega}|\boldsymbol{y}) = \frac{p(\boldsymbol{\omega}) \cdot p(\boldsymbol{y}|\boldsymbol{\omega})}{p(\boldsymbol{y})} \tag{2.14}$$

which combines the prior distribution $p(\boldsymbol{\omega})$ containing the recent "degree of belief" about arbitrary parameters $\boldsymbol{\omega} = (\omega_1, \ldots, \omega_K)$ with the likelihood $p(\boldsymbol{y}|\boldsymbol{\omega})$ of new observed data $\boldsymbol{y}$ being described by parameters $\boldsymbol{\omega}$ in the posterior distribution $p(\boldsymbol{\omega}|\boldsymbol{y})$. The unscaled form of the posterior distribution

$$p(\boldsymbol{\omega}|\boldsymbol{y}) \propto p(\boldsymbol{\omega}) \cdot p(\boldsymbol{y}|\boldsymbol{\omega}) \tag{2.15}$$

can be used to determine the shape of the posterior or to identify the modes of the posterior. Only the full scaled form of Bayes' theorem can be used for inference. However, the scaling factor $p(\boldsymbol{y})$ is the full dimensional integral

$$p(\boldsymbol{y}) = \int \ldots \int p(\boldsymbol{\omega}|\boldsymbol{y})\, d\omega_1 \ldots d\omega_K. \tag{2.16}$$

Obviously, when $\boldsymbol{\omega}$ becomes high-dimensional, the numerical determination of $p(\boldsymbol{Y})$ is not feasible, such that the exact determination of the posterior distribution is intractable [71]. In such cases, Markov chain Monte Carlo approaches can be used to estimate the posterior distribution as is explained in a later section.

By integration of the PBPK model approach from Section 2.2.1 into the Bayesian framework, $\boldsymbol{\omega}$ is defined as

$$\boldsymbol{\omega} = (\boldsymbol{\theta}^I, \boldsymbol{\theta}^G, \boldsymbol{M}, \boldsymbol{S}, \boldsymbol{\sigma}_M^2), \tag{2.17}$$

and the unscaled Bayesian theorem is formulated as

$$p\left(\boldsymbol{\theta}^I, \boldsymbol{\theta}^G, \boldsymbol{M}, \boldsymbol{S}, \boldsymbol{\sigma}_M^2|\boldsymbol{y}\right) \propto p\left(\boldsymbol{y}|\boldsymbol{\theta}^I, \boldsymbol{\theta}^G, \boldsymbol{M}, \boldsymbol{S}, \boldsymbol{\sigma}_M^2\right) \cdot p\left(\boldsymbol{\theta}^I, \boldsymbol{\theta}^G, \boldsymbol{M}, \boldsymbol{S}, \boldsymbol{\sigma}_M^2\right) \tag{2.18}$$

The PBPK model structure allows to further modify this equation. First, the likelihood term (the first term on the right side of Equation 2.18) is not influenced by the

population parameters $\boldsymbol{M}$ and $\boldsymbol{S}$, since these parameters are no direct variables of the PBPK model. Furthermore, we assume independence between the single individuals, since the PBPK model output as well as the experimental data for a certain individual i are not influenced by another individual. Therefore, the likelihood can be factorized:

$$p\left(\boldsymbol{y}|\boldsymbol{\theta}^I, \boldsymbol{\theta}^G, \boldsymbol{M}, \boldsymbol{S}, \boldsymbol{\sigma}_M^2\right) \propto \prod_{i=1}^{N} p\left(\boldsymbol{y}_i|\boldsymbol{\theta}_i^I, \boldsymbol{\theta}^G, \boldsymbol{\sigma}_M^2\right) \tag{2.19}$$

Regarding the definition of the prior, the mechanistic formulation of the PBPK model further allows assuming independence between the individual and global, substance-specific parameters. In addition, independence can be assumed between the measurement error and the model parameters. The only *a priori* relationship between parameters has to be considered between $\boldsymbol{\theta}^I$ and the population parameters which is a natural consequence of the hierarchical model formulation including the covariate approach. However, this part of the prior can also be factorized, due to the assumption of independence between the individuals [73].

Finally, the Bayesian theorem is defined in log space for easier computation. Due to these assumptions, Equation 2.18 can be written as:

$$\begin{aligned}\log\left(p\left(\boldsymbol{\theta}^I, \boldsymbol{\theta}^G, \boldsymbol{M}, \boldsymbol{S}, \boldsymbol{\sigma}_M^2|\boldsymbol{y}\right)\right) \propto & \\ & \sum_{i=1}^{N} \log\left(p\left(\boldsymbol{y}_i|\boldsymbol{\theta}_i^I, \boldsymbol{\theta}^G, \boldsymbol{\sigma}_M^2\right)\right) \\ & + \sum_{i=1}^{N} \log\left(p\left(\boldsymbol{\theta}_i^I|\boldsymbol{M}, \boldsymbol{S}\right)\right) \\ & + \log\left(p\left(\boldsymbol{\theta}^G\right)\right) + \log\left(p\left(\boldsymbol{M}\right)\right) + \log\left(p\left(\boldsymbol{S}\right)\right) \\ & + \log\left(p\left(\boldsymbol{\sigma}_M^2\right)\right).\end{aligned} \tag{2.20}$$

By such consideration, the Bayesian formulation also emphasizes the separation of the individual level model (Equation 2.4) that is included in the likelihood term (row 2 of Equation 2.20), the population level model (Equation 2.3) which is represented in row 3 and the prior distributions (rows 4 and 5).

2.3.2 Specification of the likelihood

The likelihood function represents the link between PBPK model and Bayesian framework, as the likelihood function evaluates how well the experimental data are described by the PBPK model given a specific parameter vector (remember that $\tilde{\boldsymbol{y}}_i = f(\boldsymbol{\theta}_i^I, \boldsymbol{\theta}^G, \boldsymbol{\nu}_i, \boldsymbol{t}_i, D_i)$). In particular, the PBPK model is evaluated with the current parameter vector to determine the residuals between simulation output $\tilde{\boldsymbol{y}}_i$ and experimental data $\boldsymbol{y}_i$. The likelihood is then obtained under consideration of the defined error model and the assumption that the residuals are normally distributed with mean equal to zero (Equation 2.4). Consequently, the smaller the residuals, the larger the likelihood.

A specific form of experimental data is data below the lower limit of quantification (LLOQ). In such cases, no exact experimental data point $y_{i,o,j}$ can be determined. Especially when concentrations of metabolites of the given drug are

measured or the administered dose has been small, concentrations fall below the limit of the method of measurement and cannot be determined anymore. Nevertheless, a data point below LLOQ represents a valid and informative part of the data and needs to be included into the determination of the likelihood. Hence, the likelihood is defined separately for all data points larger than LLOQ and all data points smaller than LLOQ. Here, we adapted an approach by Beal et al. [74]. For individual i, the log-likelihood as defined in Equation 2.20 can be written as:

$$\log\left(p\left(\boldsymbol{y}_i|\boldsymbol{\theta}_i^I,\boldsymbol{\theta}^G,\sigma_M^2\right)\right)=\sum_{o=1}^{O}\sum_{j=1}^{J}\log\left(p\left(y_{i,o,j}|\boldsymbol{\theta}_i^I,\boldsymbol{\theta}^G,\sigma_{M_o}^2\right)\right), \tag{2.21}$$

with the likelihood of a specific time point j of an observed species o as

$$p\left(y_{i,o,j}|\boldsymbol{\theta}_i^I,\boldsymbol{\theta}^G,\sigma_{M_o}^2\right)=\frac{1/\left(\sqrt{2\pi\sigma_{M_o}^2}\cdot\tilde{y}_{i,o,y}\right)\cdot\exp\left(-\frac{1}{2}\cdot r_{i,o,j}^2(y_{i,o,j})\right)}{1-\Phi\left(r_{i,o,j}(0)\right)} \tag{2.22}$$

for $y_{i,o,j} > LLOQ$ and

$$p\left(y_{i,o,j}|\boldsymbol{\theta}_i^I,\boldsymbol{\theta}^G,\sigma_{M_o}^2\right)=\frac{\Phi\left(r_{i,o,j}\left(LLOQ\right)\right)-\Phi\left(r_{i,o,j}\left(0\right)\right)}{1-\Phi\left(r_{i,o,j}(0)\right)} \tag{2.23}$$

for $y_{i,o,j} < LLOQ$, whereby

$$r_{i,o,j}(x)=\frac{x-\tilde{y}_{i,o,j}}{\sigma_{M_o}\cdot\tilde{y}_{i,o,j}}. \tag{2.24}$$

Φ denotes the standard normal cumulative distribution function. For an explicit concentration measurement $y_{i,oj} > LLOQ$, Equation 2.22 determines the likelihood that the residuals are normally distributed with zero mean and a variance proportional to the simulation output $\tilde{y}_{i,o,j}$. Thereby, the probability is corrected by the assumption that concentration measurements cannot be negative to achieve higher accuracy [74]. For a concentration measurement $y_{i,oj} \leq LLOQ$, also called censored data point, in Equation 2.23 the cumulative probability is calculated for $y_{i,o,j}$ being within the range of $(0; LLOQ]$. Thereby, all censored data points are also corrected for the assumption of always being positive. The chosen way for dealing with LLOQ data has shown to cause a smaller bias to the optimization results than setting LLOQ values to LLOQ/2 or to zero, or even discard LLOQ data [74,75].

2.3.3 Specification of the prior distributions

The prior distributions contain all available initial information about the parameters $\boldsymbol{\omega}$ (see Equation 2.17) that need to be identified. Based on the heterogeneous amount of information that can be found in physiological databases or publications, the form of the prior distributions vary. Therefore, different types of distributions are considered according to the present knowledge.

In cases where a lot of information is available for a certain parameter, such as for the organ volumes, so-called informative prior distributions are defined. Notably, the common assumption is that physiological values are distributed lognormally in

a population [76–78]. In this work, normal or lognormal distributions are chosen together with information about lower and upper bounds, because the considered literature provides data describing both types of distributions [63] (please refer also to Section 2.2.3).

If no information about a parameter exist, so-called uninformed prior distributions are chosen. These distributions contain only vague information about a parameter and usually only a parameter range is defined by a lower and upper bound. Notably, the definition of upper and lower bounds for the model parameters, also including the measurement uncertainty $\boldsymbol{\sigma}_M^2$, is very important. In particular, absolute constraints form a major part of the prior since they define the scientifically and physiologically reasonable range for each parameter [30]. In large models, like PBPK models, several parameters can be weakly informed or even uninformed by the experimental data. Such parameters are then only influenced by the prior. If only vague information is available about the respective parameter, unphysiological values could be obtained if no absolute constraints are set. In this work, uninformed priors are defined for the global parameters $\boldsymbol{\theta}^G$ and for few population parameters $\boldsymbol{M}$ and $\boldsymbol{S}$, since only sparse literature information is available for these parameters.

In the following, the prior definitions for the various types of parameters of the Bayesian population PBPK approach are specified.

Global substance-specific parameters $\boldsymbol{\theta}^G$

Related to Equation 2.20, a continuous uniform distribution of the form

$$\log\left(p\left(\boldsymbol{\theta}^G\right)\right) = \sum_{l=1}^{L} \log\left(p\left(\theta_l^G\right)\right) \tag{2.25}$$

and

$$p\left(\theta_l^G\right) = \frac{1}{\theta_l^{G,max} - \theta_l^{G,min}},\ \theta_l^{G,min} \leq \theta_l^G \leq \theta_l^{G,max} \tag{2.26}$$

is defined for the global substance-specific parameter θ_l^G, where $\theta_l^{G,min}$ and $\theta_l^{G,max}$ describe the lower and upper bound. Notably, independence is assumed between the global parameters *a priori*.

The definition of informative prior distributions for substance-specific parameters is challenging when performing the first investigation with a specific drug. Literature values of parameters like lipophilicity or *fu* are derived only with large uncertainties, since the measurements are often performed in unphysiological environments. In particular, the *logP* is used to determine the lipophilicity of a drug thereby representing the ability to dissolve in fatty liquids. In contrast, the lipophilicity in a PBPK model defines the ability of a drug to permeate the cellular membrane. Therefore, uninformed truncated uniform distributions are used for each θ_l^G.

Population parameters $\boldsymbol{M}$ and $\boldsymbol{S}$

Since population parameters $\boldsymbol{M}$ and $\boldsymbol{S}$ are also varied in the Bayesian population PBPK approach they are assigned prior distributions, themselves. These are called hyper priors since they define the prior distribution for a parameter of a prior

distribution, particularly for that of an individual parameter $\theta_{i,k}^{I}$ (Equation 2.20). Hyperpriors are characterized by hyperparameters.

As no further information is available *a priori*, independence is assumed between the K population mean values, furthermore, independence is also assumed between the different grid points related to age and gender, such that

$$\begin{aligned} \log\left(p\left(\boldsymbol{M}\right)\right) &= \sum_{k=1}^{K} \log\left(p\left(\boldsymbol{M}_k\right)\right), \\ \log\left(p\left(\boldsymbol{M}_k\right)\right) &= \sum_{p=1}^{P}\sum_{q=1}^{Q} \log\left(p\left(M_{A_p,G_q}^{k}\right)\right). \end{aligned} \tag{2.27}$$

Most population mean values M_{A_p,G_q}^{k} are assigned informative hyper prior distributions, since for parameters such as organ volumes or blood flow rates probability distributions are obtained from physiological databases. A truncated normal distribution is defined for M_{A_p,G_q}^{k}:

$$p\left(M_{A_p,G_q}^{k}\right) = \mathcal{T}\left(M_{A_p,G_q}^{k}, \mu_{M_{A_q,G_q}^{k}}, \Sigma_{M_{A_q,G_q}^{k}}^{2}, M_{A_p,G_q}^{k,min}, M_{A_p,G_q}^{k,max}\right), \tag{2.28}$$

where $\mathcal{T}$ is the function representing the truncated normal distribution as defined in Equation 2.1, $M_{A_p,G_q}^{k,min}$ and $M_{A_p,G_q}^{k,max}$ denote the lower and upper bound, respectively, for the population mean value for parameter k at grid point p, q. $\mu_{M_{A_p,G_q}^{k}}$ represents the hyper mean value of the prior distribution for M_{A_p,G_q}^{k} and $\Sigma_{M_{A_p,G_q}^{k}}^{2}$ represents the hyper standard deviation of the prior distribution for M_{A_p,G_q}^{k}.

The informative hyper prior distribution for the population standard deviations S_{A_p,G_q}^{k} are defined related to Equation 2.28.

Both, $\boldsymbol{\mu}_{M^k}$ and $\boldsymbol{\mu}_{S^k}$ are parameterized by the grid values in the physiological database; however, the uncertainties $\boldsymbol{\Sigma}_{M^k}^{2}$ and $\boldsymbol{\Sigma}_{S^k}^{2}$ are unknown. A common assumption is to define the coefficient of variation (CV) to lie between 20% and 100% [30,73,79]. However, this always depends on the degree of belief in the respective values. In our case, the database entries rely on measurements of large numbers of individuals. Therefore, we trust in the given mean values such that we generally define a CV of 20% as the uncertainty of each M_{A_p,G_q}^{k} and a CV of 50% for each S_{A_p,G_q}^{k}. If other uncertainties are chosen, these changes are stated in the application examples below.

For uniformed M_{A_p,G_q}^{k} the prior is defined in accordance to Equation 2.26. However, uninformed prior distributions for S_{A_p,G_q}^{k} are defined as inverse-gamma distribution

$$S_{A_p,G_q}^{k} \sim invGamma(a,b),\ S_{A_p,G_q}^{k,min} \leq S_{A_p,G_q}^{k} \leq S_{A_p,G_q}^{k,max}. \tag{2.29}$$

Due to the assumption of a rather homogeneous population, we use a skewed distribution that has higher probability for small values of S_k instead of a uniform distribution and generally parameterize the inverse gamma distribution with $a = 1$ and $b = 0.22$, leading to a CV of about 50% [79]. However, the long tail allows large variabilities in cases of unexpected heterogeneity within the population.

Measurement uncertainties $\boldsymbol{\sigma}_M^2$

The prior for the measurement uncertainties $\boldsymbol{\sigma}_M^2$ are defined as Jeffrey's priors. Jeffrey's prior is a scale-invariant prior and is a common uninformed prior for measurement uncertainties [71,80]:

$$\log(p(\boldsymbol{\sigma}_M^2)) = \sum_{o=1}^{O} \log(\frac{1}{\sigma_{M_o}^2}),\ \sigma_{M_o}^{2^{min}} \leq \sigma_{M_o}^2 \leq \sigma_{M_o}^{2^{max}}, \tag{2.30}$$

where $\sigma_{M_o}^{2^{min}}$ and $\sigma_{M_o}^{2^{max}}$ describes the lower and upper bound for the measurement uncertainty of the observed species o.

Individual parameters $\boldsymbol{\theta}^I$

The prior distribution for the individual parameters $\boldsymbol{\theta}^I$ is given by the population model in Equation 2.12, such that:

$$\log\left(p\left(\boldsymbol{\theta}_i^I|\boldsymbol{M},\boldsymbol{S}\right)\right) = \sum_{k=1}^{K} \log\left(p\left(\theta_{i,k}^I|\boldsymbol{M},\boldsymbol{S}\right)\right) \tag{2.31}$$

and for a normally distributed individual parameter $\theta_{i,k}^I$:

$$p\left(\theta_{i,k}^I|\boldsymbol{M},\boldsymbol{S}\right) = \mathcal{T}\left(\theta_{i,k}^I, M^k(A_i,G_i,H_i), S^k(A_i,G_i,H_i), \theta_{i,k}^{I,min}, \theta_{i,k}^{I,max}\right), \tag{2.32}$$

where $\mathcal{T}$ is the function representing the truncated normal distribution as defined in Equation 2.1, $\theta_{i,k}^{I,min}$ and $\theta_{i,k}^{I,max}$ describes the lower and upper bound, respectively, for individual parameter k and individual i, $M^k(A_i,G_i,H_i) = m \cdot sc$ and $S^k(A_i,G_i,H_i) = s \cdot sc$ describe the age-, gender- and height-scaled mean values and standard deviations, respectively, as previously defined by Equations 2.12 and 2.9. For a log normally distributed individual parameter $\theta_{i,k}^I$, population mean value $M^k(A_i,G_i,H_i)$ and standard deviation $S^k(A_i,G_i,H_i)$ are defined by Equations 2.13 and 2.9 and Equation 2.32 describes the truncated normal distribution for $\log\left(\theta_{i,k}^I\right)$.

The clear demarcation of the prior distributions further highlights the effect of the hierarchical model definition. Population variability of a parameter k is described by S^k. The hyper priors specify the uncertainty about such variability in the parameters b of the inverse gamma distribution in Equation 2.29 or $\Sigma_{S^k}^2$ of the truncated normal distribution (Equation 2.28). Additionally, uncertainty of the population mean value is defined by $\Sigma_{M^k}^2$. Therefore, a clear separation between variability and uncertainty is achieved [73].

2.4 Classic Markov chain Monte Carlo sampling

As described above in section 2.3.1, the direct determination of the posterior distribution is intractable for high-dimensional parameter vectors. The assessment of the parameter space of a PBPK model leads to very high-dimensional vectors, especially when large cohorts of individuals are included and due to the hierarchical approach. As an example how quick the parameter space can enlarge, we can consider a first in-man study during the drug development process, which usually includes about 10 healthy male individuals aged between 20 and 40 years. Within our PBPK model around 40 parameters should be integrated, including e.g. organ volumes, blood flow rates and enzyme activities. In addition, population parameters are considered for each age bin. This example would already result in 640 parameters that have to be identified (N *individuals* $\times K$ *parameters* $+3$ *age bins* $\times 2$ *population parameters* $\times$ K *parameters*), even without the number of global parameters $\boldsymbol{\theta}^G$ and measurement uncertainties $\boldsymbol{\sigma}_M^2$ that additionally need to be considered. Therefore, for the determination of the posterior distribution, a Markov chain Monte Carlo approach is used.

In this section, we present a blockwise Metropolis-Hastings (MH) approach to cope best with our described model structure and the properties of our PBPK model as well as the high dimensionality of our parameter space. First we describe the classic MH algorithm in Section 2.4.1. In Section 2.4.2 the block structure is illustrated. In Section 2.4.3 we present how organ volume constraints need to be treated adaptively during the sampling procedure due to an additional sum constraint.

2.4.1 Metropolis-Hastings algorithm

Markov chain Monte Carlo (MCMC) approaches describe a growing class of sampling algorithms that allow estimating the posterior distribution by drawing a large sample out of it. In contrast to classical Monte Carlo sampling, MCMC methods sample along a Markov chain that has the posterior distribution as its long-run stationary distribution [81]. After a so-called burn-in period which is necessary to converge from an initial parameter vector to the stationary distribution, each iteration of the MCMC approach represents a parameter vector out of the posterior distribution. To ensure that sampling is performed along a Markov chain that has the posterior distribution as its stationary distribution the reversibility theorem must be satisfied

$$p(\boldsymbol{\omega}|\boldsymbol{y}) \cdot q(\boldsymbol{\omega}, \boldsymbol{\omega}') = p(\boldsymbol{\omega}'|\boldsymbol{y}) \cdot q(\boldsymbol{\omega}', \boldsymbol{\omega}) \tag{2.33}$$

where $q(\boldsymbol{\omega}, \cdot)$ is the candidate or proposal density that generates a new value $\boldsymbol{\omega}'$ given the current value $\boldsymbol{\omega}$ [71].

MCMC approaches have been first developed by Metropolis et al. [33] and Hastings [82], who generalized the Metropolis algorithm. This MH algorithm forms the basis of most MCMC algorithms that have been developed so far. For more information about the vast amount of MCMC approaches and the important concepts such as convergence, please refer to [55].

A sampling step of the MH algorithm is performed as follows:

1. Let $\boldsymbol{\omega}_0$ be the initial parameter vector and let $\boldsymbol{\omega}(n)$ be the parameter vector after n steps.

2. Propose a candidate vector $\boldsymbol{\omega}'$ from a predefined proposal density $q(\boldsymbol{\omega}(n), \cdot)$.

3. With the Hastings ratio

$$r_H = \frac{p\left(\boldsymbol{\omega}'|\boldsymbol{y}\right) \cdot q\left(\boldsymbol{\omega}', \boldsymbol{\omega}(n)\right)}{p\left(\boldsymbol{\omega}(n)|\boldsymbol{y}\right) \cdot q\left(\boldsymbol{\omega}(n), \boldsymbol{\omega}'\right)}, \tag{2.34}$$

   the candidate vector $\boldsymbol{\omega}'$ is accepted with acceptance probability p_{Ac}

$$p_{Ac}(\boldsymbol{\omega}(n), \boldsymbol{\omega}') = \min\left[1, r_H\right]. \tag{2.35}$$

4. Draw a uniform distributed random variable $u \sim \mathcal{U}(0,1)$. If $u < p_{Ac}(\boldsymbol{\omega}(n), \boldsymbol{\omega}')$, then $\boldsymbol{\omega}(n+1) = \boldsymbol{\omega}'$, otherwise $\boldsymbol{\omega}(n+1) = \boldsymbol{\omega}(n)$.

By including the ratios of transition probabilities, r_H guarantees that the reversibility condition is always satisfied, even under consideration of asymmetric proposal distributions [55,71].

The careful consideration of the proposal density is crucial to the performance of the MH algorithm. If the proposal density is badly chosen, the MH algorithm would converge very slowly to the stationary distribution of the Markov chain. The most common proposal approach is the random-walk algorithm, where

$$q(\boldsymbol{\omega}(n), \cdot) = \mathcal{N}\left(\boldsymbol{\omega}(n), \boldsymbol{\sigma}_P^2 \mathcal{I}_K\right) \tag{2.36}$$

where $\mathcal{I}_K$ is the identity matrix of dimension K. The challenge here is to find well-scaled variances $\boldsymbol{\sigma}_P^2$. If a certain $\sigma_{P_k}^2$ is too small, the acceptance rate would be very high, but the movements would be small such that mixing of the chain would be bad. However, if $\sigma_{P_k}^2$ is too large, mixing would also be very bad due to a very low acceptance rate [55]. Roberts et al. [83] proved that the optimal acceptance rate for dimension $K \to \infty$ is 23.4%, whereby an efficiency of about 80% would be obtained for acceptance rates between around 15% and 50% [84]. To efficiently scale the variances several pre-runs with different values for $\sigma_{P_k}^2$ can be considered to find a sufficient proposal distribution [55].

2.4.2 Blockwise sampling

Based on the formulation of the Bayesian model framework of Section 2.3, the whole parameter vector $\boldsymbol{\omega}$ of the multidimensional posterior distribution is defined in Equation 2.17 as

$$\boldsymbol{\omega} = (\boldsymbol{\theta}^I, \boldsymbol{\theta}^G, \boldsymbol{M}, \boldsymbol{S}, \boldsymbol{\sigma}_M^2).$$

Due to the large number of parameters, the application of the standard MH algorithm would lead to a very small acceptance rate of the Markov chain, since the probability is small that all parameters iterate in the direction of higher probability.

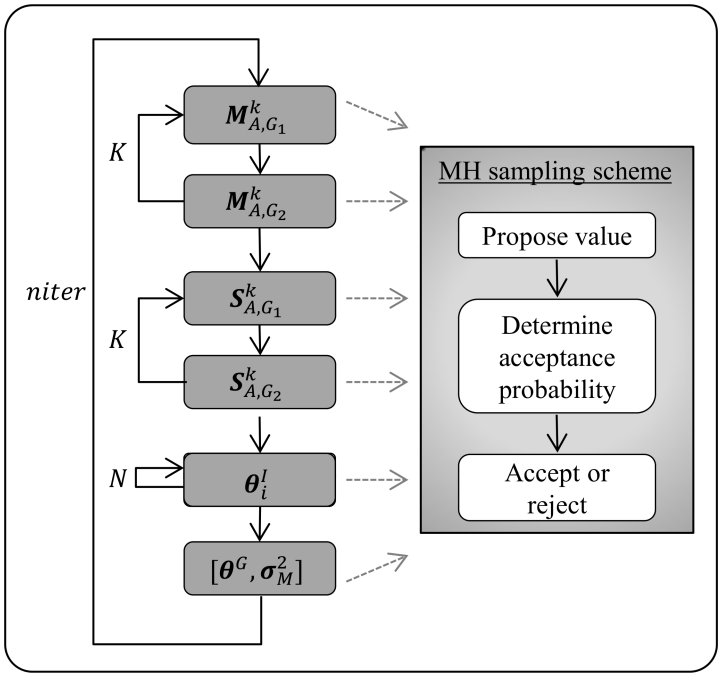

Figure 2.6: Schematic illustration of the block-wise sampling process considered for effective parameter sampling. Separate blocks are considered for all types of parameters. The population parameters $\boldsymbol{M}$ and $\boldsymbol{S}$ are sampled related to gender G and individually for each of K parameters. Individual parameters are sampled blockwise for each of N individuals. In each block, the full MH sampling scheme is performed. The sampling scheme is carried out in each of *niter* iterations.

Therefore, we adapt the standard procedure and does not vary the full parameter vector $\boldsymbol{\omega}$ in one sampling step.

In particular, a blockwise MH approach is applied in our Bayesian population PBPK approach [11,71]. It separates the parameter space into several blocks $b = 1, \ldots, B$ with regard to the biological interpretation of the parameters. The arrangement into blocks is depicted in Figure 2.6 and considered as follows: All parameter types of $\boldsymbol{\omega}$ (Equation 2.17) are assumed to be independent or only slightly dependent from each other such that they can be considered into independent sampling groups. The measurement uncertainties $\boldsymbol{\sigma}^2_M$ are added into the sampling group of the global substance-specific parameters $\boldsymbol{\theta}^G$ since the number of $\boldsymbol{\sigma}^2_M$ tends to be small and $\boldsymbol{\sigma}^2_M$ also vary globally. The individual parameters $\boldsymbol{\theta}^I$ are divided into N groups such that all parameters of a certain individual are varied in a certain block. The population parameters $\boldsymbol{M}$ and $\boldsymbol{S}$ are further divided into $2K$ groups, such that all grid points for a specific parameter k and a specific gender are sampled in one group. On the one hand, this should account for the assumption that two population parameters are only little correlated on a population level and for different genders, such that a consideration in separated block is possible. On the other hand, a certain population parameter of a specific age bin, e.g. liver volume at the age of 30 years, however, may be dependent to the parameters at the age bins nearby, due to the linear interpolation approach in the covariate model (Equation 2.9). Therefore, these parameters are sampled in one group.

Sampling is performed independently for each block. In each block, the standard MH workflow is used as described in Section 2.4.1. The Hastings ratio (Equation 2.34) is therefore defined as:

$$r_H = \frac{p(\boldsymbol{\omega}_b'|\boldsymbol{y}, \boldsymbol{\omega}_{-b}(n))}{p(\boldsymbol{\omega}_b(n)|\boldsymbol{y}, \boldsymbol{\omega}_{-b}(n))} \cdot \frac{q\left(\boldsymbol{\omega}_b', \boldsymbol{\omega}_b(n)\right)}{q\left(\boldsymbol{\omega}_b(n), \boldsymbol{\omega}_b'\right)}, \tag{2.37}$$

where $\boldsymbol{\omega}_b$ are all parameters of block b and $\boldsymbol{\omega}_{-b}$ are all other parameters of $\boldsymbol{\omega}$. $\boldsymbol{\omega}_b(n)$ is a parameter vector containing the recent parameter values of the model after n steps. $\boldsymbol{\omega}_b'$ is the candidate vector after sampling from a proposal density

$$q = \mathcal{T}\left(\cdot, \boldsymbol{\omega}_b(n), \boldsymbol{\sigma}^2_{P_b}, \boldsymbol{\omega}_b^{min}, \boldsymbol{\omega}_b^{max}\right), \tag{2.38}$$

where $\mathcal{T}$ is the function of the truncated normal distribution as defined in Equation 2.1, $\boldsymbol{\omega}_b^{min}$ and $\boldsymbol{\omega}_b^{min}$ are the lower and upper bound, respectively, of the parameters included in $\boldsymbol{\omega}_b$. The parameter constraints need to be considered during the sampling process. As long as all $\boldsymbol{\mu}'_{P_b}$ and $\boldsymbol{\mu}_{P_b}(n)$ are far away from the defined absolute constraints, the proposal distribution is approximately symmetric since usually $\boldsymbol{\Sigma}^2_{P_b} << (\boldsymbol{\omega}_b^{max} - \boldsymbol{\omega}_b^{min})$. However, if $\boldsymbol{\omega}_b'$ is close to a border the proposals become asymmetric and must be corrected.

2.4.3 Sampling of organ volumes

A subset of the individual parameters $\boldsymbol{\theta}_i^I$ is formed by the organ volumes $\boldsymbol{\theta}_i^{I,OV} = \left(\theta_{i,1}^{I,OV}, \ldots, \theta_{i,V}^{I,OV}\right)$. These volumes are constrained by a special property of the PBPK model: All organ volumes are assumed to have a density of 1 such that organ volume equals organ mass. In addition, the sum of all organ volumes of individual i represents the individual's BW, such that $BW = \sum_{v=1}^{V} \theta_{i,v}^{I,OV}$ [8]. Thus, due to a number of V organ volumes the allowed parameter space reduces to a $(V-1)$-dimensional hyperplane, such that the exact sampling of all V organ volumes including the sum-constraint is impossible. Instead, multivariate sampling of the hyperplane would be possible after a transformation of the parameters and parameter borders. To avoid complex transformations the sampling process is performed under consideration of a consecutive adaption of the lower and upper bound of a certain organ volume, conditional on the remaining proportion of BW. This is performed as follows:

1. Sort $\boldsymbol{\theta}_i^{I,OV}$ in ascending order related to the difference of the parameter-specific lower and upper bound $\boldsymbol{\theta}_i^{I,OV,max} - \boldsymbol{\theta}_i^{I,OV,min}$ and set $BW_{rem} = BW$.

2. Sample a new organ volume candidate $\theta_{i,v}^{I,OV\prime}$ according to Equation 2.38 with $\theta_{i,v}^{I,OV,min^*} < \theta_{i,v}^{I,OV\prime} < \theta_{i,v}^{I,OV,max^*}$, where

$$\begin{aligned} \theta_{i,v}^{I,OV,min^*} &= \max\left(\theta_{i,v}^{I,OV,min}, BW_{rem} - \sum_{v+1}^{V} \theta_{i,v}^{I,OV,max}\right), \\ \theta_{i,v}^{I,OV,max^*} &= \min\left(\theta_{i,v}^{I,OV,max}, BW_{rem} - \sum_{v+1}^{V} \theta_{i,v}^{I,OV,min}\right). \end{aligned} \tag{2.39}$$

3. Determine the remaining BW $BW_{rem} = BW - \theta_{i,v}^{I,OV\prime}$.

4. Repeat the steps 2 and 3 until $v = V - 1$. Then set $\theta_{i,v=V}^{I,OV\,\prime} = BW_{rem}$.

The adaptation of lower and upper bounds allows an efficient independent sampling of each organ volume $\theta_{i,v}^{I,OV}$. Apart from the dynamic lower and upper bounds, the organ volumes can be treated the same way as all other individual parameters and the transition probabilities can be easily calculated as stated in Equation 2.37, such that the blockwise MH algorithm is unaffected by the additional sum-constraint of the organ volumes.

2.5 Adaptive Markov chain Monte Carlo sampling

As mentioned above in Section 2.4.1, mixing of a Markov chain in a classical random-walk algorithm is determined by the scaling of the proposal density. If the proposal density is too broad the chain mixes very slow although single steps of the chain can be large, because the acceptance rate is very slow. If the proposal density is too narrow, mixing is also bad although the acceptance rate is high, because the accepted steps are very small and highly correlated with each other. Especially when a large number of parameters is sampled simultaneously, it is very difficult to scale the proposal density such that efficient sampling and mixing is performed. This results in slow convergence of the chain, because for full convergence of all single parameter chains need to be converged. Overall, this prolongs the run time of the approach, since a very large number of samples has to be drawn [55]. Even if several pre-runs are performed to manually select a proper proposal scaling, a sufficient density is hard to find.

To improve this manual process we here present a combined adaptive MCMC sampling approach based on the manifold Metropolis-adjusted Langevin algorithm (mMALA) from Girolami et al. [43] and the adaptive Metropolis (AM) and single-component adaptive Metropolis (SCAM) approach, respectively, from Haario et al. [44,58] to efficiently sample the different types of parameters in our approach. The two basic approaches are briefly explained in Sections 2.5.2 and 2.5.1. In Section 2.5.3, our combination of the methods based on the specific structure of the PBPK model is presented.

2.5.1 Single-component adaptive Metropolis algorithm

The finding of an optimal acceptance rate by Roberts et al. [83] led to the development of adaptive MCMC approaches, where the proposal is scaled during the MCMC run, such that pre-runs are no longer necessary. One of the first approaches was the AM algorithm of Haario et al. [57,58], which has been further extended to an adaptive Metropolis-Hastings algorithm, especially the SCAM algorithm [44]. The general idea is motivated by Gelman et al. [30] and Roberts et al. [84], who showed that

$$\boldsymbol{\Sigma}_P = k \cdot \boldsymbol{\Sigma}, \tag{2.40}$$

where $\boldsymbol{\Sigma}_P$ is the optimal proposal covariance, which is proportional to the covariance of the target posterior distribution $\boldsymbol{\Sigma}$, whereby the optimal proportionality factor k is

$$k = \frac{2.38^2}{d}, \tag{2.41}$$

where d is the dimension of the covariance matrix.

The AM algorithm uses such observation by step-wise adapting the proposal covariance matrix $\boldsymbol{\Sigma}_P$ during the MCMC run. The proposal distribution for iteration n and parameter vector $\boldsymbol{\theta}(n)$ with dimension K is defined as

$$q_n(\boldsymbol{\theta}(n), \cdot) = \begin{cases} \mathcal{N}\left(\boldsymbol{\theta}(n), \boldsymbol{\Sigma}_0\right), & n \leq n_{eq} \\ \mathcal{N}\left(\boldsymbol{\theta}(n), \frac{2.38^2}{K} \cdot \boldsymbol{\Sigma}_P(n) + \epsilon \mathcal{I}_K\right), & n > n_{eq} \end{cases} \tag{2.42}$$

where n_{eq} is a short burn-in period to have a reasonable proposal covariance matrix $\boldsymbol{\Sigma}_P(n)$ and $\boldsymbol{\Sigma}_0$ is the initial covariance matrix based on prior knowledge.

$\boldsymbol{\Sigma}_P(n)$ can be determined via simple recursion formulas, such that computation time is not an issue. A very important issue instead is the ergodicity of the algorithm, which means that it produces samples out of a Markov chain with a stationary distribution which is the posterior distribution. Brooks et al. [55] summarize and explain the conditions, whereby the most important condition is the vanishing adaption condition, which in words says that the difference of $q_n(\boldsymbol{\theta}(n), \cdot)$ and $q_{n+1}(\boldsymbol{\theta}(n), \cdot)$ must vanish when $n \to \infty$. For more detailed explanations please refer to [55,85,86]. This assumptions holds for the AM algorithm when adding $\epsilon \mathcal{I}_K$ to $\boldsymbol{\Sigma}_P$ at each iteration, where $\epsilon > 0$. This guarantees that $\boldsymbol{\Sigma}_P$ is always non-zero. In practical applications where it can be observed that $\boldsymbol{\Sigma}_P$ will not collapse to zero after few iterations, ϵ can be set to zero or to a really small value [57].

An adaptation of the AM algorithm is the SCAM algorithm which is not adapting the full dimensional covariance but updates the variances one at a time, thereby using the MH algorithm with a one-dimensional proposal. The algorithm is analog to the AM algorithm, but samples, accepts and adapts each parameter independently, such that only one-dimensional variances are adapted. Such representation of the AM algorithm can be considered for high-dimensional parameter spaces, where a determination of the full covariance and simultaneous sampling of the full parameter vector would be very time consuming and only very small sampling steps would be achieved [44].

2.5.2 Manifold Metropolis-adjusted Langevin algorithm

The mMALA is a sophisticated sampling algorithm which still has similarities to the random-walk algorithm of Equation 2.36. The original Metropolis-adjusted Langevin algorithm (MALA) has been developed by Roberts and Tweedie [87], Roberts and Rosenthal [88] and has been further adjusted by Atchade [89].

In 2011, Girolami and Calderhead [43] published the mMALA, which is based on the Riemann geometry and provides an efficient way to use local gradient and curvature information to draw samples of a high-dimensional and strongly correlated posterior density. Under assumption of a constant curvature, sampling of a candidate parameter vector $\boldsymbol{\theta}'$ is defined as

$$\boldsymbol{\theta}' = \boldsymbol{\theta}(n) + \frac{\epsilon^2}{2} \cdot \boldsymbol{G}^{-1}(\boldsymbol{\theta}(n)) \cdot \nabla_{\boldsymbol{\theta}(n)} \left(\mathcal{L}(\boldsymbol{\theta}(n))\right) + \epsilon \cdot \sqrt{\boldsymbol{G}^{-1}(\boldsymbol{\theta}(n))} \cdot \boldsymbol{z}(n), \tag{2.43}$$

where

$$\boldsymbol{G}^{-1}(\boldsymbol{\theta}(n)) \cdot \nabla_{\boldsymbol{\theta}(n)} \left(\mathcal{L}(\boldsymbol{\theta}(n))\right)$$

is the gradient of the logarithmic posterior

$$\mathcal{L}(\boldsymbol{\theta}(n)) = \log(p(\boldsymbol{\theta}(n)|\boldsymbol{Y}))$$

under consideration of the metric tensor $\boldsymbol{G}(\boldsymbol{\theta}(n))$, which is the expected Fisher information matrix of the log likelihood plus the negative Hessian of the logarithmic prior. The last right hand term provides a position-specific vector of independent

random variables $\boldsymbol{z} \sim \mathcal{N}(0, \mathcal{I}_K)$ based on the local metric given by $\sqrt{\boldsymbol{G}^{-1}(\boldsymbol{\theta}(n))}$. The scaling parameter ϵ determines the integration step size.

In contrast to the MH algorithm, the optimal acceptance rate of the mMALA was shown to be 57.4%, whereby a sufficient performance can be achieved for acceptance rates between 40% and 80% [88]. To achieve such acceptance rates, scaling is advised to be $\epsilon = K^{-\frac{1}{3}}$, where K is the dimension of the sampled parameter vector $\boldsymbol{\theta}$ [43].

Since the algorithm is based on the structure of a standard MH algorithm, the Hastings ratio r_H of Equation 2.34 can be easily applied for determination of the acceptance probability $p_{Ac}(\boldsymbol{\theta}(n), \boldsymbol{\theta}')$, since based on Equation 2.43

$$\begin{aligned} q\left(\boldsymbol{\theta}', \boldsymbol{\theta}(n)\right) &= \mathcal{N}\left(\boldsymbol{\mu}_{\boldsymbol{\theta}(n),\epsilon}, \boldsymbol{\Sigma}_{\boldsymbol{\theta}(n),\epsilon}\right), \\ \boldsymbol{\mu}_{\boldsymbol{\theta}(n),\epsilon} &= \boldsymbol{\theta}(n) + \frac{\epsilon^2}{2} \cdot \boldsymbol{G}^{-1}(\boldsymbol{\theta}(n)) \cdot \nabla_{\boldsymbol{\theta}(n)} \left(\mathcal{L}(\boldsymbol{\theta}(n))\right), \\ \boldsymbol{\Sigma}_{\boldsymbol{\theta}(n),\epsilon} &= \epsilon^2 \cdot \boldsymbol{G}^{-1}(\boldsymbol{\theta}(n)). \end{aligned} \tag{2.44}$$

The assumption of a constant curvature does not hamper the correctness of the sampling approach, however, it may decrease the efficacy of the approach depending on the real geometry of the posterior density. However, the mMALA allows to omit the pre-runs which are often necessary for classical MH approaches to tune the proposal density as described in Section 2.4.1 [43].

This method hence provides an automated adaption of the proposal density based on the local gradient and curvature such that the target density is explored quickly and the resulting Markov chain converges very fast. A possible drawback of the approach is the number of function evaluations which are needed for the numerical determination of the first and second derivatives. These evaluations increase linearly with the dimension of the parameter vector, such that sampling of high-dimensional parameter vectors under consideration of complex model structures can be difficult and very time consuming [43,55].

2.5.3 Combined mMALA and SCAM sampling

Sampling population parameters

For sampling of the population mean values $\boldsymbol{M}$ and population standard deviations $\boldsymbol{S}$ we consider the mMALA approach by Girolami et al. [43]. In contrast to recent applications of this approach, the application of manifold Metropolis-adjusted Langevin algorithm (mMALA) to population parameters does not need additional evaluations of the respective model, since the first and second derivatives do not need to be determined numerically but can be obtained analytically due to our defined model structure in Section 2.2.3. Changes in $\boldsymbol{M}$ or $\boldsymbol{S}$ only affect the prior probability but not the likelihood, as described in Equation 2.20. Thus, the gradient of the log posterior simplifies to the gradient of the log prior and the metric tensor simplifies to the negative Hessian of the log prior. Sampling is performed for each $\boldsymbol{M}_k$ and $\boldsymbol{S}_k$ independently (for definition of $\boldsymbol{M}_k$ and $\boldsymbol{S}_k$ please refer to Equation 2.5).

For example, a new $\boldsymbol{M}_k'$ is therefore sampled after n steps as

$$\boldsymbol{M}_k' \sim \mathcal{N}\left(\boldsymbol{\mu}_{\boldsymbol{M}_k(n),\epsilon}, \boldsymbol{\Sigma}_{\boldsymbol{M}_k,\epsilon}\right), \tag{2.45}$$

with $\boldsymbol{\mu}_{\boldsymbol{M}_k(n),\epsilon}$ and $\boldsymbol{\Sigma}_{\boldsymbol{M}_k,\epsilon}$ according to Equation 2.44 and

$$\mathcal{L}\left(\boldsymbol{M}_k(n)\right) = \log\left(\sum_{i=1}^{N} p\left(\theta_{i,k}^{I} | \boldsymbol{M}_k(n), \boldsymbol{S}_k(n)\right)\right) + \log\left(p\left(\boldsymbol{M}_k(n)\right)\right) \tag{2.46}$$

Assuming a normal distributed individual parameter k and based on the defined prior distributions in Equations 2.32 and 2.28 as well as according to Equations 2.9-2.11, the partial derivative with respect to the affected grid point $M^k_{A_a,G_i}$ for individual i is

$$\begin{aligned}
&\frac{\partial \mathcal{L}\left(\boldsymbol{M}_k(n)\right)}{\partial M^k_{A_a,G_i}(n)} = \\
&sv_a \cdot \frac{\theta^I_{i,k}(n) - \left(M^k_{A_a,G_i}(n)\cdot sv_a + M^k_{A_b,G_i}(n)\cdot sv_b\right)\cdot sv_c\left(A_i, G_i, BH_i, \boldsymbol{H}, \alpha_k\right)}{\left(S^k_{A_a,G_i}(n)\cdot sv_a + S^k_{A_b,G_i}(n)\cdot sv_b\right)^2 \cdot sv_c\left(A_i, G_i, BH_i, \boldsymbol{H}, \alpha_k\right)} \\
&- \frac{M^k_{A_a,G_i}(n) - \mu_{M^k_{A_a,G_i}}}{N\cdot \Sigma^2_{M^k_{A_a,G_i}}},
\end{aligned} \tag{2.47}$$

while the corresponding entry of the Hessian is

$$\frac{\partial^2 \mathcal{L}\left(\boldsymbol{M}_k(n)\right)}{\partial M^k_{A_a,G_i}(n)^2} = -\frac{sv_a^2}{\left(S^k_{A_a,G_i}(n)\cdot sv_a + S^k_{A_b,G_i}(n)\cdot sv_b\right)^2} - \frac{1}{N\cdot \Sigma^2_{M^k_{A_a,G_i}}}. \tag{2.48}$$

For clarity, $\mu_{M^k_{A_a,G_i}}$ and $\Sigma^2_{M^k_{A_a,G_i}}$ denote the hyperprior of population mean value $M^k_{A_a,G_i}$ for parameter k at grid point A_a, G_i, as defined in Equation 2.28. $\boldsymbol{\mu}^*_{M_k}$ and $\boldsymbol{\Sigma}^*_{M_k}$ represent mean values and covariance matrix in the mMALA sampling process of a new vector of population mean values for parameter k.

The full gradient and Hessian matrix are obtained by determination of the first and second derivatives with respect to all grid points of $\boldsymbol{M}^k$ and $\boldsymbol{S}^k$, corresponding to the example shown in Equations 2.45 - 2.48. For each parameter, the specific prior distribution needs to be taken into account as described in Equations 2.32 - 2.29. The structure of the mMALA sampling approach allows then to calculate the standard Metropolis-Hastings (MH) acceptance criteria as defined in Equation 2.35.

Sampling individual and global parameters

For individual parameters $\boldsymbol{\theta}^I$ and global parameters $[\boldsymbol{\theta}^G, \boldsymbol{\sigma}^2_M]$, application of mMALA as the sampling algorithm would need to determine the derivatives numerically. Sampling of these parameters with mMALA would affect the full posterior probability and thus derivation of the full PBPK model would be necessary. A large number of additional model evaluations would be needed for numerical derivation which would be extremely time consuming. Instead, we consider the adapted approach by Haario et al. [44,58] (see Section 2.5.1) for the individual and global model parameters. We consider the SCAM algorithm, which adapts, samples and accepts one parameter at a time, but extend and apply it to the described blockwise sampling scheme as described in Section 2.4.2.

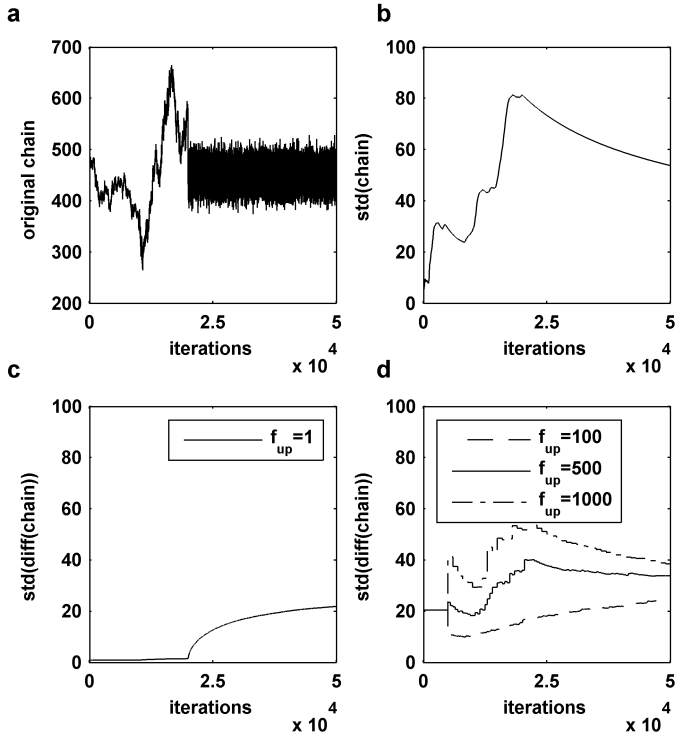

Figure 2.7: Comparison of different proposal densities for adaptive MCMC methods. (**a**) Markov chain for an arbitrary parameter. (**b**) Development of the stepwise-calculated standard deviation of the growing chain. This standard deviation is used as proposal density in the SCAM algorithm [44]. (**c**) Development of the stepwise-calculated standard deviation of the difference of adjacent elements of the growing chain. (**d**) Development of the standard deviation under consideration of the here proposed adaptive approach with $\omega_{j0} = 450$, $n_{eq} = 5000$ and $f_{up} = 500$. For comparison, two other update frequencies f_{up} are shown.

In contrast to recent approaches, we here do not adapt the proposal density based on the original sequence $(\boldsymbol{\omega}_0, \boldsymbol{\omega}_1, \ldots, \boldsymbol{\omega}_n)$ of the Markov chain, where $\boldsymbol{\omega}_n$ is the last sampled full parameter vector $\boldsymbol{\omega}_n = [\boldsymbol{\theta}^I, \boldsymbol{\theta}^G, \boldsymbol{\sigma}^2_M]$. We use the sequence of the difference of adjacent elements of the Markov chain $(\boldsymbol{\omega}_1 - \boldsymbol{\omega}_0, \boldsymbol{\omega}_2 - \boldsymbol{\omega}_1, \ldots, \boldsymbol{\omega}_n - \boldsymbol{\omega}_{n-1})$ for adaptation. Such consideration reduces overestimation of the posterior variance at the beginning of the MCMC run where the Markov chain often behaves like a Brownian motion, before converging to a stable distribution (Figure 2.7a,b). However, a continuous adaptation of the proposal density by using the standard deviation of difference of adjacent elements of the growing chain would also lead to insufficient results, since a very low proposal standard deviation would be used during the first 20,000 iterations (Figure 2.7c).

Therefore, the algorithm is defined as follows, whereby adaptation of the proposal standard deviation is performed independently for each single parameter $\omega_{b,j},\ j = 1 \ldots J$ of a certain block b. For simplicity, we write only ω_j in the following.

Before start:

- Define a start proposal standard deviation for each ω_j

$$\sigma_{p_0}^j = \frac{2.4}{\sqrt{3d}} \cdot (\omega_{j_0} \cdot 0.2)\,, \tag{2.49}$$

  where ω_{j_0} is the start value of ω_j, d is the dimension of sampling block b.

- Define the length of equilibration steps n_{eq} of the MCMC run in which $\sigma_p^j = \sigma_{p_0}^j$.

- Define the update frequency f_{up}

for $n = 1 : n_{end}$

1. Perform a Metropolis-Hastings (MH) step for the full parameter block $\boldsymbol{\omega}_b$ as described in Section 2.4.

2. If iteration $n > n_{eq}$ and n is a multiple of f_{up}, adapt the proposal standard deviation

$$\sigma_p^j = \frac{2.4}{\sqrt{3d}} \cdot \sqrt{var\left(\omega_{j_{seq(2)}} - \omega_{j_{seq(1)}}, \ldots, \omega_{j_{seq(n/f_{up})}} - \omega_{j_{seq((n-f_{up})/f_{up})}}\right)} + \epsilon, \tag{2.50}$$

   where var is the variance, $seq = (f_{up}, 2 \cdot f_{up}, \ldots, n - f_{up}, n)$ is the sequence of all iterations of the chain that are multiples of f_{up} and ϵ is a very small number to prevent σ_p^j to collapse to zero.

Based on this algorithm, updating the standard deviation of the proposal density only each f_{up} steps leads to a reasonable adaptation along the growing Markov chain (Figure 2.7d).

The literature provided variance scaling factor of $\frac{2.4^2}{d}$ [30,58,83] was found to be little too high in the case of our approach. Since we sample each parameter independently but have a dependent parameter space smaller proposals are needed. Therefore we use $\frac{2.4^2}{3d}$.

Notably, the blockwise sampling process as described in Section 2.4.2 is in principle unaffected by the here presented adaptive sampling framework, since both approaches are based on the structure of the MH algorithm. Instead of the presented random walk sampling with a constant proposal density standard deviation as described in Equation 2.38, we now consider the proposal density parameter-dependent as described in Equation 2.45 or the adapted proposal standard deviation of Equation 2.50. Furthermore, the algorithm does not affect the ergodicity of the Markov chain, since all relevant conditions (see Section 2.5.1 and [55,86]) are satisfied.

2.6 Application of the posterior results

In this section we describe how the posterior results are considered to perform model simulations for each of the integrated individuals using the individual parameter distributions in Section 2.6.1. In addition, we explain how to simulate new individuals out of the assessed population distributions in Section 2.6.2. Thereby, we present an approach to integrate the *a posteriori* dependency between the population parameters into the population simulation.

2.6.1 Individual model simulations

The application of the described Bayesian population PBPK approach generates a large high-dimensional chain of parameter vectors for $\boldsymbol{\theta}^I$, $\boldsymbol{\theta}^G$, $\boldsymbol{M}$, $\boldsymbol{S}$ and $\boldsymbol{\sigma}^2_M$. After discarding the first part of the chain which is needed for equilibration as described in Section 2.4.1, the rest of the chain represents a sample out of the posterior distribution. First, a subsample out of the posterior is generated to reduce autocorrelation of the chain and to simplify handling with the posterior distribution. For a model simulation of individual i including parameter uncertainty, the PBPK model is parameterized and evaluated with all parameter vectors $\boldsymbol{\theta}^I_{i,z}$ and $\boldsymbol{\theta}^G_z$, successively, where $z = 1 \dots Z$ represents the single parameter vectors of the posterior subsample. Subsequently, the 95% confidence interval of the simulation results is calculated.

2.6.2 Population model simulations using an *a posteriori* dependency structure

To check whether the derived posterior distributions of the population parameters correctly describe the experimental data, a population simulation is performed as described by Willmann et al. [8]. Thus, virtual individuals are created based on the anthropometry of the respective population. This step is necessary to generate the fixed parameters $\boldsymbol{\nu}$ (see Equation 2.2) for each individual.

Next, all variable parameters are generated, thereby taking into account the uncertainty of the population parameters $\boldsymbol{M}$ and $\boldsymbol{S}$, since such uncertainty is an essential part of the full posterior distribution. To include the uncertainty of population parameters into the simulations, the posterior subsamples $\boldsymbol{M}_z$ and $\boldsymbol{S}_z$ are considered together with the population model in Equation 2.12 to generate new parameterizations for new individuals out of our assessed population.

However, we do not consider the prior assumption of independent standard normal distributed random effects $\boldsymbol{\eta}_i$ (see Equation 2.8) for our posterior population simulations. Instead, we obtain the posterior random effects by inverting the population function g (see Equation 2.12):

$$\eta_{i,k,z} = \frac{\theta^I_{i,k,z} - M^{k,z}\left(A_i, G_i, H_i\right)}{S^{k,z}\left(A_i, G_i, H_i\right)}, \tag{2.51}$$

where $M^{k,z}\left(A_i, G_i, H_i\right)$ and $S^{k,z}\left(A_i, G_i, H_i\right)$ denote the age-, gender- and height-scaled mean value and standard deviation for parameter k and subsample z. We

then assume a multivariate Gaussian mixture model

$$p(\boldsymbol{\eta}) = \sum_{z=1}^{Z} \mathcal{N}\left(\overline{\boldsymbol{\eta}}_z, \boldsymbol{\Sigma}_z\right), \tag{2.52}$$

where $\overline{\boldsymbol{\eta}}_z = \left(\overline{\eta}_{1,z}, \ldots, \overline{\eta}_{K,z}\right)$ and $\overline{\eta}_{k,z} = \frac{1}{N}\sum_{i=1}^{N}\left(\eta_{i,k,z}\right)$ is the mean value of the random effects for parameter k and subsample z of all N individuals and Σ_z is the covariance matrix of all random effects for subsample z, such that a new individual parameter vector $\boldsymbol{\theta}_i^*$ can be generated by consideration of a randomly chosen subsample z, where

$$\boldsymbol{\theta}_{i,z}^{I*} = \boldsymbol{M}^z\left(A_i, G_i, H_i\right) + \boldsymbol{S}^z\left(A_i, G_i, H_i\right) \cdot \boldsymbol{\eta}_z^*,\ \boldsymbol{\eta}_z^* = \mathcal{N}\left(\overline{\boldsymbol{\eta}}_z, \boldsymbol{\Sigma}_z\right). \tag{2.53}$$

We then check whether the new individual parameters define an individual out of our population, which means that BW and body mass index (BMI) are within the predefined ranges. Otherwise, the individual parameterization is discarded and need to be sampled again.

With our new obtained individual parameters the PBPK model is parameterized and evaluated, successively, for each subsample $\boldsymbol{\theta}_{i,z}^{I*}$ together with the substance-specific parameters $\boldsymbol{\theta}_z^G$. Subsequently, the 95% confidence interval of the simulation results is calculated to represent the interindividual variability within the population.

It is also possible to perform population simulations based on maximum posterior estimates, thereby neglecting the derived uncertainty of the population parameters. In such cases, the population distribution is defined by $\boldsymbol{M}_{z_M}$, $\boldsymbol{S}_{z_M}$, $\overline{\boldsymbol{\eta}}_{z_M}$ and $\boldsymbol{\Sigma}_{z_M}$, where z_M is the iteration with the highest determined posterior probability.

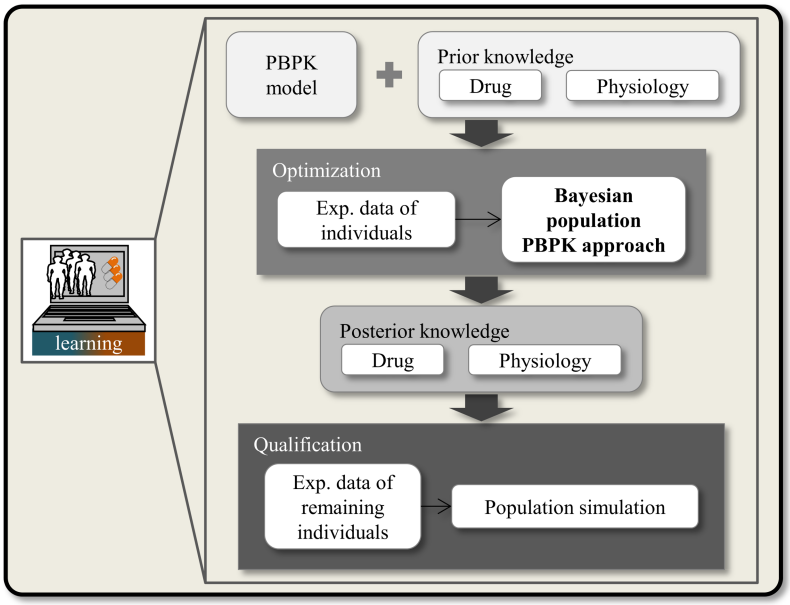

Figure 2.8: Single learning step of the translational learning workflow. The presented scheme is performed in each step of the translational learning workflow (Figure 2.9). The central element is the Bayesian population PBPK approach. Prior knowledge is updated with new experimental data, and posterior knowledge on both the drug and population physiology is inferred. Assessed knowledge is qualified by comparing a population simulation with remaining experimental data.

2.7 Workflow for translational learning

In this section, we describe a workflow for translational learning based on our developed Bayesian population PBPK approach. The Bayesian paradigm of our method allows to use initial information about parameters and combine it with information extracted from new experimental data. Such an approach cannot only be used as single investigations to estimate parameters and their uncertainty or the interindividual variability within a population. It is further ideally suited for an iterative assessment where generated knowledge can be translated to new scenarios. In a clinical context, the value of such translational learning is the growing amount of initial knowledge about e.g. the physiology of a diseased population which is available before a clinical study is performed. Such knowledge can be used for improved planning of clinical trials. For example, a profound prediction of the expected PK profile in a diseased population can be generated before starting a clinical phase II study based on recent applications of the Bayesian PBPK analysis with other drugs.

In particular, the translational learning workflow consists of several consecutive learning blocks, each containing an optimization step using Bayesian population PBPK and a qualification step, where a population simulation is performed to evaluate the results with additional experimental data (Figure 2.8).

After each learning block, a part of the assessed posterior distribution can be translated to the prior distribution for the next learning step. This either allows to accumulate derived knowledge about the properties of a drug or to learn about the physiology of a specific-patient population. Such learning process is possible due to

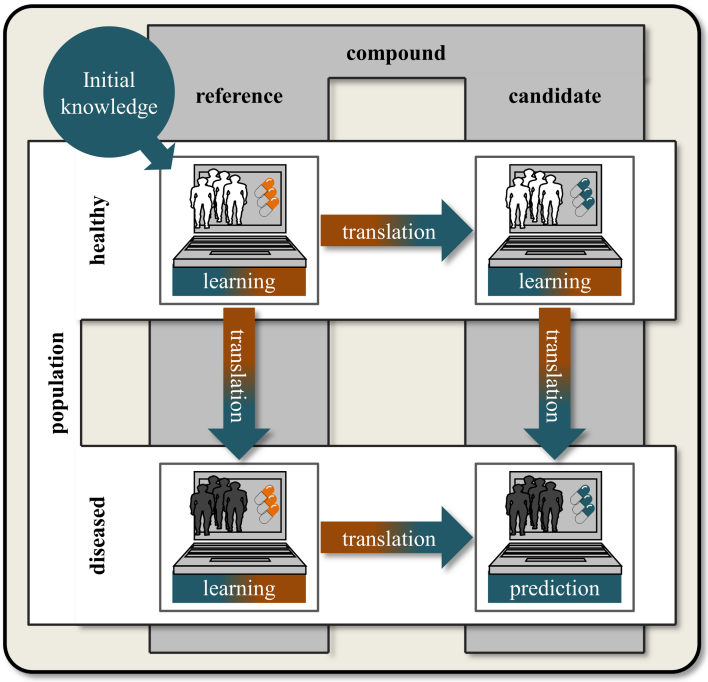

Figure 2.9: Schematic illustration of the translational learning approach. A learning step contains a full Bayesian analysis where initial knowledge is used in combination with new experimental data to refine and acquire knowledge about physiological and drug-specific parameters (Figure 2.8). A translation step transfers the acquired knowledge to a new investigation where the acquired knowledge is used as initial knowledge in a new Bayesian analysis. In this illustration, learning starts from the healthy population treated with a reference drug and ultimately leads to prediction of the effects of a candidate drug in a diseased population.

the separated consideration of physiological parameters and drug-specific parameters in the PBPK models. Finally, the gained knowledge about a drug as well as the physiological properties of a specific population can be used for a prediction of the PK behavior of a certain drug within a certain population.

A possible transfer of knowledge from a clinical phase I to a clinical phase II can be obtained as follows (Figure 2.9):

In step one, the Bayesian population PBPK approach is performed for a given reference drug in a reference cohort of healthy individuals. Thereby the posterior distributions characterizing interindividual variability in physiological parameters are quantified and the physicochemistry of the reference drug is established. The results are qualified by the population simulation which is compared against further individuals of the corresponding reference population. In the second step, a novel candidate drug is investigated within the same healthy population as before. At this step, posterior distributions of physiological parameters acquired in the previous step are now translated to another Bayesian analysis where they are used as prior information. This second step hence refines the physiological characterization of the healthy population and further infers the physicochemistry of the novel candidate drug. Qualification of the results is again performed by a population simulation which is compared against further individuals of the reference popula-

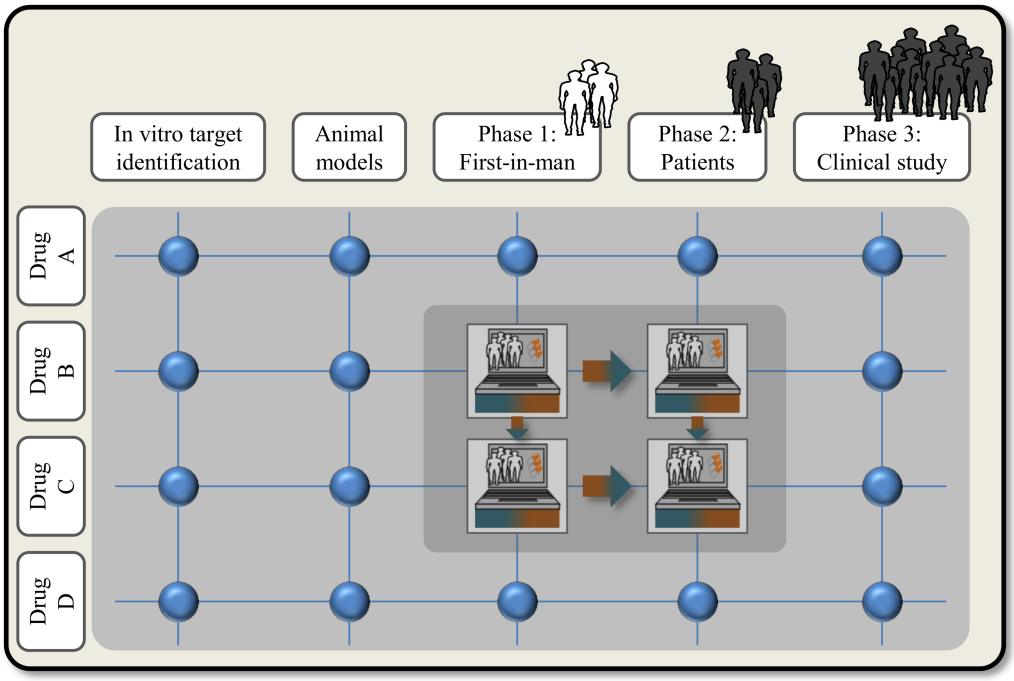

Figure 2.10: Iterative administration of the translational learning workflow in the clinical drug development process. The translational learning workflow of Figure 2.9 can be iteratively used across and within clinical development programs. As proof of concept example we presented translation between two drugs and between clinical phase I and II.

tion. The third step of the translational learning approach is performed with the reference drug again, but now experimental PK data of a diseased population are considered. The posterior distributions acquired before in the two analyses of the healthy reference population are now taken as initial estimate for another Bayesian analyses in the diseased population. This third step is of particular relevance to infer possible pathophysiological changes in this novel cohort of patients. After these three preparatory Bayesian analyses, both, the posterior physiological information of the diseased population and the posterior physicochemical information about the candidate drug were combined and used for a de novo prediction of the PK behavior of the candidate drug in the diseased population.

In principle, the number of learning steps is not restricted before predicting the PK behavior of a new drug. Furthermore, such translational workflow can be considered along the full drug development program starting from early clinical development and ending at the prediction of large clinical phase III studies (Figure 2.10).

2.8 Implementation

The PBPK models were created using the software tools PK-Sim® and MoBi® (Version 5.5.3). PK-Sim and MoBi are both part of the Computational Systems Biology Software Suite, which is a commercial software package from Bayer AG (`www.systems-biology.com`). Notably, academic licenses are available free of charge. The Software Suite further consists of R and MATLAB Toolboxes, which represent interfaces to MoBi, such that parameterization and simulation of a PBPK model created within PK-Sim is possible also in external software (Figure A.1) [63]. This allows to integrate the simulation into complex workflows.

PK-Sim is a software tool for PBPK modeling. It includes a generic compartmental structure as described in Section 2.2.1. Several generic distribution models can be selected using different methods for calculation of partition coefficients [61,62,65–67]. This allows the description of neutral compounds as well as acidic or basic compounds. Based on the anthropometry of an individual, all physiological parameters like organ volumes and blood flow rates are determined using an integrated physiological database [8,56,63].

MoBi is an expert tool for mechanistic and dynamic modeling of biological processes. A previously generated PBPK model in PK-Sim can be imported into MoBi for further modification, parameter identification processes or population simulations. MoBi offers full access to all parameters in the model and allows integration of complex cellular reaction networks etc. Furthermore, MoBi allows to couple several PBPK models, such that the simultaneous evaluation of a parent compound and its metabolites is possible. PK-Sim and MoBi have both been explained in detail before [23,56,67,90]

The full Bayesian population PBPK approach including the MCMC methods and the hierarchical model structure was implemented in MATLAB (version R2013b; MathWorks®, Natick, MA). Figure 2.11 shows a schematic view of the implementation steps that are needed in MATLAB together with references to the respective sections and equations that are described above. Priority in the implementation process of the MCMC sampling routine must be given to the sampling process itself and the determination of the prior probability and the likelihood within the blockwise sampling structure (Section 2.4.2). Thereby, the correct assignment of the covariate scaled population parameters during determination of the prior probabilities requires special consideration. Furthermore, sampling of organ volumes (Section 2.4.3) and the number of parameters that are accepted in one step for a certain type of parameter (population, individual, global) need to be implemented carefully (Section 2.4.2).

2.9 Discussion

For the establishment of our described Bayesian population PBPK workflow, several model concepts have been combined and adapted. The resulting approach allows to efficiently assess interindividual variability and at the same time generate personalized descriptions of the PK behavior of drugs. The underlying consideration of mechanistic PBPK models enables a clear attribution of assessed information to a

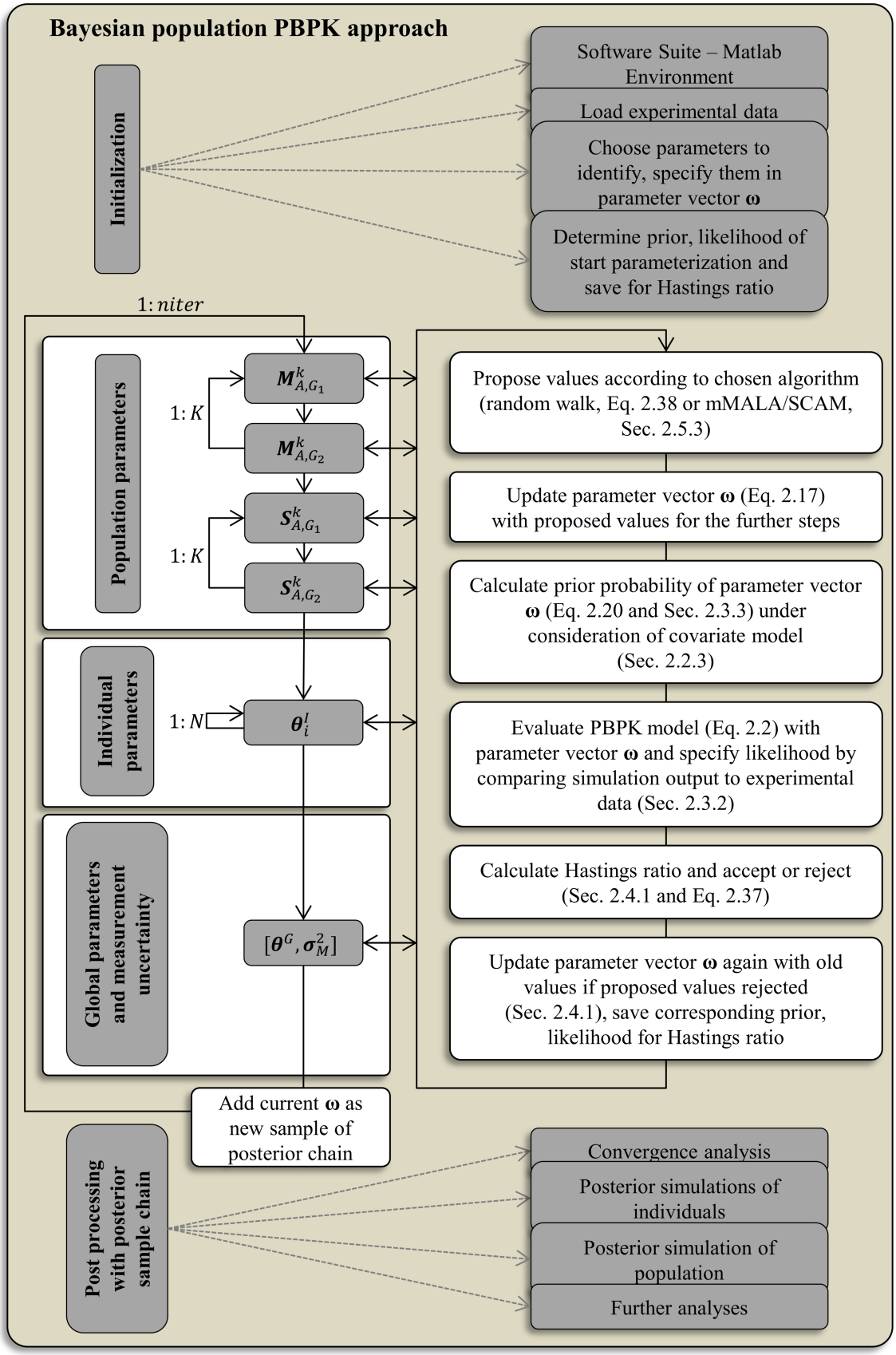

Figure 2.11: Scheme for implementation of the Bayesian population PBPK approach in MATLAB.

biological process in a certain individual or to a physicochemical property of a drug.

During development of the approach, assumptions have been made which significantly facilitate efficient parameter estimation and the setup of the Bayesian framework, for example the assumption of independence of several parameters, distribution assumptions for population distributions or independence of prior distributions. In particular, prior information represents the subjective current "degree of believe" about a parameter or a set of parameters [71]. The parameters within PBPK models all have an underlying biological equivalent due to the mechanistic consideration, or describe physicochemical properties of the drug. Thus, a lot of prior information about most physiological parameters is available from databases; however, the measurements e.g. of volumes of organs are usually independent from each other, such that no information about possible dependencies is available. Furthermore, it is unlikely, that for example the protein expression of a certain enzyme is dependent on an organ volume or the lipophilicity of a drug, which strengthens the trust on the assumption of *a priori* independence. The assumption that the different parameter types such as population parameters, individual parameters and global parameters are independent from each other allows for the formulation of the blockwise sampling structure as explained in Section 2.4.2. Notably, the consideration of blockwise sampling would not be possible if parameters that are highly correlated with each other are sampled in different blocks. High correlation of two parameters sampled in different blocks would strongly decrease the acceptance rate of the proposed samples in both blocks. Thus, the performance of the MCMC run would clearly indicate that the classification of the parameters into the different sampling block is not feasible.

Notably, assumptions made during definition of prior distributions can be overruled in the posterior distribution, as the posterior represents the updated "degree of believe" after integration of new information that can be extracted from new experimental data. This also includes covariance information between parameters. An interesting aspect is that based on the definition of Bayes' theorem, different prior assumptions lead to different posterior distributions, however, asymptotically and with enough available data, the posterior is independent from the prior distribution [91]. This further strengthens the concept of translational learning, where the iterative assessment of the Bayesian population PBPK approach also increased the impact of integrated information compared to the initial prior information.

Structural assumptions such as the definition of normal and lognormal population distributions influence the resulting posterior distribution more strictly. For example, no bimodal population distributions could be identified with our approach; in such cases probably a very broad normal distribution would be obtained. Therefore, our hierarchical model works under the assumption of a homogeneous population. In cases where heterogeneous populations are expected, additional sublevels could be included into the hierarchical model or a pre-run without a population model could be used to identify possible heterogeneous subgroups, which are then considered separately.

Another important aspect during setup our approach is the selection of the parameters to be identified. In general, there is no fix set of parameters; the choice of parameters strongly depends on the question that should be answered in an inves-

tigation. However, for a thorough characterization of the PK behavior of a drug all aspects of drug ADME should be included, otherwise significant parts of interindividual variability could be explained inadequately. As described in Section 2.2.1, the distribution model is parameterized by few drug-specific parameters, mainly lipophilicity and molecular weight. Molecular weight can be determined precisely, but lipophilicity is hard to determine and the measurement method is subject to large uncertainty, such that only a vague prior can be defined. This parameter should therefore always be identified within the Bayesian population PBPK approach; as it has such large influence on drug distribution it is highly informed by the experimental data, which results in a sharp marginal of the posterior distribution.

Parameters that characterize active processes such as transport across membranes or enzymatic metabolization also need to be identified for a thorough characterization of interindividual variability of the elimination behavior of drugs. The absorption of a drug is a more complex process and strongly depends on the formulation of a drug, for example as tablet, solution or small pellets. Therefore, the choice of parameters that need to be included can vary. Solubility is important to describe dissolution in stomach and intestine in cases where the drug is administered orally. If the dissolution of the drug is pH-dependent, also the pKa value could be considered.

For healthy individuals, interindividual variability of physiological parameters such as organ volumes and blood flow rates can be assumed to be fully explained by the covariates [36]. In such cases, these parameters do not need to be identified; however, the integration of physiological parameters into the Bayesian population PBPK approach allows to check whether the assumed relationships to covariates can be validated. In cases where a pathological population is physiologically characterized, these parameters need to be considered to assess the underlying pathophysiological alterations.

The covariate model itself also represents an assumption about structural variability and is subject to change and development. Several covariate models have been developed so far as stated at the end of Section 2.2.2. It was shown that other covariate models exist that explain physiological variation even better than the one used in this thesis [70]. However, the change to another covariate model would hamper the efficient use of the available prior information in the physiological database of the considered software suite. Furthermore, the use of a less effective covariate model does not lead to wrong results, but to more unexplained variability in the population model (Equation 2.3). An interesting extension of our developed approach in the future could be the identification of additional covariates based on the integrated experimental data. It could be expected that, especially in diseased patients, further covariates such as the diseased state could explain significant amounts of the observed interindividual variability.

Main focus in general development of MCMC approaches is on the sampling procedure. Large numbers of different sampling methods have developed during recent years which have become very sophisticated and aim for specific purposes or specific fields of applications. Thereby, the sampling methods can be divided into two classes: gradient-free (such as classic, adaptive or multi-chain MH algorithms [33,44,92]) and gradient-based samplers (such as Hamiltonian Monte Carlo methods

(HMC) or MALA [43]). In several applications and technical assessments it has been shown that gradient-based samplers are superior to gradient-free sampling methods, showing a higher time-normalized effective sampling size (nESS) [93]. Thereby, HMC shows a much higher nESS than MALA, however, the advantage of MALA is that it needs almost no tuning and is computationally less expensive [93]. Therefore, MALA is well suited for identification of our high dimensional parameter distributions.

Nevertheless, also gradient-free methods show reasonable performance when they are tuned properly. Tuning can be performed e.g. by the consideration of adaptive MCMC samplers or by comprehensive sensitivity analyses before starting an MCMC run. Furthermore, they are much less computationally expensive than gradient-based samplers, which are therefore not ideal in cases of very high dimensional problems [55]. This is why we developed the combined mMALA/SCAM algorithm, that combines the advantages of gradient-free and gradient-based samplers regarding the specific parameter types in the Bayesian population PBPK approach. Such combinations are also proposed by other workers just recently [93,94].

In summary, there is no general superior method for MCMC sampling, instead, the algorithm should fit for purpose and should be chosen carefully. In this work, this was done regarding our specific workflow, thereby taking into account the specific properties of mechanistic PBPK models, the consideration of large cohorts of individuals and the resulting high dimensionality. Further discussion about performance and the overall concept is only possible focusing on specific applications with the developed Bayesian population PBPK approach and can be found in the following chapters.

Chapter 3

Subgroup stratification related to identified inhomogeneities in enzyme activity

In this chapter, we present an application example of our Bayesian PBPK approach considering pravastatin PK [10]. Pravastatin is a cholesterol lowering drug. Its PK behavior is characterized by a large genotype-mediated interindividual variability [95–98]. In case of pravastatin, the arising interindividual variability can lead to severe adverse effects. To ensure the patient' safety it is very important to identify patient subgroups which can manifest adverse effects as early as possible. Therefore, the objective of this application example is to establish a thorough characterization of the sources of interindividual variability and to generate a comprehensive understanding of the processes that govern the PK behavior.

Section 3.1 describes the PBPK model building and the biological and pharmacological background of pravastatin. In Section 3.2 the specific setting of the Bayesian PBPK approach is described, including the selection of model parameters and the execution of MCMC runs. Section 3.3 presents the results, followed by a discussion in Section 3.4.

3.1 Pravastatin: background, data and model

Pravastatin is a 3-hydroxy-3-methyl-glutaryl-Coenzyme A (HMG-CoA) reductase inhibitor which lowers the cholesterol level within the body and thereby contributes to prevention of cardiovascular diseases. Compared to other statins, it has a low lipophilicity [97] such that pravastatin uptake is mainly distributed by active transporters [96]. On the one hand, the organic anion transporting polypeptide 1B1 (OATP1B1) transports pravastatin into the intracellular space of the liver and on the other hand the organic anion transporter 3 (OAT3) inserts pravastatin in the intracellular space of the kidneys [96]. In the liver, pravastatin is excreted by biliary excretion, leading to enterohepatic circulation, while tubular secretion is the main pathway to excrete pravastatin from the kidneys [99]. Thereby, both routes of excretion are also performed by an active transporter, the multidrug resistance-associated protein 2 (MRP2) (Figure 3.1). MRP2 is also significantly expressed in the apical

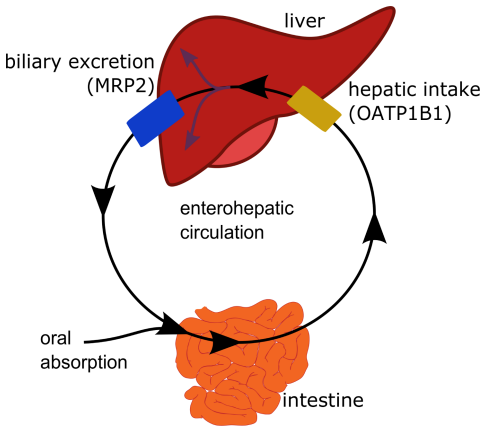

Figure 3.1: Schematic representation of the enterohepatic circulation and the key transporting enzymes in pravastatin pharmacokinetics. Notably, this is only a simplified consideration for a better representation of the processes that are integrated into the mechanistic whole-body physiologically-based pharmacokinetic model.

membrane of enterocytes in the duodenum and jejunum. The bioavailability of pravastatin is low due to an incomplete absorption in the small-intestine [96].

Notably, significant alterations in pravastatin PK are associated to three different genotypes (SNP; c.521T→C, p.Val174Ala) of solute carrier organic anion transporter family member 1B1 (SLCO1B1) encoding for OATP1B1 [96,100]. These genotypes (homogeneous TT, heterogeneous TC and homogeneous CC) determine the transporter activity [5]; the CC genotype has decreased activity compared to the normal TT genotype, which leads to higher pravastatin concentrations in the body. In contrast, no such effect is known for MRP2.

For our analyses we considered a previously established and validated PBPK model of pravastatin [5] for an oral dose of 40 mg administered orally. In this model, active transport processes were established in the interstitial (OATP1B1) and the intracellular space (MRP2) of the liver as well as in the interstitial space of the kidneys (OAT3). Additionally, MRP2-mediated transport was considered in the gastrointestinal compartment of our model as well as the intracellular space of the kidneys. Tissue specific enzyme activity was estimated by using gene expression data as a proxy for protein abundance. Notably, this allows the discrimination between organ-specific protein levels and the global catalytic rate constant (k_{cat}) [101]. A luminal clearance reaction in the small intestine accounted for the low bioavailability of pravastatin.

The experimental data was provided from previously published studies [100]. Out of the dataset of 32 individuals, 10 individuals were chosen randomly to lower computational costs. It was taken into consideration that all above mentioned genotypes are represented equal in number within the dataset. Figure 3.2 shows the chosen individuals and their respective genotype of OATP1B1.

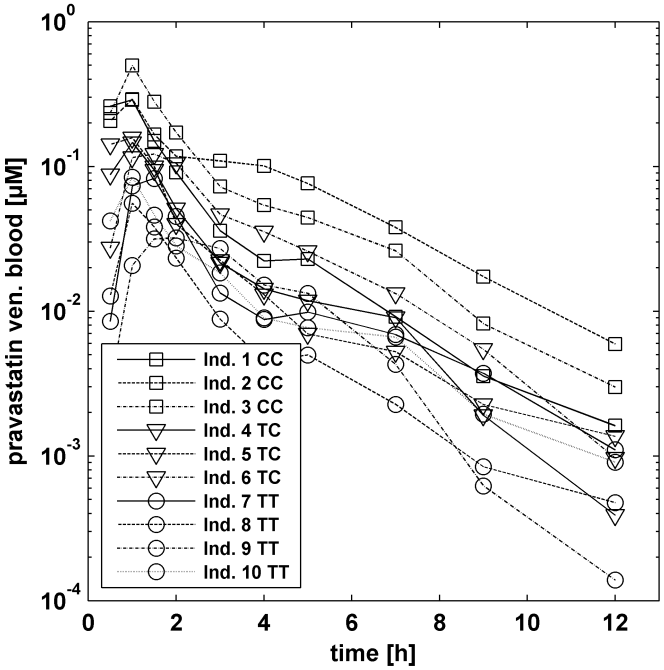

Figure 3.2: Experimental data of the ten patients which were integrated into the Bayesian-PBPK approach. The patients have been chosen out of a dataset of 32 patients provided by Niemi et al. [100].

3.2 Statistical computation

8 individual parameters together with 4 global parameters were chosen for the Bayesian analysis (Table 3.1), which means the variation of 84 parameters in total. These parameters have chosen such that all important ADME processes were considered for a comprehensive description of the PK behavior and an assessment of the interindividual variability on a parameter level. An individual model approach is used including a proportional error model as defined in Equation 2.4. By consideration of the blockwise sampling described in Section 2.4.2, individual parameters and global parameters were sampled in separate blocks. The proposal density is chosen as defined in Equation 2.38. Thereby, all parameters are sampled independently with the mean value defined as the last sampled parameter of the Markov chain and the standard deviation as $0.01 \cdot (\omega_b^{max} - \omega_b^{min})$. Prior distributions were defined as log normal distributions in case of previous information about that parameter, or as uninformed prior. The start parameters as well as geometric mean and standard deviation for the informative prior distributions are provided in Table 3.2.

During the separation of the parameters into different blocks, it is very important to know if parameters are correlated, since correlated parameters have to be sampled in one block [102]. Our block structure is driven by the clear separation between drug and individual physiology in the PBPK model, therefore, we can assume that all parameters of different blocks are independent and uncorrelated (see also the discussion) and we can assure that no lumped parameters exist which depend on physiological and drug-specific information.

With the established PBPK model, the combined Bayesian PBPK approach was

Table 3.1: Parameters of the pravastatin model that are identified in the Bayesian-PBPK approach

parameter	**unit**	**abbreviation**	**type**
intestinal permeability	cm/min	$intP$	individual
intestinal transit time	min	ITT	individual
gastric emptying time	min	GET	individual
luminal clearance factor	μM/min	CL_{lum}	individual
k_{cat} OATP1B1	-	k_{cat_O}	individual
k_{cat} MRP2	-	k_{cat_M}	individual
lag time of enterohepatic circulation	min	$EHClagtime$	individual
measurement error	-	σ_M	individual
lipophilicity	-	$logP$	global
unbound protein fraction	%	fu	global
K_m OATP1B1	μM	K_{M_O}	global
K_m MRP2	μM	K_{M_M}	global

Table 3.2: Start values and prior definition for all identified parameters

parameter	**start value**	**prior type**	**geo mean**	**geo std**
$intP$	0.004	informative	0.007	1.6
ITT	240	informative	240	1.6
GET	16.9	informative	30	1.4
CL_{lum}	0.012	informative	0.013	1.4
k_{cat_M}	503.696	uninformative	-	-
k_{cat_O}	2242.631	uninformative	-	-
$EHClagtime$	193	uninformative	-	-
σ_M	0.35	Jeffreys	-	-
$logP$	0.749	informative	2.2	1.8
fu	0.561	uninformative	-	-
K_{M_M}	223	uninformative	-	-
K_{M_O}	11.5	uninformative	-	-

processed and 300,000 iteration steps were calculated. The computation time was 3.6 s/iteration and was performed on a quad core i5 processor running under Windows 7. Although MCMC runs are in principle independent from the start parameterization regarding the identification of the correct posterior distribution, parameter start values were optimized via a standard point optimization process for a single individual to reduce convergence time, which increases when the MCMC run starts in regions with very low probability (Table 3.2). During the first 150,000 steps, the parameter vectors did not sample from the correct distribution. For this so-called burn-in period the samples were discarded. By subsampling 200 parameter vectors of each individual from the remaining 150,000 steps (Figure A.2), an independent sample of the posterior distribution was drawn to derive the results presented below.

3.3 Results

As a first result, we simulated the interindividual variability of pravastatin PK in the population. Simulations were performed for each individual by evaluating the PBPK model for pravastatin with each of the 200 parameter vectors which were subsampled out of the posterior distribution. Next, the 95% confidence interval (CI) was calculated over all individuals (with all 2,000 samples) and compared against the experimental data. The resulting range of interindividual variability is shown in Figure 3.3a. The resulting visual predictive check shows a good agreement with the experimental data except a little too broad interval around 3 to 5 h.

To further check that the depicted interindividual variability did not result from large uncertainty of the single individuals, simulations were performed for three exemplary individuals by simulating the PK of pravastatin with each of the 200 parameter vectors which were subsampled out of the posterior distribution (Figure 3.3b). The 95% CI was calculated and plotted for each individual together with the median and compared to the experimental data. The obtained uncertainty is small and furthermore the individuals show also good agreement with the experimental data, whereby individual 1 shows a less good fit to the experimental data around 3 to 6 h.

To better illustrate the quality of the obtained results, a comparison of the predicted mean values and the experimental data of all individuals was performed and shows good agreement (Figure 3.4).

Notably, beside the PK range which is kind of a “macroscopic” result of the posterior parameter distribution, a lot of other information can be obtained by directly analyzing the posterior. The calculation of correlations between the 8 individual parameters provided information about dependencies between the various parameters in the model. For example, a strong correlation between intestinal permeability ($intP$) and the enzyme activity of MRP2 (k_{cat_M}) was observed, as depicted in Figure 3.5.

We next asked whether our approach can also be used for the identification of specific subgroups within a population. This is a challenging task in particular in early phases of drug development, since only little prior knowledge may be available. Therefore, we asked if our Bayesian PBPK approach enabled the identification of such homogeneous groups of individuals even if no additional information was taken

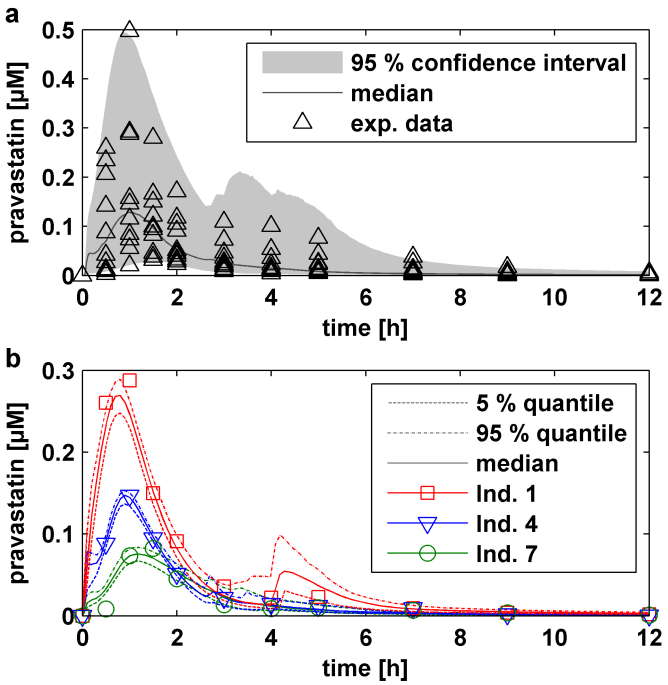

Figure 3.3: Inter-individual variability of pravastatin pharmacokinetics (venous blood plasma). (**a**) Population variability is shown under consideration of simulations with 2000 parameter sets as described in the text. The variability is shown together with the median curve and the experimental data. (**b**) Individual simulations are illustrated for three exemplary individuals. The 95 % confidence interval representing uncertainty is shown together with the median and the experimental data.

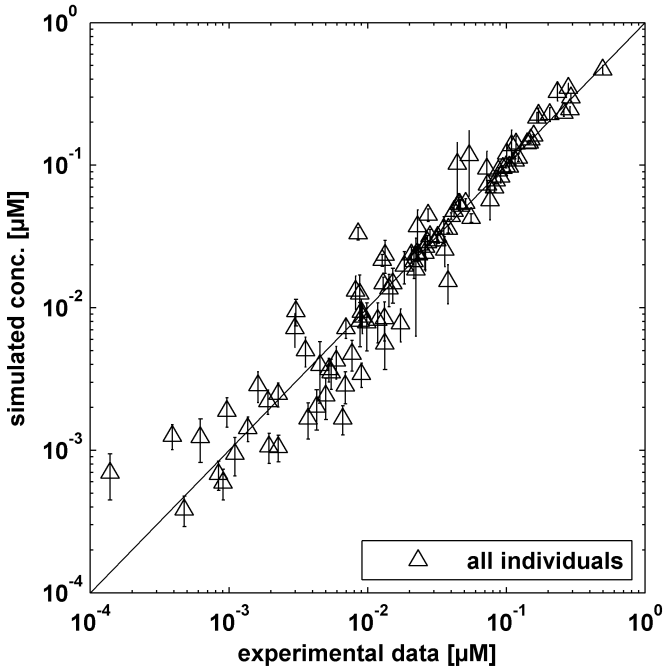

Figure 3.4: Correlation between simulated mean values and experimentally obtained pravastatin data (venous blood plasma). Mean concentration values and standard deviations of the 200 simulations for each individual were monitored at the same time points as the experimental data.

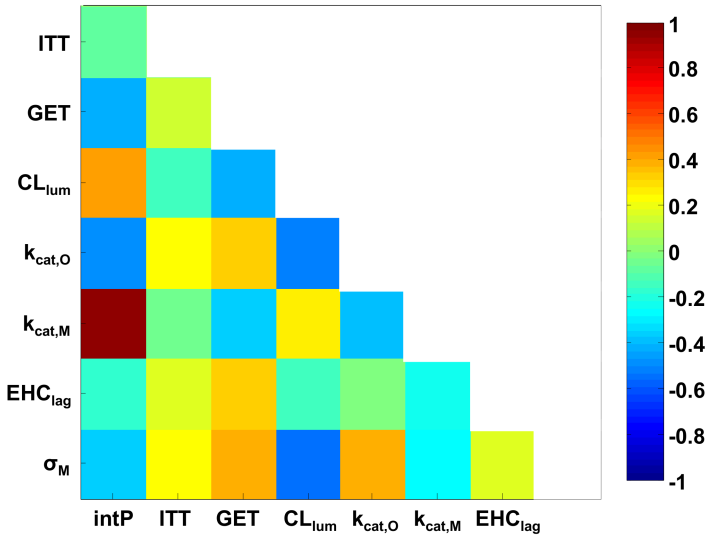

Figure 3.5: Correlation matrix of all individual parameters. Spearman correlation coefficients were calculated from the overall subsample of 2000 parameter vectors for all parameter combinations to identify structural connections. To improve the visualization of the correlations the main diagonal was set to zero.

into account and considered the transporter activities of MRP2 and OATP1B1 as a putative source for subgroup stratification. First, we performed a Shapiro-Wilk test for normal distribution [103] of the logarithmic mean values of the 200 samples of every individual, since enzyme activity has found to be log normally distributed in homogeneous groups of individuals [78,104]. The results supported the hypothesis of log normal distribution for MRP2 ($p > 0.75$) and gave a strong indication of rejection of the hypothesis for OATP1B1 ($p < 0.1$). Visual inspection of the estimated kernel densities [105] of the logarithmic mean values supported this, since two groups of individuals were monitored for OATP1B1, but the density of MRP2 was clearly normally distributed, as shown in Figure 3.6.

Thus, with regard to OATP1B1 the individual mean values were analyzed individually to examine which individual can be attached to which group (Figure 3.6). A clear separation into two groups of four and six individuals, respectively, was found. It should be noted that this separation of the OATP1B1 transporter activity was not an implicit property of the model structure, but emerged as a result during the Bayesian PBPK approach.

This grouping of individuals was compared to the different OATP1B1 genotypes, which is known to significantly influence PK. This consideration led to a clear separation of the two homozygous genotypes, which demonstrated the capability of the approach to give strong hints about the reasons for subgroup stratification, even when only little experimental data of a small population was available.

3.4 Discussion

In the present application example, the combined Bayesian PBPK approach was performed to assess the interindividual variability in ADME-related and drug-specific

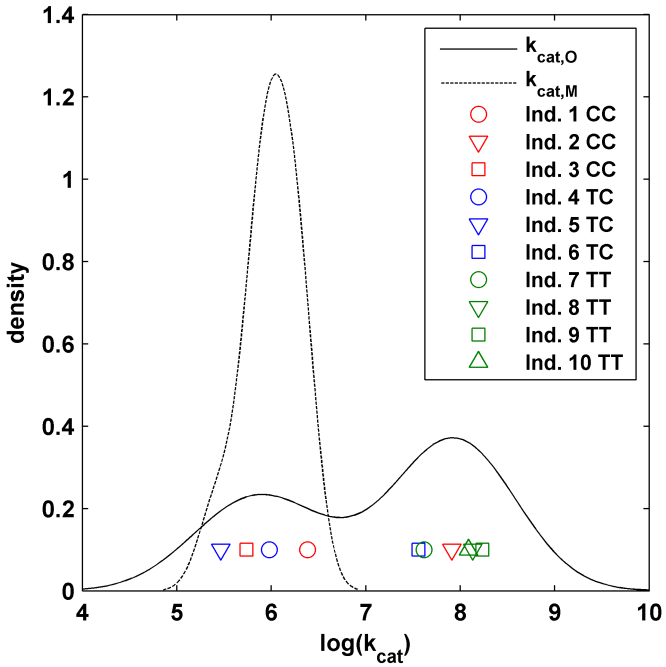

Figure 3.6: Identification and assignment of subgroups of individuals. A density estimation of the logarithmic mean values of the transporter activities for OATP1B1 and MRP2 supported the identification of specific subgroups of individuals. The logarithmic mean values of the transporter activities for MRP2 and OATP1B1 were calculated from the subsample of the posterior and the kernel densities were quantified. The density for OATP1B1 provided the separation into two groups, such that the single values were also plotted with symbols. Additionally, they were colored related to their specific genotype.

parameters. Based on the resulting high dimensional posterior distribution, individual uncertainty in PK behavior as well as an estimation of the interindividual variability in the PK of pravastatin was provided. Furthermore, an analysis at the parameter level revealed at least two subgroups in the population related to the transporter activity of OATP1B1. A comparison of the logarithmic posterior estimates showed that the subgroups can be approximately linked to different genetic predispositions of the individuals.

Overall the approach demonstrated the successful identification of the interindividual PK variability of pravastatin. However, an important process in pravastatin PK is enterohepatic circulation (Figure 3.1), which leads to a second peak in the PK profile due to gallbladder emptying. This process was not well described in the population, leading to a too broad PK range in the simulation (Figure 3.3a). Possible reason for this could be the small number of experimental data points, which hampered a correct identification of the time point of gall bladder emptying, even by visual inspection.

For the performed MCMC run, it was assumed that the population distributions of the physiological parameters were known, such that no population level was estimated in the approach. The individuals were created based on the prior knowledge integrated into the physiological database of the considered PBPK software tool [8]. Hence, interindividual variability in physiological parameters was integrated into the approach, however, it was assumed that unexplained interindividual variability can be neglected and all variability is explained by the covariate relationships to age, gender and BH. Such assumptions have also been made in other applications e.g. in the field of TK [36]. Furthermore, physiological parameters have not been varied at an individual level which constitutes that we assumed negligible uncertainty in physiological parameters compared to ADME-related parameters. The presumption of a known population variability was also made for definition of informed prior probabilities as defined in Table 3.2.

As convergence analysis, visual inspection was performed. In addition, it was checked if the results change significantly during growth of the Markov Chain. After 150,000 iterations overall results were robust such that the burn-in period was defined as the first 150,000 steps. Here, a methodological convergence analysis could be performed in future work, however, recent analyses approaches also have relatively high probabilities to fail [106].

The integration of a population level would improve the approach concerning its extrapolation capabilities. The consideration of the individual level allows for an estimation of the population based on 10 individuals. However, the identification of whole individual's and population's physiology and the integration of as much experimental data as possible would result in a more reliable identification of the population distribution. In our model this would lead to the identification of hundreds of parameters per individual and thousands of parameters for a large population. Due to computational restrictions we here chose only a population of 10 individuals and made the aforementioned assumptions on the populations physiology. Nevertheless, the varied parameters were chosen in a way such that all the important ADME processes were represented. Therefore, no different results would be expected on the PK level. However, the integration of more physiological param-

eters such as organ volumes could lead to a less clear information of parameters such as the enzyme activities. Here, a multidimensional analysis could be necessary to identify the subgroups, as the hepatic clearance process is described by liver volume as well as enzymatic capacity.

A concept for reduction of computational restrictions would be the parallelization of the individual MH blocks, which would reduce the computation time by the number of individuals if enough computational power is available. Notably, the presented concept is not constrained in its dimensionality, therefore also the investigation of large populations and hundreds of parameter is possible, which provides great opportunities for the assessment of interindividual variability in clinical trials.

The several MH blocks allowed the separation between individual parameters and global parameters and reduced the convergence time of the run, since each block could converge faster as if all parameters would had been varied in one large block. In following investigations, different algorithms such as adaptive approaches [44,107,108] could be tested to be able to further reduce convergence time or improve the mixing of the Markov chains.

Concerning the global parameters it has to be noted that such parameters have to be chosen very carefully, since they have by definition a large effect on all obtained individuals. In our application example, the *fu* was defined as a global parameter. Since it is also determined by the composition of the blood serum it can as such also be defined as individual parameter. However, the unbound fraction also depends on the lipophilicity of the drug, which is varied in our approach. Therefore, both parameters had to be sampled in the same MH block to consider the covariance between these parameters [73,102].

Advantages of using the highly-detailed mechanistic PBPK model were demonstrated by analyzing the example of pravastatin. Relationships between the physiological parameters were provided directly from the posterior and could be easily identified, for example a strong correlation was found between the enzyme activity of the MRP2 transporter and the intestinal permeability of pravastatin in all individuals. This results from a contrary transport of pravastatin in the gastrointestinal tract, because MRP2 transports pravastatin back into the intestinal lumen. Therefore, by the analysis of the posterior, structural information about the model can be inferred.

Furthermore, beside the derivation of structural information about the PBPK model the identification of clinically-relevant subgroups within the population was demonstrated. By investigating the logarithmic mean values of the single individuals with a Shapiro-Wilk test the assumption of more than one homogenous group was confirmed for OATP1B1. Additionally, the two groups of individuals were assigned to different homozygous genotypes. This demonstrates the ability of our approach to make physiological inferences with very little prior information and only few individuals. The heterozygous genotype could not be assigned to an own group. However, Niemi et al. also showed that a significant separation of the heterozygous genotype is not possible [100]. Notably, the separation of different subgroups itself may also be possible with smaller models. However, the use of a mechanistic PBPK model can point out the relation between subgroup and genotype which makes our Bayesian PBPK approach a suitable alternative to rather phenomenological

methods [109].

Chapter 4

Identification and characterization of interindividual variability in physiological-realistic parameters

In this chapter we present an application example of the presented Bayesian population PBPK approach for the identification and characterization of interindividual variability in physiologically realistic parameters [11]. Beside assessment of the interindividual variability in theophylline PK, the objective is to compare resulting population simulations using previous methods and our approach. We thereby infer population distributions for ADME parameters in the model as well as physiological parameters. Furthermore, the consideration of the dependency structure of the high dimensional parameter space accounts for the co-variability of physiological properties within the population.

As a second objective, we evaluate the performance and resulting posterior distributions of the new adaptive MCMC sampling as described in Section 2.5.3 compared to the MH approach.

Section 4.1 describes the background, available data and specific ADME processes that were integrated into the model. Section 4.2 illustrates the chosen setting of the Bayesian population PBPK approach including an overview of the selected parameters and defined start values. Section 4.3 presents the results related to interindividual variability. Section 4.4 describes the results after using the new adaptive MCMC approach, followed by a discussion in Section 4.5.

4.1 Theophylline: background, data and model

We here considered the PK of theophylline, a methylxanthine drug that acts against asthma and chronic obstructive pulmonary disease. Individual dosings are considered in theophylline therapy due to large interindividual variability. Thereby, the sources of variability vary widely and no clear relationship to classical covariates like age, gender or BW can be observed. In addition, a variety of other factors influence theophylline PK such as e.g. different diseases [110–113]. A free available theophylline dataset [114] was taken to demonstrate the abilities of our approach (the data is accessible in the software environment “R” as “theoph” data frame).

It consists of 11 theophylline venous blood samples for each of 12 individuals together with the administered doses and the BWs of the individuals. In addition, one data point for the fraction of unchanged theophylline in urine after 36 hours was considered [112]. An individual PBPK model was created for each of the 12 individuals. Since no age or height was stated in the dataset, it was assumed that all individuals are 30 years old, but differ in BH. BH was randomly chosen such that BMI is in normal ranges (in between 19 and 25). This assumption indicates a very homogenous group of individuals simulating e.g. a first in man study of a new drug. Table B.1 shows the anthropometry and related administered dose together with appropriated BH. Two clearance processes were integrated into the model, hepatic metabolization via cytochrome P450 1A2 and a renal excretion process [112]. For both clearance routes a first order process was considered in the PBPK model.

4.2 Statistical computation

To identify reasonable start parameters for our investigation, a parameter identification process was performed for a mean value model to identify a good guess for the specific clearance rates and the intestinal permeability, which is an important parameter defining the absorption of the drug. For the drug-specific parameters literature information was used to define reasonable start values. The physiology was specified using the respective entry of the integrated physiological database of the PBPK modeling platform PK-Sim [8,56]. All in all, 40 parameters which define the individual physiological and global drug-specific parameters, respectively, were varied in the approach (Table B.2). The full Bayesian population PBPK approach was considered as described in Chapter 2, including the individual and the population level. Thus, each individual parameter was assigned two population parameters, the population mean and the population standard deviation, respectively. Blockwise sampling was performed as described in Section 2.4.2. For each type of experimental data, a measurement error was considered. Thereby, the error for the venous blood samples was also varied, while the variance of the measurement error for urinary excretion was set to an assumed fixed value of 5%, since only one data point was available. Due to 12 individuals considered, this resulted in 535 parameters that were identified in the approach. The proposal density was chosen as defined in Equation 2.38, whereby independent standard deviations were considered. Several pre-runs were performed to adapt the proposal densities which are critical for a good performance of the MCMC approach. After each pre-run, the proposal densities and the start values of all parameters were adapted. The start values were defined as the last sampled parameter of the previous run. The standard deviation of the proposal densities were defined as a proportion of the standard deviation of the previous posterior sample chain. In our final MCMC run, a posterior sample of about 1,000,000 iterations was created. A burn-in period of 200,000 parameter samples was cut off since after 200,000 iterations convergence of the posterior chain could be assumed by visual inspection and determination of Gelman and Rubin convergence criterion ($\hat{R}$) [106,115]. Since our MCMC approach consists of one long run but the calculation of $\hat{R}$ requires at least two chains, we split our chain into two chains with equal length and calculated $\hat{R}$. Table B.3 shows the obtained values for

for important parameters. From the remaining 800,000 samples, a subsample of 500 parameter vectors was drawn to derive an independent subsample of the posterior.

4.3 Results

Individual-specific model simulations

As a qualification of the individual level model and the structural properties of the PBPK model, individual simulations were performed out of the posterior sample and compared to the experimental data. Figure 4.1 shows the individual PK behavior for all individuals in linear scale, Figure A.3 depicts the individual PK behavior in semi-log scale. The PBPK model was parameterized one after another with all of the 500 posterior subsamples and the PK was simulated. The 95% confidence interval for the PK is shown together with the experimental data and the mean value curve. Except for individual no. 10, the PK behavior is described well and all experimental data points can be described by the full model including the inferred measurement error (Equation 2.4). Individual no. 10 seems to have a much slower absorption of the drug which can be related e.g. to a tablet which does not dissolve completely. Such effects cannot be described by our model.

In addition, Figure 4.2 shows the mean simulation at time points of the observed data versus the observed data for a better visual inspection of the quality of the fit.

Inference on parameter level

The Bayesian inference that is generated with the Bayesian population PBPK approach is represented by the high dimensional posterior distribution of all parameters. Simulations and extrapolations on the PK level can only be performed by using high dimensional samples of the posterior. However, the consideration of marginal parameter distributions is an appropriate instrument to illustrate parameter inference. Figure 4.3 shows the marginal posterior population distributions based on the posterior estimates for the population mean value and the population standard deviation for nine exemplary parameters: the intestinal permeability (intP), the specific hepatic clearance rate (CLspec), the specific tubular secretion rate (TSspec), the gastric emptying time (GET), the intestinal transit time (ITT) and four organ volumes. The truncated distributions were generated by consideration of the mean value of the hyper distributions for the posterior population mean value and population standard deviation which represent the posterior estimates of the population distribution. Truncation was applied to account for the previously defined physiological constraints in Table B.2.

The marginal posterior distributions were then compared to the prior distributions. The prior distributions were generated equivalent to the posterior distributions. The comparison, as also shown in Table 4.1, reveals shrinkage of the CV in most parameters. However, the CV of intP increases significantly. GET and ITT both increase in their mean value, indicating that the examined population has a delayed and prolonged residence time in comparison to previous studies. It can be further observed for GET and ITT, that the absolute physiological constraints as defined in Table B.2 restrict the obtained population distribution. IntP, CLspec

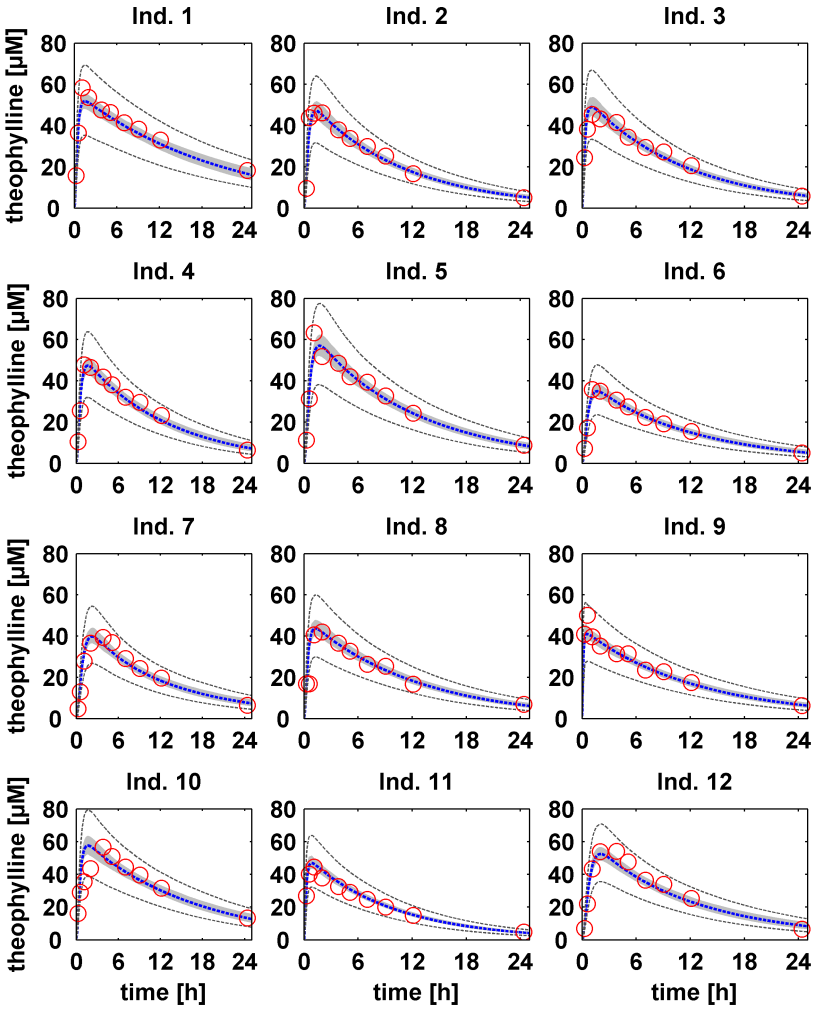

Figure 4.1: Individual-specific model simulations. For each of the 12 individuals the PBPK model was parameterized and evaluated with each of 500 individual and independent parameter vectors out of the posterior distribution. The 95 % confidence interval of all simulations (grey area) is shown together with the mean value curve (blue dotted line) and the experimental data (red circles). Dark grey dotted lines depict the upper and lower bound of the 95 % confidence interval of all simulations including the inferred measurement error under consideration of the proportional error model as described in equation 2.4.

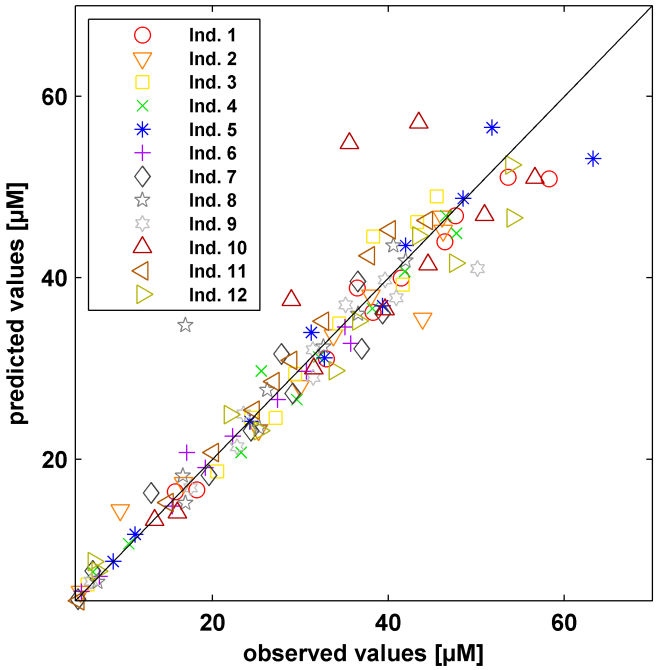

Figure 4.2: Comparison of observed experimental data and simulated values. Mean simulated values are plotted against the observed data at the same time points for all individuals.

and TSspec show a decrease in the posterior geometric mean value compared to the prior. However, it has to be noted that for these three parameters uninformed hyper prior distributions were considered for the population mean value and therefore the prior value of the population mean value was set to the middle of the interval of the hyper prior.

The uncertainty of the hyper level is often not assessed in Bayesian analyses using hierarchical models. However, Table 4.2 demonstrates how the CVs increase when including the uncertainty of the population mean value and the population standard deviation instead of consideration of the prior and posterior estimates. Especially the hyper prior distributions which were vague e.g. for intP, CLspec and TSspec cause a large variability in the population distributions.

A correlation analysis was performed to investigate possible dependencies in the high dimensional posterior population distribution. As described in Section 2.6.2 in Equations 2.51 and 2.52, the random effects include possible dependencies of parameters within the population. Consistent with the determination of the covariance matrices in Equation 2.52, the correlation matrix of all random effects was calculated between the individuals to estimate the dependency of individual parameters within the population. To account for the uncertainty within this analysis, the correlation matrix was calculated for each of the 500 subsamples out of the posterior distribution. Figure 4.4 shows the distribution of correlations between exemplary parameters. In particular, a significant mean negative correlation of about 70% ($p < 0.05$, mean confidence interval [-0.85 -0.49]) between TSspec and kidney volume can be obtained. The other three exemplary distributions do not have significant mean correlations; however, a mean positive correlation of about 30% ($p > 0.05$,

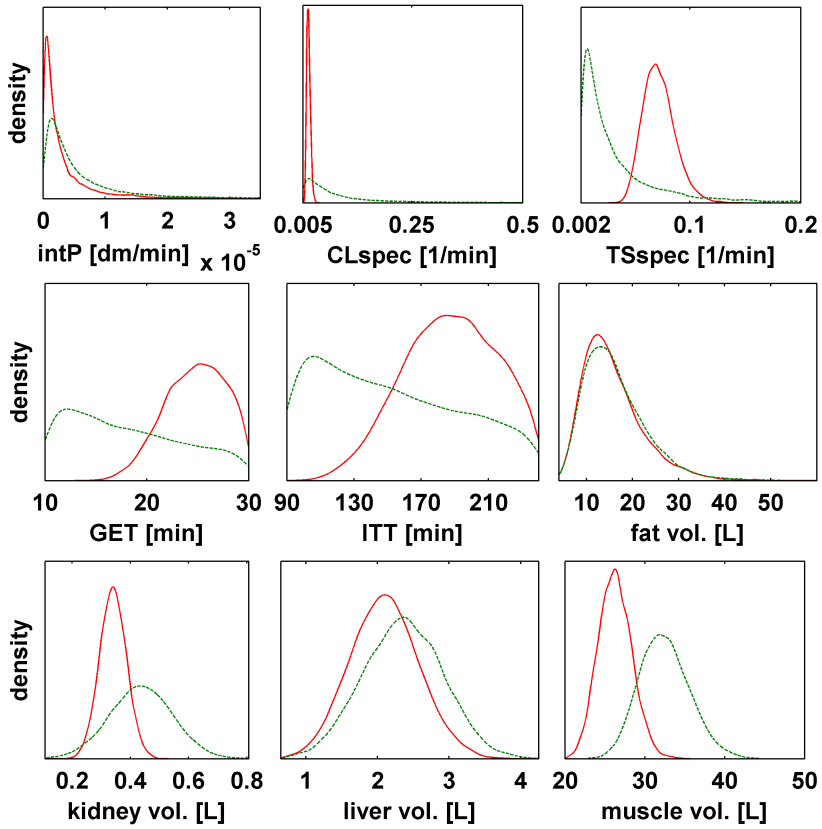

Figure 4.3: Comparison of marginal prior and posterior distributions of nine exemplary physiological parameters. For each parameter, the marginal posterior density estimate (red line) is compared to the corresponding prior distribution (green dotted line). Limits on x-axis represent physiological constraints as defined in Table B.2 (except for intP where the maximum x value was reduced by a factor of 10 for better visualization).

Table 4.1: Comparison of prior and posterior mean values and coefficients of variations for nine exemplary physiological parameters when taking only maximum posterior estimates into account. The uncertainty in the mean value and standard deviation of the population distribution was therefore not considered.

parameter	**prior estimate**		**posterior estimate**	
	mean val.	**CV [%]**	**mean val.**	**CV [%]**
intP [dm/min]	3.55E-06	172	1.70E-06	213
CLspec [1/min]	0.05	138	0.017	24
TSspec [1/min]	0.02	139	0.071	20
GET [min]	17.26	32	24.57	12
ITT [min]	146.22	29	185.33	16
fat vol. [L]	14.94	42	14.51	42
kidney vol. [L]	0.44	25	0.34	13
liver vol. [L]	2.36	23	2.097	23
muscle vol. [L]	32.33	10	26.2	8

Table 4.2: Comparison of prior and posterior mean values and coefficients of variations for nine exemplary physiological parameters taking all assessed information into account.. The population distribution is based on the prior and posterior distributions of the hyper parameters including the assessed uncertainty in the mean value and standard deviation.

parameter	**prior estimate**		**posterior estimate**	
	mean val.	**CV [%]**	**mean val.**	**CV [%]**
intP [dm/min]	3.68E-06	2843	1.76E-06	221
CLspec [1/min]	0.05	204	0.017	26
TSspec [1/min]	0.02	206	0.071	30
GET [min]	17.25	31	24.45	14
ITT [min]	146.41	28	184.57	18
fat vol. [L]	14.98	65	14.47	46
kidney vol. [L]	0.44	30	0.34	25
liver vol. [L]	2.36	28	2.1	30
muscle vol. [L]	32.099	26	26.27	11

mean confidence interval [-0.31 0.70]) can be obtained between CLspec and TSspec. No further significant correlations could be found after performing a complete analysis of all possible individual parameter combinations (results not shown). Notably, such correlations are derived despite the prior assumption of independent random effects as defined in Equation 2.8. Furthermore, the distinction between individual level and population level is important for the correct meaning of parameter correlations. For population simulations, parameter correlations along individuals are important since such correlations need to be included for the parameterization of a new individual. For model characterization, the aforementioned correlations of individual parameters along the samples of the Markov chain are important. For example, a significant positive correlation of about 42% can be identified for intP and GET ($p < 0.05$) along the autocorrelation-free samples. Such dependencies denote an essential part of intraindividual uncertainty and need consideration when simulating individual PK profiles as demonstrated in Figure 4.1.

Visual predictive check of population pharmacokinetics

Next, a visual predictive check (VPC) was performed to investigate the quality of simulations using the posterior distribution of the population parameters [116]. The VPC diagnoses the fixed effects as well as the random effects by calculating the CI of the median and the 5% and 95% percentile of a large amount of simulations of the experimental setting. This was important to interpret objectively if the simulations with the posterior results describe the data well.

For each individual, 500 parameters sets were randomly drawn from the posterior population distribution and the population simulation approach of Section 2.6.2 was applied. Thereby, no new individuals were simulated, instead, the 12 integrated individuals were recreated with the new *a posteriori* parameter sets. For the VPC, all 12 individuals were then simulated and evaluated for each subsample, successively. Next, median and 5% and 95% percentiles were calculated for

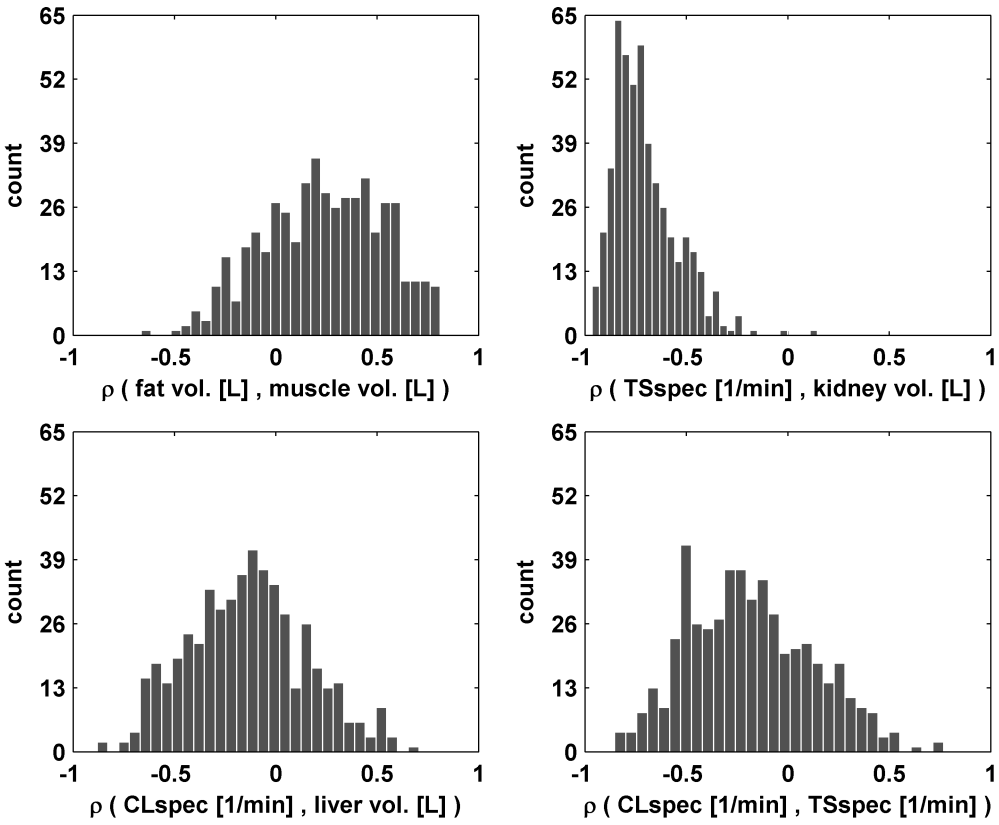

Figure 4.4: Exemplary representation of derived distributions of correlation between the population parameters. The correlation of a pair of parameters along all individuals was calculated for each of the 500 subsamples of the posterior distribution. For each pair of parameters the histogram of all correlations is shown, representing the variability of the respective correlation.

each subsample simulation. Finally, the 95% CI is determined for the 500 curves of medians and percentiles, quantifying the uncertainty in the predictions.

Figure 4.5a depicts the resulting 95% CIs for the median and the 5% and 95% percentiles. For this VPC, the posterior population distribution was created from the posterior estimates of the population mean values and the population standard deviations (see also Table 4.1). In addition, the experimental data together with the corresponding median and percentiles are illustrated. The CIs describe the experimental data very well and with small uncertainty, especially in the mean value. However, the 95% CI slightly underestimates the elimination phase compared to the experimental data.

A second VPC was performed in Figure 4.5b, where the posterior population simulation was estimated considering the full uncertainty of the hyper parameters (see also Table 4.2). It can be observed that the CI of the 5% and 95% percentiles increase, especially the 5% CI shows large uncertainty. The CI of the mean value is in good agreement with the experimental data.

A third VPC was then performed using the population PBPK approach of Willmann et al [8] to compare against the VPCs using the presented Bayesian population PBPK approach. Here, the parameter distributions which need to be considered for the approach consist of the prior knowledge that was integrated into our population PBPK approach. For the three uninformed parameters intP, CLspec and TSspec a lognormal distribution with a geometric standard deviation of 1.5 was considered. That should provide reasonable values regarding to the literature [117,118]. The mean value was assumed to be the respective parameter value of the adjusted mean value model. The resulting confidence intervals are shown in Figure 4.5c and show considerably different results. Especially in the terminal phase (time $>$ 12 h), the confidence interval of the 95% percentile is much wider than the one in Figure 4.5a or 4.5b. More variability can also be observed when comparing the confidence intervals of the median. With regard to the experimental data, the simulated confidence interval of the 95% percentile overestimates the 95% percentile of the experimental data. The confidence interval of the median overestimates the data in the absorption phase but fits the experimental data well in the elimination phase.

4.4 Improving performance by adaptive sampling

A drawback in the recent MCMC runs are bad mixing properties of the Markov chain in some parameters. This results in large autocorrelation of the chain and prolongs the run time of the approach, since a very large amount of parameter vectors has to be sampled. For example, this led to sampling of 1,000,000 steps in the run presented above. The main reason for the bad mixing properties is the defined scaling of the proposal density in Section 4.2: After each pre-run, the proposal density for the next run was determined from the posterior variance of the pre-run.

In order to improve this manual process we here present the results of our combined adaptive MCMC sampling approach based on the mMALA [43] and the SCAM approach, respectively [44,58]. The implementation of the approach was already described above in Section 2.5.

With the described combined mMALA/SCAM approach of Section 2.5.3, a new

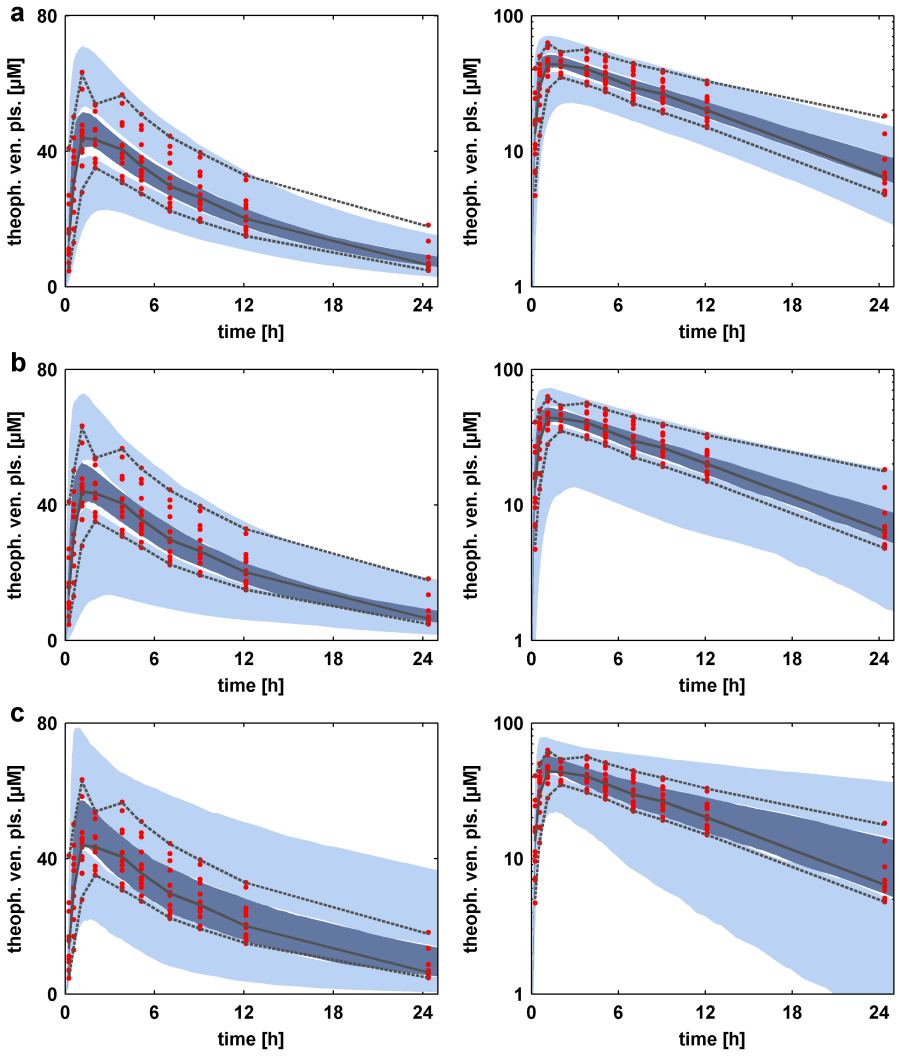

Figure 4.5: Comparison of visual predictive checks (VPCs) of population simulations. (a) VPC of the PK behavior using the posterior distributions based on posterior estimates of the population parameters. (b) VPC of the PK behavior using the posterior distributions based on the population parameters including their uncertainty. (c) VPC of the PK behavior using the prior distributions of all parameters [8]. Each VPC is presented in linear scale (left) and logarithmic scale (right). The VPCs were performed as described in the text. In each VPC, the 5% and 95% percentiles (black dotted lines) and the median (black line) of the experimental data (red dots) are compared against the 95% confidence intervals of the 5% and 95% percentile of the simulation (light blue area) and the median (blue area).

MCMC run was performed and 200,000 parameter samples were generated. For the adaptation of σ_P^j we chose $n_{eq} = 5,000$ and $f_{up} = 500$. Furthermore, a new MCMC run was performed with the standard MH proposal for comparison. Both runs started from the identical starting condition. After discarding the first 50,000 iterations as burn-in, analyses of convergence, acceptance rate and autocorrelation are considered to compare the performance of both runs by using a sample of 10,000 iterations out of the remaining 150,000 samples.

Table 4.3 shows the respective values for autocorrelation and convergence. Convergence was determined as $\hat{R}$ as described in Section 4.2 and Table B.3. The MH-based run shows significantly larger values for $\hat{R}$ compared to the mMALA/SCAM run. At perfect convergence all values should be equal to 1. $\hat{R}$ values for the mMALA/SCAM run indicate full convergence of the run, while several parameters are not converged in the MH run, indicating that the full run has not been reached convergence, yet. Furthermore, autocorrelation is four times higher in the MH run, indicating inferior mixing properties.

Figure 4.6 shows the development of the acceptance rate for both, the MH and the mMALA/ SCAM run, for three exemplary individuals. For each iteration n, the acceptance rate was calculated based on the sequence of $1 \dots n$ iterations. The three individuals chosen out of the MH run show different acceptance rates also after 20,000 iterations. Thereby, especially the acceptance rate of individual 3 is around 50% which accounts for a lower efficacy of the sampling than in the other individuals. Here, further tuning of the proposal standard deviation and restart of the MCMC run would be necessary to obtain an equal sampling quality for all individuals.

In contrast, the acceptance rates for the three individuals in the mMALA/SCAM run start to adapt their proposal standard deviation after $n_{eq} = 5,000$ iterations as described above. After 20,000 iterations and $20,000/f_{up} = 40$ updates of the proposal standard deviations, they are already converged to an acceptance rate around 20% which fits well in light of the optimal acceptance rate of 23.4% [84].

In contrast to an improved performance, the overall results should not differ significantly. Figures A.4 and A.5 show the individual model predictions according to Figure 4.1. Furthermore, Figure 4.7 compares the VPC of the MH approach using pre-runs and fixed proposal densities per run with the new adaptive mMALA/SCAM approach. Figure 4.7a shows the VPC of the MH run, Figure 4.7b the VPC of the mMALA/SCAM run. It can be demonstrated, that both figures show the same overall result.

Regarding the parameter level, a comparison of the distribution of correlations reveal an even sharper distribution of the correlation between TSspec and kidney volume for the mMALA/SCAM (mean negative correlation of 74%, $p<0.05$) run than the distributions of the old (mean negative correlation of 70%, $p<0.05$) and new MH (mean negative correlation of 62% $p<0.1$) runs (see Figures A.6, 4.4 and A.7, respectively).

Table 4.3: Performance comparison of MH and mMALA/SCAM algorithms. Analyses have been performed for each run using the same sample of 10,000 iterations out of all 150,000 iterations which remain after discarding the first 50,000 iterations as burn-in period.

parameter	**type**	$\hat{R}$		**autocorrelation**	
		MH	mMALA/ SCAM	MH	mMALA/ SCAM
intP	individual	1.070	1.011	475	114
CLspec	individual	1.060	1.001	560	324
TSspec	individual	1.390	1.047	1236	581
GET	individual	1.104	1.008	502	149
ITT	individual	1.007	1.003	170	112
plasma protein SF	individual	1.061	1.004	354	105
logP	global	1.120	1.022	647	277
fu	global	1.036	1.023	96	305
fat vol.	individual	1.015	1.036	536	175
kidney vol.	individual	1.306	1.008	1116	516
liver vol.	individual	1.022	1.012	259	82
muscle vol.	individual	1.016	1.029	415	175
CLspec x liver vol.	individual	1.021	1.017	201	158
TSspec x kidney vol.	individual	1.085	1.013	369	287
intP	population	3.391	1.008	2620	111
CLspec	population	1.169	1.000	2420	316
TSspec	population	4.126	1.034	2373	555
GET	population	1.007	1.000	397	58
ITT	population	1.001	1.001	331	124
plasma protein SV	population	1.014	1.000	125	69
fat vol.	population	1.001	1.033	451	169
kidney vol.	population	1.383	1.003	1033	508
liver vol.	population	1.005	1.016	457	81
muscle vol.	population	1.004	1.038	508	182
CLspec x liver vol.	population	2.296	1.052	1757	542
TSspec x kidney vol.	population	1.082	1.012	563	226
largest value		**4.126**	**1.052**	**2620**	**581**

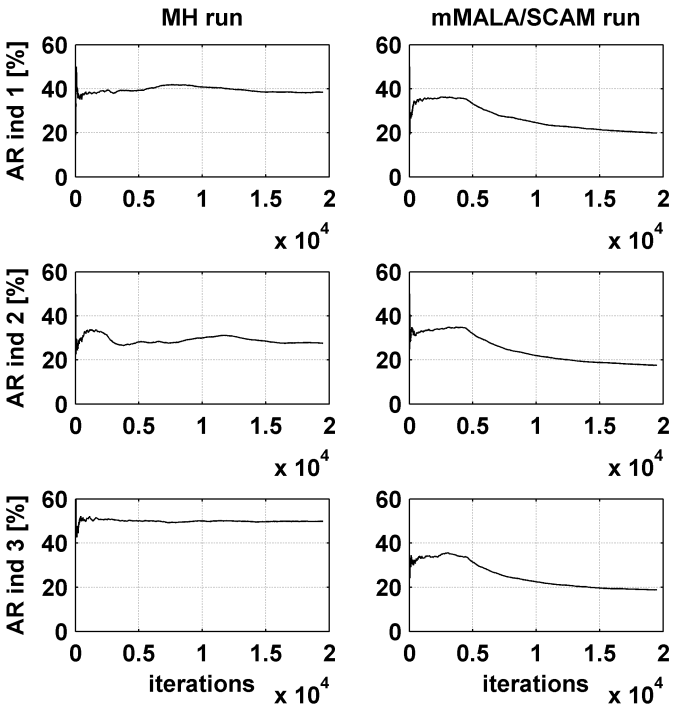

Figure 4.6: Development of acceptance rates during MH and mMALA/SCAM run for three exemplary individuals. Left column shows MH run and right column shows mMALA/SCAM run.

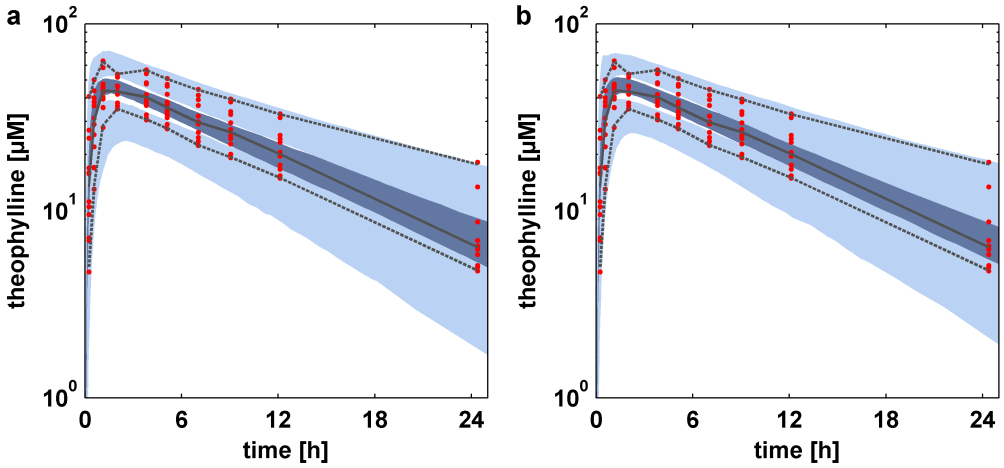

Figure 4.7: Comparison of VPCs using standard MH and the combined mMALA and SCAM algorithm. (a) Standard MH algorithm. (b) New combined adaptive algorithm. For further explanation of the legend please refer to Figure figure 4.5 on page 84.

4.5 Discussion

The application example simulating theophylline PK revealed the variety of information that can be obtained by using the Bayesian population PBPK approach. As a first result, individual-specific simulations under consideration of assessed parameter uncertainty described the experimental data in good agreement and with little uncertainty on the PK level. Such information can be considered e.g. to identify possible heterogeneities in the population or even to identify subgroups related to genetic or physiological differences or diseases [10], as also demonstrated within the first application example in Chapter 3.

Furthermore, a comparison of marginal population distributions of the posterior and the prior distributions demonstrated which information can be inferred from the experimental data. Since the experimental data represented the PK of a very homogeneous population with respect to their physiology, several population parameter distributions showed a decrease of their variance. Additionally, changes in the mean values indicated a different behavior of the drug, for example in the absorption processes. In particular, theophylline seemed to be absorbed more slowly, which was represented by prolonged GET and ITT. A possible reason could be that the individuals have not been in fasted state during the experimental investigation. Moreover, the posterior population distributions of the organ volumes suggested a lower average BW of the individuals, since e.g. the mean muscle volume decreases and BW is composed of the organ volumes in the PBPK model [8].

However, simple observation of the marginal distributions is insufficient to thoroughly analyze the posterior distribution. Only the investigation of the complete high dimensional posterior distribution provides the full information, at least if the prior assumption of independence between parameters cannot be assumed anymore. The distributions of correlations in Figure 4.4 indicated that the assumption of independence between the parameters does not hold and information about the model and the physiology of the population can only be described by the complete multivariate posterior. This can be seen as a natural consequence of incorporation of a physiologically-realistic PBPK model into the Bayesian framework, since effective parameters like a total clearance rate are divided into physiological relationships of e.g. catalytic constants of enzymes and the corresponding volume of an organ. However, it has to be noted though that large uncertainty could be observed on the estimated correlations. A possible reason could be the small sample size of 12 individuals that were considered for the determination of the correlations. Here, investigations that integrate a larger population would deliver more precise results regarding the correlations.

The findings of a dependent multivariate posterior distribution were further supported by the VPCs (Figure 4.5). The use of independent prior information of the parameters led to a too large interindividual variability and would provide vague information about the PK behavior of theophylline in a homogeneous population. The Bayesian population PBPK approach provided a smaller interindividual variability especially in the mean value, and the shape of the intervals was in better agreement with the experimental data. Hence, the VPC also served as a validation for the estimated high dimensional posterior distribution of the population parameters.

The comparison of a VPC based on the maximum posterior estimate and the

VPC based on the full posterior information revealed the influence of parameter uncertainty at the population level. Due to the small population that was investigated in our application, large uncertainty is expected in the identified distributions of population parameters. Such uncertainty should also be taken into account in model extrapolations; otherwise the extrapolations would underestimate the interindividual variability. Nevertheless, for validation of our approach, the maximum posterior estimate appropriately demonstrates the successful estimation of the population distributions.

Notably, the assumption of a multivariate normal distribution for the estimation of the dependency structure of the random effects could also be crosschecked against other dependency structures, such as copulas [119]. However, we do not expect large variations in the effect of different dependency structures, since only one significant correlation was identified and all correlations were subject to large uncertainty. Nevertheless, the analyses revealed the existence of correlations between population parameters.

In classical population pharmacokinetics approaches (PopPK), various additional covariates are tested during model identification, such as BW or creatinine clearance [54,120]. In this work we used an approach by Willmann et al. [8], where age, gender and height were chosen as covariates to create a large physiological database. We used this database for definition of our prior distributions and to implement the covariate approach. This is in line with de la Grandmaison et al. [121], who demonstrated that the organ weights were better correlated with body height than with BMI or BW. However, other approaches show contrary results and could be tested in future studies to use e.g. lean body mass as covariates [70]. For the theophylline dataset used in our approach, in a PopPK approach Tornøe et al. [110] showed that BW is no significant covariate, however, BW has also been shown to be a covariate of e.g. clearance of theophylline in markedly obese patients [122,123].

The use of a standard MH proposal density with a fixed standard deviation led to a poor performance of the MCMC run. A sample of 800,000 iterations was needed to create an independent sample of the posterior and convergence was achieved only after 200,00 iterations. Furthermore, the acceptance rates of individual and population parameters were bad, such that the mixing of the Markov chain was insufficient, especially for the population parameters. However, poor performance of the MCMC run does not mean a bad identification of the parameter space and the interindividual variability of the PK behavior. Robustness of the results could be assumed since several checks of the posterior results after e.g. 400,000 or 600,000 iterations showed similar results as the ones illustrated above (results not shown). Nevertheless, the long computation time and the efficiency of the MCMC sampler should be improved for faster convergence, better mixing and more reliable results on the parameter level, especially for the application of the approach to later clinical studies of phase II or III, where up to thousands of patients would be included.

Therefore, other MCMC samplers were considered to improve the performance of the Bayesian population PBPK approach. Thereby, a possible approach should be efficient in time and should be able to cope with the PBPK model structure. One of the most efficient sampling methods is the mMALA approach as described in Section 2.5.2. However, in case of numerical determination of the derivatives,

it can become inefficient due to increasing computation times. Therefore, we considered a combined approach of mMALA sampling and the SCAM approach. One advantage of our approach is that no further proof of successful convergence to the stationary distribution is needed anymore, since the basic approaches are already well established. However, the combination of both approaches and the application to the population level are new.

Notably, the PBPK structure and the different types of parameters in the hierarchical model were well suited for the consideration of different adaptive approaches. The acceptance criterion for parameter sampling at the population level is only dependent on the prior distribution and does not need a calculation of the likelihood. Hence, for application of the mMALA approach, analytic derivations of the prior distributions could be considered. Haario et al. [44] showed that SCAM can be easily applied in very high dimensional examples, such that this approach was chosen for the individual and global parameters. In particular, we used SCAM within our specified block structure, such that acceptance of sampled parameters was performed for each block and not for each parameter, separately. However, the adaption step was performed for each parameter itself. Although SCAM ignores the adaptation of an underlying dependency structure in contrast to other approaches such as the AM from Haario et al. [58], we decided to consider SCAM, since the posterior dependency structure could be estimated from the posterior distribution as described in Section 2.6.2.

Few assumptions were integrated into the overall computation, such as adaption of only the diagonal entries of the covariance or using mMALA with constant curvature. Notably, these assumptions affect only the performance of the approach such that it is possible to use such simplifications for better applicability with large and complex model structures and large numbers of parameters [43].

The obtained results of the adaptive mMALA/SCAM approach showed a largely improved performance compared to the standard MH approach. The comparison run with standard MH was clearly not yet converged, such that more iterations would be needed or probably more tuning steps should be performed to manually adapt the proposal standard deviations.

The comparison of posterior results such as the VPC or the correlations demonstrated that the new adaptive mMALA/SCAM approach provided the same findings as the standard MH before. The VPC of mMALA/SCAM showed less uncertainty in the interindividual variability, which is, however, also the case for the new standard MH run. This is therefore no effect of the new algorithm, but is due to different starting conditions and sharper prior distributions for the population parameters.

Chapter 5

Prediction of drug pharmacokinetics in clinically-relevant populations using a translational learning approach

In this chapter, the objective is to apply translational learning as described in Section 2.7 to predict drug PK in a specific patient population based on physiological and physicochemical information acquired before in several applications of the Bayesian population PBPK analysis [12]. The approach is applied on clinical data from a specifically-designed study program [124]. In brief, Midazolam PK in healthy individuals and obese patients as well as torsemide PK in healthy individuals is used to identify physicochemical and physiological distributions of PBPK model parameters. The acquired information is then used to predict torsemide PK in a population of obese patients.

In Section 5.1, results of the clinical study are presented, Section 5.2 describes background and model building of the two considered compounds midazolam and torsemide. Section 5.3 introduces the chosen prior distributions and parameters of the Bayesian population PBPK approaches and Section 5.4 presents the achieved results, followed by a discussion in Section 5.5

5.1 Clinical study

The translational learning approach was applied to a clinical study in healthy volunteers on the one hand and obese to morbidly obese patients on the other hand. Both cohorts were administered a cocktail of six marketed drugs (midazolam, torsemide, talinolol, pravastatin, codeine and caffeine) at sub-therapeutic doses [124]. The drugs in the cocktail were selected because each of them is dominantly cleared by a single enzyme or transporter-mediated pathway thereby excluding the occurrence of drug-drug-interactions. In our analysis, we focused on midazolam and torsemide since the metabolization scheme of these two compounds has a comparable com-

Table 5.1: Anthropometric information of both the cohort of healthy individuals and the cohort of diseased individuals

	n	**male [%]**	**age [years]**		**body weight [kg]**		**body height [cm]**		**body mass index**	
			median	[min max]	median	[min max]	median	[min max]	median	[min max]
healthy	103	52.4	28	[18 56]	74.5	[48.5 113]	174	[154 194]	23.5	[18.8 32.3]
diseased	79	41.8	45	[20 77]	138	[52 206]	175	[156 192]	47.3	[19.7 67.1]

Table 5.2: Summary of weight normalized PK parameters of midazolam and torsemide data

	healthy geo. mean	CV [%]	**diseased** geo. mean	CV [%]	**p-val**
midazolam cmax [μmol/l/kg]	0.00017	50	0.00011	76	<1e-5
torsemide cmax [μmol/l/kg]	0.0011	33	0.00045	62	<1e-21
midazolam AUC [μmol*min/l/kg]	0.018	77	0.012	93	<1e-5
torsemide AUC [μmol*min/l/kg]	0.13	62	0.049	78	<1e-21

plexity. In the clinical study, plasma samples from 103 healthy individuals and 79 obese to morbidly obese patients were taken and analyzed. The anthropometry of the individuals and patients are summarized in Table 5.1. The main difference between the two cohorts is BW, where the median is 74.5 kg and 138 kg, respectively. Summary statistics of important PK parameters are shown in Table 5.2. While non-normalized PK parameters are apparently similar for both healthy volunteers and patients (data not shown), analysis of maximum concentration (C_{max}) and area under curve (AUC) revealed a significant negative correlation of PK parameters with respect to BW (Figure 5.1a). Due to this dependency on BW, the PK analyses of Table 5.2 were performed weight-normalized. Significant differences between the healthy and the diseased PK data were obtained for both midazolam and torsemide for C_{max} and AUC, respectively, as also illustrated in Figure 5.1b. Further analyses of the diseased population revealed significant correlations between BW and fatty degeneration of the liver. A positive correlation was also revealed between the nonalcoholic steatohepatitis (NASH) score and BW, which showed that BW is a strong indicator for pathophysiological conditions (Figure 5.1c). The NASH score sums up the grade of fatty degeneration, inflammation and fibrosis. An analyses of the fractions of individuals that show strong fatty degeneration or a high NASH score (Figure 5.1d and e) revealed that although only 7% of the patients have high fatty degeneration, 25% show a NASH score larger than 3, indicating that many individuals have other diseases than fatty liver alone.

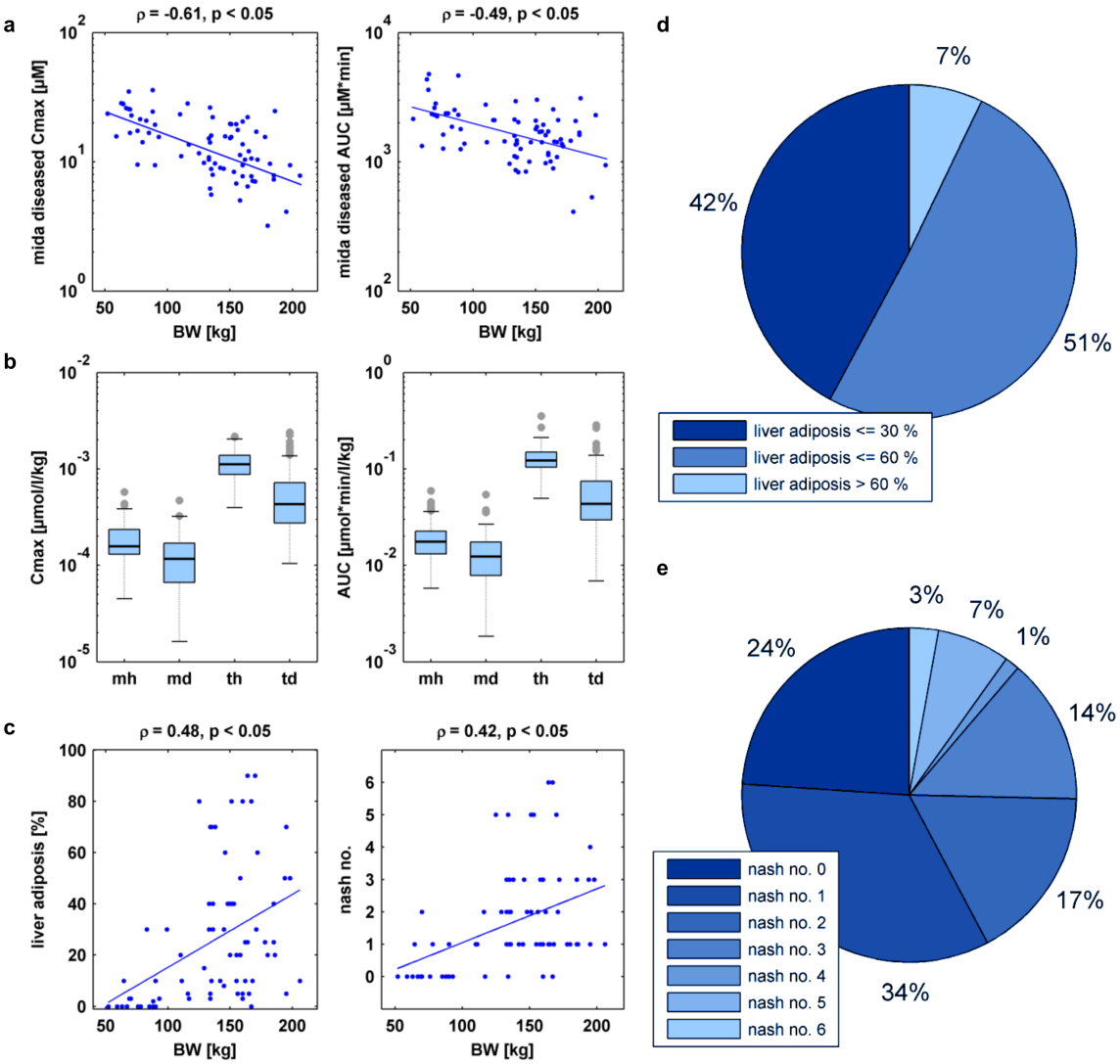

Figure 5.1: Results of the clinical study regarding patient properties and experimental data of midazolam and torsemide in healthy and diseased individuals [124]. (**a**) Correlation analyses regarding weight of individuals. Scatter plots together with the linear regression line are shown comparing the C_{max} (left panel) and the AUC (right panel) of the experimental data for midazolam (mida) in diseased individuals versus body weight. Correlation coefficients ρ are shown above both subfigures together with the corresponding p-values. (**b**) Boxplots of C_{max} (left panel) and AUC (right panel) from healthy individuals and midazolam (mh), diseased individuals and midazolam (md), healthy individuals and torsemide (th) and diseased individuals and torsemide (td) are compared against each other. Black line represents the median, the edges of the box are the 25th and 75th percentiles, the whiskers extend to the most extreme data not considered outliers, and outliers are plotted individually. (**c**) Correlation analyses regarding the diseased state of the patients compared to body weight. Scatter plots together with the linear regression line are shown comparing the fatty degeneration of the liver (liver adiposis) and the NASH score of the experimental data for each individual with the respective body weight. Correlation coefficient ρ together with the corresponding p-value are depicted above both subfigures. (**d**) Pie chart representing the fractions of individuals with liver adiposis below 30%, between 30% and 60% and above 60%. Color code is present in the legend in the figure. (**e**) Pie chart representing the fractions of individuals with different NASH scores between 0 and 6. Color code is present in the legend in the figure.

5.2 Model building

Midazolam

Midazolam is a benzodiazepine derivative which is mainly used as sedative. It is almost exclusively metabolized via cytochrome P450 3A4 (CYP3A4). Metabolization takes place in the liver as well as in the intestine. The main metabolite is 1'-hydroxymidazolam (OH-midazolam), which is also pharmacologically active. Two other metabolites are formed via CYP3A4 and cytochrome P450 3A5 (CYP3A5), but only in small fractions (3% and 1%, respectively). Oral bioavailability of midazolam is extremely variable and due to first pass metabolism in the intestinal tract, formation rate of OH-midazolam is higher after oral administration of the drug compared to intravenous administration. Parent drug and metabolite are both glucoronidated via uridine diphosphate glucuronosyltransferase 1A4 (UGT1A4). About 75% of the administered dose is renally excreted as glucoronidated OH-midazolam. The fraction of unchanged midazolam is negligible [125–127].

The *fu* in the blood plasma is about 3% [128], and the lipophilicity is calculated as 3.89 [128], other sources provide values of between 2.9 [129] and 3.93 [130]. For OH-midazolam, lipophilicity is determined as 3.13 [130].

A combined PBPK model for midazolam and OH-midazolam was created with the PBPK modeling software PK-Sim and MoBi, considering literature information. Three active processes are integrated into the model, metabolization of midazolam to OH-midazolam via CYP3A4, glucuronidation of OH-midazolam via UGT1A4 and active transport of midazolam via P-glycoprotein (Pgp). The relative expression of the enzymes for each organ is obtained via the expression database integrated into the software [101]. CYP3A4 is mainly expressed in the liver and the intestinal compartments, UGT1A4 is mainly expressed in the kidneys, liver and small intestine and Pgp is also especially expressed in these organs. Glucoronidation of midazolam is neglected, as well as metabolization into minor metabolites via CYP3A4 and CYP3A5. All three processes are described via Michaelis-Menten kinetics to account for possible nonlinearities.

Torsemide

Torsemide is a loop diuretic acting against chronic heart failure, chronic renal failure and hypertension [131]. It leads to an increase of urinary excretion and reduces blood pressure by reducing blood volume. Renal plasma flow or the glomerular filtration rate are not affected [128]. In comparison to other loop diuretics like furosemide, torsemide possesses a large bioavailability of about 80 to 90% [132], which also indicates only very little first-pass metabolism [133]. Torsemide undergoes hepatic metabolism via cytochrome P450 2C9 (CYP2C9), forming three main metabolites M1, M3 and M5. M5, in the following named as OH-torsemide, is formed by oxidation of M1 [131,132,134]. In addition, torsemide is also metabolized by cytochrome P450 2C8 (CYP2C8) although the intrinsic clearance (Vmax/Km) of CYP2C9 is about an order of magnitude higher for CYP2C9 [135,136]. The *fu* of torsemide in blood plasma is smaller than 1% such that glomerular filtration can be neglected as a route for renal excretion. Active secretion is therefore the main route of re-

nal elimination [137]. About 75 to 80% of torsemide are metabolized in the liver, only 20 to 25% remain unchanged in urine. In addition, 11%, 3% and 44% of the administered dose can be found as M1, M3 and M5, respectively, in urine [132].

Based on the described information and the available experimental data, a combined PBPK model for torsemide and metabolite M1 was created with PK-Sim and MoBi. CYP2C9 was integrated as active second order Michaelis-Menten process for metabolization of torsemide to M1 and of M1 to M5, using the expression database from PK-Sim to obtain the relative expression profile of the enzyme for each organ. Notably, two independent kinetics were created since the dissociation constant K_m and also v_{max} are not the same for both metabolization steps. For simplification and due to the lack of experimental data, metabolization of torsemide to M3 was neglected. Two renal clearance processes were also integrated into the model, one for each of the considered compounds. Michaelis-Menten kinetics were chosen for a possible description of nonlinearities.

5.3 Statistical computation

The established Bayesian population PBPK approach of Chapter 2 was used for the single steps of the presented translational learning approach. We considered the combined mMALA/SCAM algorithm as described in Section 2.5.3 as the sampling algorithm. For each of the three applications of the Bayesian population PBPK approach, one long MCMC run was performed by drawing 150,000 samples out of the posterior. The first 50,000 iterations were defined as burn-in and were discarded from the chain. $\hat{R}$ was considered as convergence criterion [106,115]. To determine $\hat{R}$ the remaining 100,000 samples were split into two chains, whereby the first chain contained iterations 50,001:100,000 and the second chain contained iterations 100,001:150,000. An independent subsample of 500 parameter vectors out of the chain was used for the presented analyses and population simulations. For each individual, all organ volumes and blood flow rates were varied in the approach together with gastric emptying time (GET) and intestinal transit time (ITT), as already described in Section 4.2 and Table B.2. In addition, the specific ADME-related parameters and drug-specific parameters were varied as stated in Tables 5.3 and 5.4. The prior distributions were chosen as described in Section 2.3.3. The parameterization of the priors for each compound and MCMC run can be found below.

5.4 Results

Characterization of compound specific-parameters and pathophysiology

Having established the PBPK model for midazolam and torsemide, the described translational learning approach was applied for the characterization of healthy and diseased cohorts of individuals and for the identification of their interindividual variability. 20 individuals were randomly chosen out of the two cohorts consisting of either healthy volunteers or obese to morbidly obese patients. The remaining

individuals were then used for validation of each step of the translational approach by comparison with the population simulation (Figure 2.8).

In the first step of our translational learning approach we performed the Bayesian population PBPK approach in the healthy population and the PK of midazolam and OH-midazolam. Following the quantitative assessment of inter-individual variability, the identified distributions of parameters were subsequently used for a population simulation, as described in Section 2.6.2. Figure 5.2a shows the resulting population simulation for midazolam and OH-midazolam together with the remaining experimental data of the 83 healthy individuals at their original time points. Both simulations are in good agreement with the experimental data, however, the confidence interval is broader than the range of the experimental data.

Table 5.3 shows the integrated prior distributions for important parameters and the resulting posterior distributions after the application of the Bayesian population PBPK approach. A large difference can be observed between the prior and posterior of the ADME parameters for midazolam in the healthy individuals. In contrast, the posterior distributions of exemplary physiological parameters differ only slightly from the prior distributions. The drug-specific parameters do not have a population distribution; the depicted CV describes the uncertainty and not the variability in these parameters. It can be observed that besides the uncertainty of the *fu* for OH-midazolam, all drug-specific parameters were identified with very high probability.

In the next step we performed the Bayesian population PBPK approach for torsemide in the healthy population. As experimental data, the same 20 randomly chosen individuals of the first run considering midazolam and OH-midazolam PK were integrated. Figure 5.2b shows the resulting population simulation of torsemide and OH-torsemide in comparison with the remaining experimental data of the 83 healthy individuals at their original time points. In the absorption phase, the simulation of torsemide PK slightly underestimates the interindividual variability of the data; however, the interindividual variability of the distribution phase and the elimination phase is in good agreement with the experimental data. The PK behavior of OH-torsemide is not very well described regarding the shape of the experimental data over time.

Table 5.4 shows the integrated priors and the resulting posterior of the torsemide investigation. Inferred uncertainty of the drug-specific parameters is also small, as obtained before in the midazolam run. The difference between prior and posterior distributions for the physiological parameters is negligible as before for midazolam in healthy individuals. This indicates that no new information about the physiology of a healthy population could be extracted from the experimental data.

The third step in our translational workflow (Figure 2.9) accounted for midazolam PK in a diseased population. Here, experimental data of midazolam and OH-midazolam for 20 randomly chosen patients from the cohort of obese to morbidly obese patients were considered for the analyses. Table 5.3 shows the integrated priors and the resulting posterior. Notably, the inferred posterior information of the ADME parameters of the healthy population was used as prior information for the run, assuming that no better information existed for the diseased population. The drug-specific parameters were fixed at their maximum posterior values from the first run with healthy individuals (Table 5.3). This accounts for the assumption, that

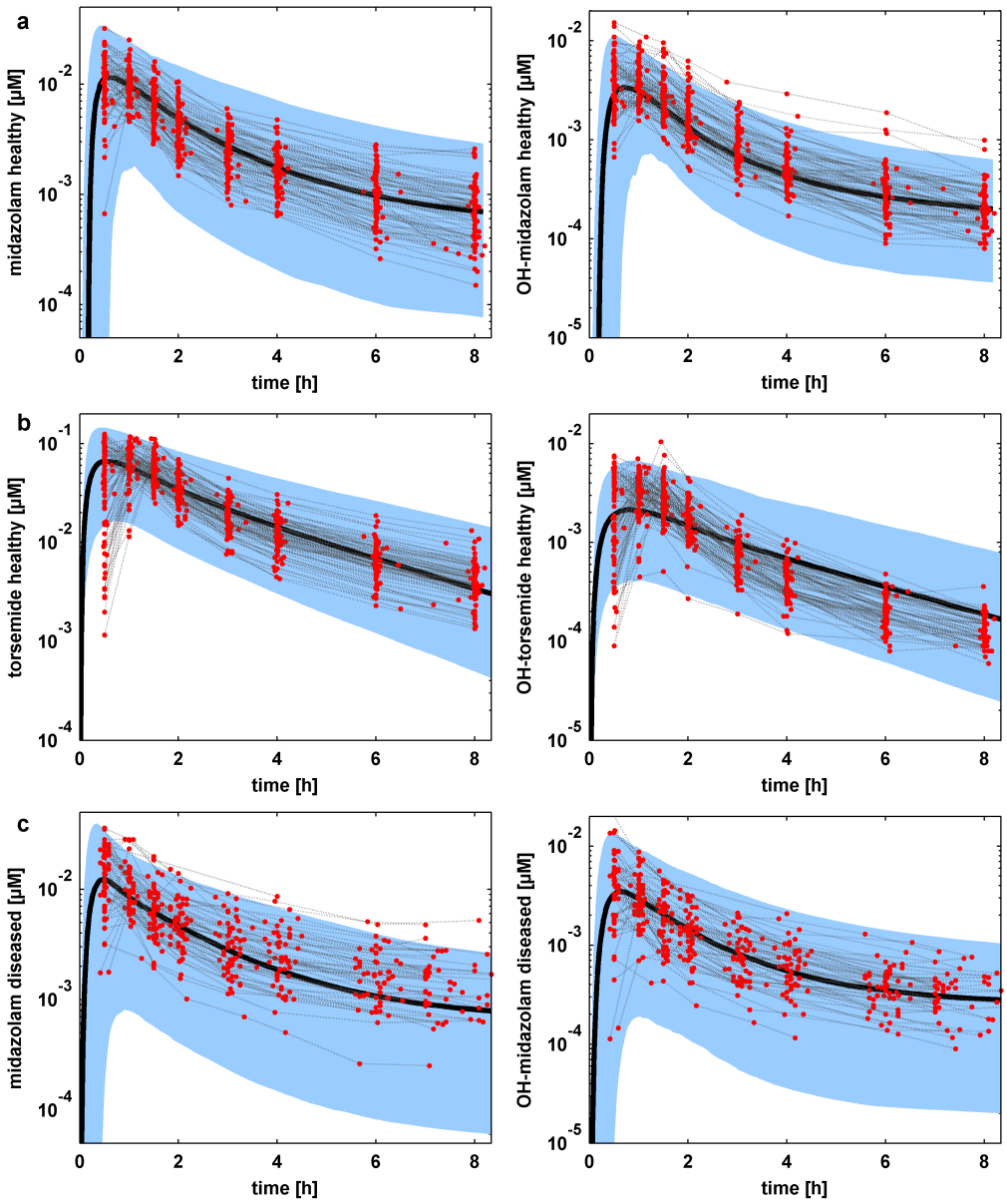

Figure 5.2: Population simulations for validation of the first three steps of the translational learning workflow. (**a**) Midazolam and OH-midazolam PK in the healthy population (**b**) Torsemide and OH-Torsemide in the healthy population. (**c**) Midazolam and OH-midazolam in the diseased population.
95 % confidence intervals (blue area) are shown together with the mean value curve (black line) and the experimental data (red dots with dark grey dashed lines). The parent compound is depicted on the left, the metabolites are depicted on the right.

Table 5.3: Prior and posterior distributions of the midazolam MCMC runs for ADME, compound-specific and exemplary physiological parameters. The distributions are characterized by geometric mean and coefficient of variation (CV).

		midazolam healthy				**midazolam diseased**			
	parameter	**prior geo. mean**	**CV [%]**	**posterior geo. mean**	**CV [%]**	**prior geo. mean**	**CV [%]**	**posterior geo. mean**	**CV [%]**
ADME	vmax PGP [μmol/l/min]	177.58	44	754.85	15	754.85	15	922.74	6
	vmax Cyp3A4 [μmol/l/min]	0.084	43	0.38	43	0.38	43	0.35	43
	vmax UGT1A4 [μmol/l/min]	45.36	44	222.18	36	222.18	36	119.91	60
compound-specific	logP mida	uniform	–	4.1	1	–	–	from healthy	–
	logP OH-mida		–	3.45	5	–	–		–
	fu mida		–	0.01	10	–	–		–
	fu OH-mida		–	0.01	32	–	–		–
physiology	fat vol. [L]	14.88	42	15.067	43	36.41	34	48.24	37
	kidney vol. [L]	0.44	25	0.44	24	0.44	26	0.44	26
	liver vol. [L]	2.36	24	2.34	24	2.36	24	2.35	25
	muscle vol. [L]	32.37	10	34.023	10	32.35	11	49.67	10
	fat Qspec [L/min/kg]	0.022	5	0.022	5	0.022	6	0.028	5
	kidney Qspec [L/min/kg]	3.026	5	3.017	5	3.024	6	3.015	6
	liver Qspec [L/min/kg]	0.18	5	0.18	5	0.18	6	0.18	6
	muscle Qspec [L/min/kg]	0.034	5	0.034	5	0.034	5	0.034	5

Table 5.4: Prior and posterior distributions of the torsemide MCMC runs for ADME, compound-specific and exemplary physiological parameters. The distributions are characterized by geometric mean and coefficient of variation (CV).

		torsemide healthy				**torsemide diseased prediction**			
	parameter	**prior geo. mean**	**CV [%]**	**posterior geo. mean**	**CV [%]**	**prior geo. mean**	**CV [%]**	**posterior geo. mean**	**CV [%]**
ADME	vmax Cyp2C9 [μmol/l/min]	91.56	37	542.1	28	–	–	542.1	28
	vmax Cyp2C9 [μmol/l/min]	523.85	36	1748.58	31	–	–	1748.6	31
	TSmax tora [μmol/min]	47.42	37	126.79	32	–	–	126.79	32
	TSmax M1 [μmol/min]	1488.47	36	6940.92	31	–	–	6940.9	31
	intP [dm/min]	5.83E-07	48	3.64E-05	24			3.64E-05	24
compound-specific	logP tora	uniform	–	2.09	4	–	–	2.09	4
	logP M1		–	2.53	8	–	–	2.53	8
	fu tora		–	0.001	9	–	–	0.001	9
	fu M1		–	0.001	11	–	–	0.001	11
physiology	fat vol. [L]	14.99	43	18.38	43	–	–	48.24	37
	kidney vol. [L]	0.44	25	0.4	27	–	–	0.44	26
	liver vol. [L]	2.35	23	2.18	25	–	–	2.35	25
	muscle vol. [L]	32.36	10	30.94	10	–	–	49.67	10
	fat Qspec [L/min/kg]	0.022	5	0.022	5	–	–	0.028	5
	kidney Qspec [L/min/kg]	3.026	5	2.92	5	–	–	3.015	6
	liver Qspec [L/min/kg]	0.18	5	0.18	5	–	–	0.18	6
	muscle Qspec [L/min/kg]	0.034	5	0.034	5	–	–	0.034	5

drug-specific information was completely inferred in the application with healthy data.

Again, after the MCMC run, a population simulation was performed with the posterior parameter distributions and compared to the 56 remaining patients of the study. Figure 5.2c depicts the resulting simulation. In the absorption phase and the distribution phase, the PK behavior of midazolam in the diseased individuals is well described. However, in the terminal phase, the simulation underpredicts the experimental data slightly, and the confidence interval overestimates the lower bound of the PK range. In contrast, the PK behavior of the metabolite is in good agreement with the experimental data over the whole time period, even though the confidence interval again overestimates the lower bound of the PK range in the terminal phase.

On a parameter level, the comparison between the healthy and the diseased cohort revealed large differences. The geometric mean of the enzyme activities of CYP3A4 and UGT1A4 decreased by 10% and 45%, respectively. In contrast activity of Pgp as well as muscle and fat volume showed a large increase. Furthermore, parameters like GET, ITT or the specific blood flow rate of fat increased partly noticeably more than 5%.

For further validation of the three examinations, the PK outcome of the simulation parameterized with the parameter vectors that showed the largest probability in the MCMC runs was compared to the experimental data. This was done for all three scenarios. Figure 5.3. shows the result for all 20 individuals that were included into the investigations. Notably, the PK outcome of midazolam was created with the 20 individuals of the healthy populations and the 20 individuals of the diseased population. Figure A.8 illustrates the simulations of the metabolites. The obtained results show a very good agreement with the experimental data. In addition, the comparison of the metabolites OH-midazolam and OH-torsemide demonstrates a good agreement with the study data, hence the Bayesian analyses provided reliable results for the individuals as well as the population.

Prediction of torsemide PK in a diseased population

The final step of the described translational learning approach was then the prediction of torsemide PK in diseased individuals. Notably, no previous MCMC run was performed to infer additional knowledge of new experimental data. Instead, the respective population distributions on the parameter level were translated from the previous runs, as depicted in Table 5.4. The drug-specific parameters including enzyme activities of the respective enzymes regarding torsemide metabolism were included from the posterior distributions of the torsemide run considering the healthy population. The physiological parameters were included from the posterior distribution of the midazolam run considering the diseased population. Measurement uncertainty was taken from the torsemide MCMC run investigating the healthy population. Figure 5.4 shows the resulting prediction of torsemide PK in the diseased population. The overall data can be well described within the simulated 95% confidence interval. However, it seems like the absorption phase is slightly underestimated while the terminal phase is overpredicted by the simulation. For OH-torsemide, the population simulation underpredicts the absorption phase, but

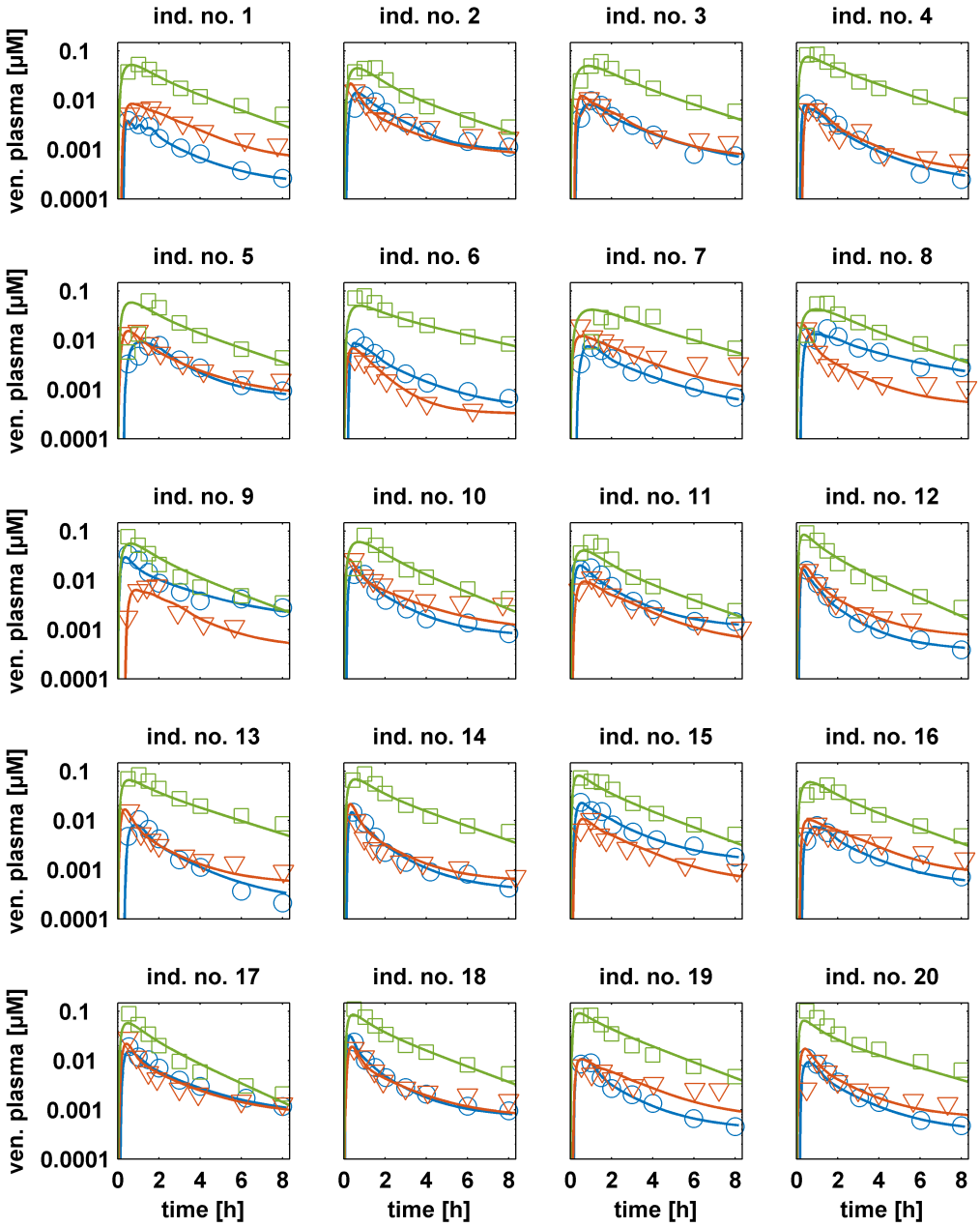

Figure 5.3: Individual model simulations of the parent compounds midazolam and torsemide. The simulation of the parameter vector with maximum posterior probability is shown for midazolam in the healthy individuals (blue line and circles), torsemide in healthy individuals (green line and squares) and midazolam in the diseased individuals (red line and triangles)

.

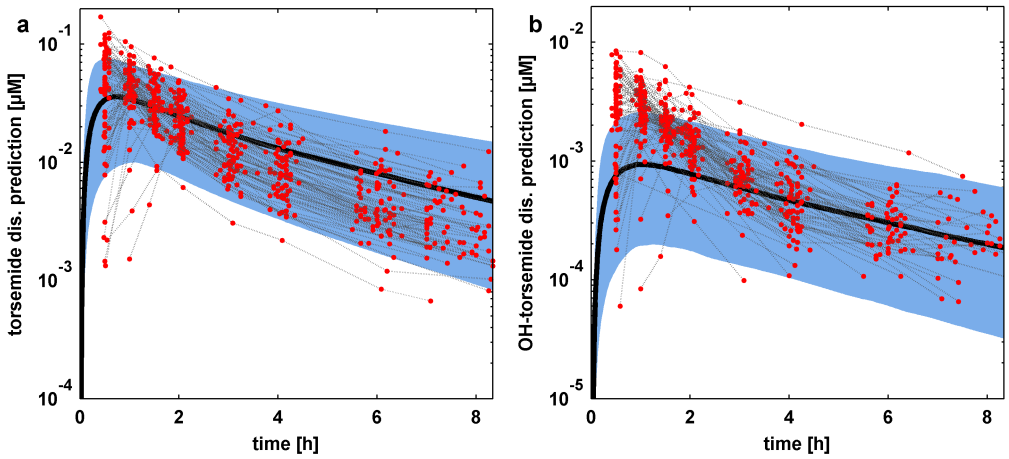

Figure 5.4: Prediction of the PK behavior of (**a**) torsemide and (**b**) OH-torsemide in a diseased population.
95 % confidence intervals (blue area) are shown together with the mean value curve (black line) and the experimental data (red dots with dark grey dashed lines)

.

the terminal phase is in good agreement with the experimental data.

To better compare the quality of the prediction, a comparison of PK parameters was performed. The distributions of C_{max}, time point, where maximum concentration is reached (t_{max}) and AUC of torsemide PK were compared between the experimental and simulated data. Figure 8 shows the obtained results for torsemide and OH-torsemide. A significant difference between healthy and diseased data and also between the simulations can be observed for the C_{max} values of torsemide. Predicted and observed C_{max} of the diseased population are in very good agreement, while C_{max} of the healthy population overestimates the data. The comparison of the AUCs shows similar results. The predicted AUCs in the healthy and diseased population are significantly different. Furthermore, predicted and AUCs from the experimental data are in very good agreement for the healthy population and the diseased population, respectively. A comparison of t_{max} reveals also significant differences between the simulations of healthy and diseased individuals. However, the agreement between predicted and observed t_{max} for healthy and diseased population, respectively, is not as good as for C_{max} and AUC.

A retrospective analysis using the Bayesian population PBPK approach was performed to quantify the quality of the obtained prediction of the PK behavior for torsemide. Therefore, the experimental data for torsemide in the diseased population were used. After the Bayesian analysis, a population simulation was performed similar to the first three steps of the translational learning approach. In addition to the predicted population simulation and the one based on the retrospective Bayesian run, a third population simulation based only on prior knowledge was assessed as a reference point. The normalized root-mean-square-error (NRMSE) was considered as a measure for the quality of the population simulations. The root-mean-square-error (RMSE) was obtained by comparison of the median of the 500 simulations and the median of the 79 experimental data sets at the time points of the experimental data. For the parent compound torsemide and the metabolite OH-torsemide,

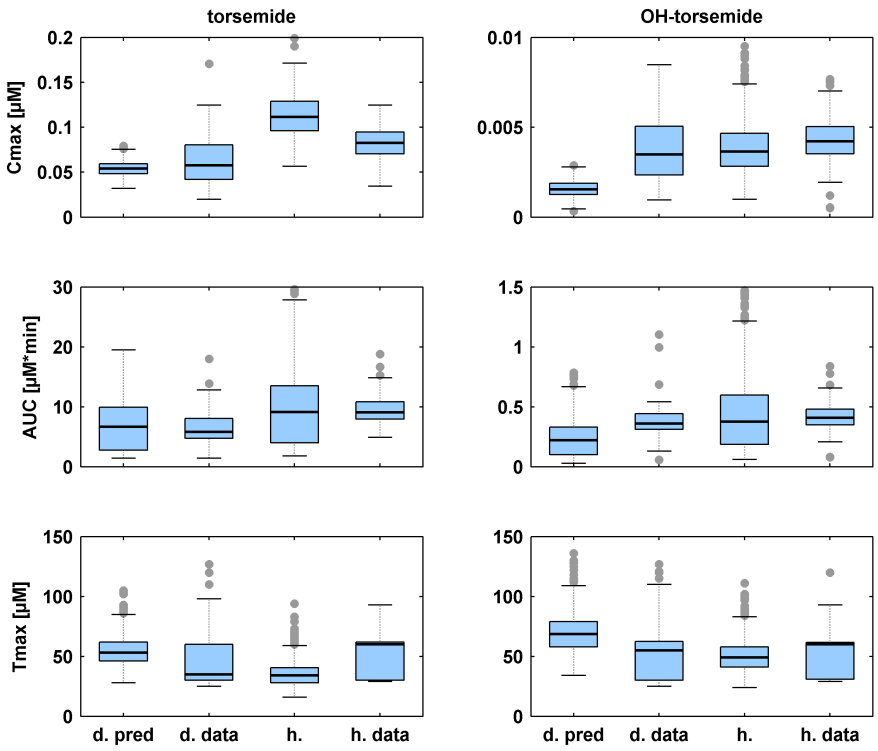

Figure 5.5: Analysis of PK parameters of the prediction of torsemide and OH-torsemide. C_{max}, AUC and t_{max} are compared between the prediction (d.pred) and the data (d.data) of the diseased individuals for torsemide (left) and OH-torsemide (right) as well as between the simulation (h.) and the experimental data (h.data) of the healthy individuals.

Table 5.5: Comparison of NRMSE to quantify the quality of the population simulations using: only **prior** knowledge; the results of the systems pharmacology approach for the **prediction** of the PK behavior; and the results of the **retrospective** analysis of torsemide in diseased individuals using the Bayesian population PBPK approach.

	NRMSE		
	prior	prediction	retrospective
torsemide	1	0.544	0.536
OH-torsemide	1	0.898	0.579

respectively, the RMSE was normalized with the maximum RMSE of all three scenarios, which was the population simulation using only prior knowledge for both cases. Table 5 shows the obtained values for the normalized root-mean-square-error (NRMSE).

The NRMSE of the prediction of the PK behavior of torsemide shows an improvement of 45.6% compared to the simulation that was created by using prior information. A slight improvement of the simulation could be further observed in the retrospective analysis. However, a visual inspection of the shape of the median simulation curve reveals a significantly better shaped median curve for the retrospective simulation, in addition (Figure A.9). For OH-torsemide, an improvement of about 11% can be observed in the prediction compared to the simulations using only prior information. Furthermore, the NRMSE of the retrospective analysis is about 35% better than the predicted one.

5.5 Discussion

In this chapter, we performed a systems-pharmacology approach to translate physiological information between different patient cohorts to ultimately predict the population PK of specific drugs in novel patient subgroups. The approach consisted of four steps. In the first three steps, new experimental data was used in combination with a Bayesian population PBPK approach to update prior information about physiological parameters and drug-specific parameters to assess the interindividual variability of drug pharmacokinetics in a population and infer posterior knowledge about all integrated parameters. The three applications described the PK of midazolam and torsemide in a healthy population and the PK of midazolam in a diseased population. The results on the parameter level were validated by performing a population simulation for each of the three applications and comparing the 95% confidence interval to new unsupervised experimental data. The last step consisted of a prediction of the PK of torsemide in the diseased population based on the derived knowledge of the three assessments before. The derived drug-specific knowledge of torsemide in a healthy population was combined with the derived pathophysiology of the diseased population to perform a population simulation. The simulation was compared to experimental data and showed a quite reasonable accordance to the experimental data.

The key idea of the presented approach was the iterative translation of drug-

specific information from investigations considering the same drug and the iterative translation of physiological information from the investigation in healthy volunteers to that in patients. That allowed to start the first investigations with very little information about the physicochemistry and the ADME-related parameters of the two compounds midazolam and torsemide and to assess information about the parameter uncertainty and variability from the experimental data in healthy individuals. This knowledge could be then transferred to assess the interindividual variability in the PK of midazolam in diseased individuals. Since the uncertainty of the parameters describing the physicochemistry of the compound such as lipophilicity and *fu* was very small, it was assumed that these parameters need not to be assessed further. Instead, all changes between the healthy and the diseased population should be explainable with changes in the physiology and the ADME-related parameters.

The PBPK model structure that was considered for the systems pharmacology approach was a generic mechanistic model structure that consisted of all important organs and tissues of the human body. Therefore, it was possible to integrate all organ volumes and blood flow rates into the analyses, whereby informative prior distributions about each parameter were provided by a large physiological data base. Starting with a cohort of healthy individuals, the analyses demonstrated that no new information could be extracted about the physiology from the experimental data, since the posterior distributions were very similar to the prior distributions. The meaning of such result is ambiguous, on the one hand the data could be uninformative related to the physiological parameters, on the other hand the information extracted from the data confirms the prior distributions that were integrated. This cannot be completely differentiated with our approach. However, the integration of these uninformed parameters into the investigation allows in principle the extraction of information from the experimental data and further enables the translation and extrapolation to new scenarios [17].

Such translation was performed for the assessment of midazolam PK in a diseased population, in which the posterior distributions of all physiological parameters were considered as prior information. The results demonstrated large changes in ADME related parameters, in organ volumes such as fat and muscle volume and also in several blood flow rates, characterizing the pathophysiology of the patients, reflecting the changes on a parameter level. Thereby, the sparse data and especially the fact that only plasma data were available led to a characterization of the pathophysiology on a functional level. That means, that the validity of a certain change of a parameter cannot be ensured, but e.g. a decrease in the liver volume or in the specific vmax of CYP3A4 both reflects a decrease of liver function. Such localization to a functional representation of biological meaning is only possible by the consideration of a whole-body PBPK model.

The results of the three applications of the Bayesian population PBPK approach were qualified by population simulations as well as individual simulations of the PK behavior, which in principle all showed good agreement with the experimental data. Several population simulations were too broad compared to the range of the experimental data. A possible reason for this could be the relatively small number of 20 individuals that have been used for the application of the Bayesian population PBPK approach. The integration of a larger number of individuals could provide

better estimations, however, in early clinical studies usually small cohorts of about 10 to 50 individuals are considered. Another reason could be an insufficient estimation of the dependency structure of the population parameters, such that effects are added up on the PK level and lead to too large variability. However, it has to be noted that all remaining unsupervised individuals that were compared with the simulations (Figure 5.2) lie within the simulated confidence interval, such that from a clinical perspective these results would not lead to any additional safety issues, which would be the case if a small number of individuals lead to too narrow ranges of estimated interindividual variability.

For torsemide in the diseased population, successful translation of information and following prediction of population PK was demonstrated: on the one hand of drug-specific parameters of torsemide from the healthy to the diseased population and on the other hand the physiology of the diseased individuals from midazolam to torsemide. Thereby, the quality of the PK prediction was further quantified and revealed a very good agreement of observed and predicted PK of the parent compound, but not of the metabolite. Visual inspection and analyses of the posterior distribution of the retrospective analysis concluded that especially the metabolization of torsemide via CYP2C9 is increased in the diseased individuals, since an improved shape could be observed in the population of the retrospective analysis, especially in the terminal phase of torsemide. This increased metabolization of torsemide led to an increased C_{max} of OH-torsemide thus increasing the quality of the population simulation of OH-torsemide.

Chapter 6

Conclusion

In conclusion, this work makes three main contributions to the literature. The first is the development of the comprehensive generic Bayesian population PBPK approach for an improved understanding of interindividual variability and the establishment of a translational learning concept. We aimed for an elaborated estimation of the parameters' uncertainty and variability and constructed a specifically-designed model framework including a nonlinear-mixed effects model, a covariate model and a proportional error model within the Bayesian framework. The second is the adaptation and tuning of the considered approaches to best suite the demands of whole-body PBPK models and translational systems pharmacology, the idea of acquisition and translation of physiological and physicochemical properties. Thereby, to the best of our knowledge, we for the first time paid particular attention to tune performance of MCMC approaches in the area of life science applications, be it the setup of the sampling or the sampling approach itself. As the third main contribution we considered several application examples that cover a wide range of issues occurring in the drug development process and demonstrate the usability of the developed Bayesian population PBPK approach.

In particular, the contributions of this work related to the overall workflow are:

- reduction of model complexity by taking into account the natural independence of model parameters that base upon a biological origin [10,11],
- integration of a covariate model that allows to infer the distribution of physiological parameters over the full age range [11],
- a specifically-designed blockwise sampling structure of the MCMC algorithm, taking into account the mechanistic deconvolution of physiological and drug-specific parameters in the PBPK model [10,11],
- definition of prior distributions in consideration of the structure and properties of a physiological database that is part of the generic PBPK modeling platform [10,11].

To improve the performance compared to recent approaches and for evaluation of the derived results as well as to facilitate translation, we:

- developed and adapted a sophisticated MCMC sampling algorithm that was designed to best suit the specific properties of the different types of parameters

that are identified by the Bayesian population PBPK approach and were able to show a clear improvement of the performance by our method compared to the conventional MH approach (Chapter 4, [12]),

- developed a retrospective estimation of the *a posteriori* dependency structure to take all derived information of a Bayesian analyses into account [11],

- established a framework for translational learning, where several iterations of the Bayesian population PBPK approach informed a de-novo prediction of an unsupervised phase of a clinical drug development program [12].

For qualification of the Bayesian population PBPK approach and for demonstration of its usability we:

- demonstrated in a pravastatin example how to use the approach to identify clinically-relevant subgroups within a cohort of individuals in an unsupervised approach. Thereby, considering our approach we were able to identify a bimodal distribution characterizing a specific biological process. We hence were able to point out the biological fundamental of the underlying stratification, in this case the enzyme activity of a key transport protein, the OATP1B1 in the liver [10].

- assessed the interindividual variability of the PK behavior of theophylline in a cohort of healthy individuals. A comparison was performed between the results of our Bayesian population PBPK approach and a conventional approach that is based more on prior knowledge and independence of parameters. Furthermore, the results generated with our new sampling method were compared against the mainly used sampling method and a clear improvement of the performance was obtained [11].

- made the translational capabilities of our approach evident. The Bayesian population PBPK approach was embedded into an iterative translational systems pharmacology approach. First, the interindividual variability of the physiology of a healthy population was assessed together with the physicochemistry of the drug midazolam; second, the physicochemical properties of the drug torsemide were identified. Third, the inferred drug-specific properties of midazolam were translated into an investigation to assess the pathophysiology of obese patients. Finally, the generated knowledge was considered for the prediction of the PK behavior of torsemide in obese patients. Thus, it was demonstrated how a translation of knowledge from early clinical phases in healthy volunteers and other previously performed studies in the patient group can successfully support the development of a new drug candidate by providing predictions of its PK behavior, which can then be considered during planning clinical trials and dosing strategies [12].

The presented thesis has envisaged to close the above mentioned limitations of previous approaches, that had been amongst others lack of a generic and systematic workflow for continuous evaluation and transfer of knowledge in clinical development programs and missing considerations of efficient MCMC sampling. To both,

the presented work could significantly contribute by providing the presented workflow for estimation and translation. Outstanding issues, that need to be tackled and could be integrated into the approach, are for example missing identification of the full covariance relationships during MCMC sampling. So far, parameters have been estimated under assumption of independence and dependencies of population parameters were subsequently identified from the posterior distribution. These dependencies were integrated and considered for improved population distributions. However, a continuous adaptation of the covariances could further increase accuracy. Furthermore, no concepts exist for use of the full covariance information for translational learning so far. Although this is beyond the scope of this work, the development of accurate methods to conserve and adapt such information over several learning steps proves to be very interesting for future investigations.

Another issue is that several parameters of the considered models were defined as fixed parameters, such as volume fractions or surface areas. In principle, these parameters could also be integrated in the estimation in the future, since they potentially provide additional information about pathophysiological conditions. However, it is unlikely that these parameters are informed by plasma PK data, such that additional data would be needed. Moreover, especially when parameters are expected to be uninformed by the experimental data, extensive prior information must be available. This is, so far, not the case for several parameters in our considered PBPK models, such that these parameters were set as fixed.

An important objective in Bayesian applications is to decrease the obtained parameter uncertainty as this increases the reliability on estimated population variability or individual parameter estimates. With mechanistic PBPK models this can be achieved by a better understanding of the actual biological processes but also by optimization of the underlying experimental design [73]. In the field of PK, experimental design means for example to optimize the number of samples to take, the actual time points where a sample should be taken or the number of individuals to participate in an experiment. Thereby, Bayesian optimal design could help to overcome a major critics of optimal design, that is the need to rely on a certain model and parameter point estimates [138]. So far, Bayesian optimal design has been applied e.g. in the field of toxicokinetics to optimize uncertainty of key parameters of small two-compartment TK models [139]. Recent approaches have been also performed in the field of population PK, but not PBPK [140–142]. The prospective application of our Bayesian population PBPK approach for optimal experimental design could be even advantageous due to its extrapolation capabilities. As an example, related to the presented application in Chapter 5, the prediction of torsemide in the diseased population could now be used for optimal experimental design of the following phase II study, thereby taking into account assessed knowledge about pathophysiological alterations and estimated population variability as well as uncertainty.

All in all, our developed workflow strongly improves previous work regarding combination of physiological models and Bayesian statistics and provides a framework for continuous integration, assessment and transfer of knowledge along the the drug development process. In the future, our approach could facilitate the streamlining of clinical studies, since a lot of information could be already available before e.g. a clinical phase II trial. This could reduce costs without increasing possible

safety issues. Thinking ahead, a systematic application in systems pharmacology would foster the establishment of a large knowledge database. This database would allow the collection of physiological and pathophysiological information about specific populations where only sparse data is available, leading to a continuous increase of safety and efficacy in the development of new drugs and furthermore strengthens confidence in personalized medicine efforts.

References

[1] M. Hay, D. W. Thomas, J. L. Craighead, C. Economides, and J. Rosenthal. Clinical development success rates for investigational drugs. *Nat Biotechnol*, 32(1):40–51, 2014.

[2] S. M. Paul, D. S. Mytelka, C. T. Dunwiddie, C. C. Persinger, B. H. Munos, S. R. Lindborg, and A. L. Schacht. How to improve R&D productivity: the pharmaceutical industry's grand challenge. *Nat Rev Drug Discov*, 9(3):203–14, 2010.

[3] B. M. Agoram, S. W. Martin, and P. H. van der Graaf. The role of mechanism-based pharmacokinetic-pharmacodynamic (PK-PD) modelling in translational research of biologics. *Drug Discov Today*, 12(23-24):1018–24, 2007.

[4] R. L. Lalonde, K. G. Kowalski, M. M. Hutmacher, W. Ewy, D. J. Nichols, P. A. Milligan, B. W. Corrigan, P. A. Lockwood, S. A. Marshall, L. J. Benincosa, T. G. Tensfeldt, K. Parivar, M. Amantea, P. Glue, H. Koide, and R. Miller. Model-based drug development. *Clin Pharmacol Ther*, 82(1):21–32, 2007.

[5] J. Lippert, M. Brosch, O. von Kampen, M. Meyer, H. U. Siegmund, C. Schafmayer, T. Becker, B. Laffert, L. Gorlitz, S. Schreiber, P. J. Neuvonen, M. Niemi, J. Hampe, and L. Kuepfer. A mechanistic, model-based approach to safety assessment in clinical development. *CPT Pharmacometrics Syst Pharmacol*, 1:e13, 2012.

[6] M. Maliepaard, C. Nofziger, M. Papaluca, I. Zineh, Y. Uyama, K. Prasad, C. Grimstein, M. Pacanowski, F. Ehmann, S. Dossena, and M. Paulmichl. Pharmacogenetics in the evaluation of new drugs: a multiregional regulatory perspective. *Nat Rev Drug Discov*, 12(2):103–15, 2013.

[7] R. Evers, R. L. Blanchard, A. W. Warner, D. Cutler, N. G. Agrawal, and P. M. Shaw. A question-based approach to adopting pharmacogenetics to understand risk for clinical variability in pharmacokinetics in early drug development. *Clin Pharmacol Ther*, 96(3):291–5, 2014.

[8] S. Willmann, K. Hohn, A. Edginton, M. Sevestre, J. Solodenko, W. Weiss, J. Lippert, and W. Schmitt. Development of a physiology-based whole-body population model for assessing the influence of individual variability on the pharmacokinetics of drugs. *J Pharmacokinet Pharmacodyn*, 34(3):401–31, 2007.

[9] K. Venkatakrishnan, L. E. Friberg, D. Ouellet, J. T. Mettetal, A. Stein, I. F. Troconiz, R. Bruno, N. Mehrotra, J. Gobburu, and D. R. Mould. Optimizing oncology therapeutics through quantitative translational and clinical pharmacology: challenges and opportunities. *Clin Pharmacol Ther*, 97(1):37–54, 2015.

[10] M. Krauss, R. Burghaus, J. Lippert, M. Niemi, P. Neuvonen, A. Schuppert, S. Willmann, L. Kuepfer, and L. Gorlitz. Using Bayesian-PBPK modeling for assessment of inter-individual variability and subgroup stratification. *In Silico Pharmacol*, 1:6, 2013.

[11] M. Krauss, K. Tappe, A. Schuppert, L. Kuepfer, and L. Goerlitz. Bayesian Population Physiologically-Based Pharmacokinetic (PBPK) Approach for a Physiologically Realistic Characterization of Interindividual Variability in Clinically Relevant Populations. *PLoS One*, 10(10):e0139423, 2015.

[12] M. Krauss, U. Hofmann, W. von Schoenfels, S. Igel, C. Schafmayer, J. Schlender, C. Mueller, M. Brosch, A. Schuppert, M. Block, E. Schäffeler, G. Böhmer, L. Goerlitz, J. Hoecker, J. Lippert, R. Kerb, J. Hampe, L. Kuepfer, and M. Schwab. Translational learning from clinical studies predicts drug pharmacokinetics across patient populations. in preparation, 2016.

[13] J. F. Schlender, M. Meyer, K. Thelen, M. Krauss, S. Willmann, Eissing T., and U. Jaede. Development of a Whole-Body Physiologically Based Pharmacokinetic Approach to Assess the Pharmacokinetics of Drugs in Elderly Individuals. *Clin Pharmacokinet*, pages 1–17, 2016.

[14] V. Baier. Investigation of extrapolation within the Bayesian population PBPK modelling on the example of erythromycin and midazolam. Master's thesis, 2015.

[15] M. J. Waring, J. Arrowsmith, A. R. Leach, P. D. Leeson, S. Mandrell, R. M. Owen, G. Pairaudeau, W. D. Pennie, S. D. Pickett, J. Wang, O. Wallace, and A. Weir. An analysis of the attrition of drug candidates from four major pharmaceutical companies. *Nat Rev Drug Discov*, 14(7):475–486, 2015.

[16] D. A. Katz, B. Murray, A. Bhathena, and L. Sahelijo. Defining drug disposition determinants: a pharmacogenetic-pharmacokinetic strategy. *Nat Rev Drug Discov*, 7(4):293–305, 2008.

[17] T. A. Leil. A bayesian perspective on estimation of variability and uncertainty in mechanism-based models. *CPT Pharmacometrics Syst Pharmacol*, 3:e121, 2014.

[18] I. Nestorov. Whole-body physiologically based pharmacokinetic models. *Expert Opin Drug Metab Toxicol*, 3(2):235–49, 2007.

[19] A. N. Edginton, F. P. Theil, W. Schmitt, and S. Willmann. Whole body physiologically-based pharmacokinetic models: their use in clinical drug development. *Expert Opin Drug Metab Toxicol*, 4(9):1143–52, 2008.

[20] I. Nestorov. Modelling and simulation of variability and uncertainty in toxicokinetics and pharmacokinetics. *Toxicol Lett*, 120(1-3):411–20, 2001.

[21] K. S. Pang and M. R. Durk. Physiologically-based pharmacokinetic modeling for absorption, transport, metabolism and excretion. *J Pharmacokinet Pharmacodyn*, 37(6):591–615, 2010.

[22] W. Schmitt and S. Willmann. Physiology-based pharmacokinetic modeling: ready to be used. *Drug Discov Today Technol*, 1(4):449–56, 2004.

[23] S. Willmann, J. Lippert, and W. Schmitt. From physicochemistry to absorption and distribution: predictive mechanistic modelling and computational tools. *Expert Opin Drug Metab Toxicol*, 1(1):159–68, 2005.

[24] A. N. Edginton and S. Willmann. Physiology-based simulations of a pathological condition: prediction of pharmacokinetics in patients with liver cirrhosis. *Clin Pharmacokinet*, 47(11):743–52, 2008.

[25] T. Eissing, J. Lippert, and S. Willmann. Pharmacogenomics of codeine, morphine, and morphine-6-glucuronide: model-based analysis of the influence of CYP2D6 activity, UGT2B7 activity, renal impairment, and CYP3A4 inhibition. *Mol Diagn Ther*, 16(1):43–53, 2012.

[26] J. J. Swen, T. W. Huizinga, H. Gelderblom, E. G. de Vries, W. J. Assendelft, J. Kirchheiner, and H. J. Guchelaar. Translating pharmacogenomics: challenges on the road to the clinic. *PLoS Med*, 4(8):e209, 2007.

[27] D. Calvetti and E. Somersalo. Life sciences through mathematical models. *Rend Lincei*, 26(2):193–201, 2015.

[28] B. Efron. Mathematics. Bayes' theorem in the 21st century. *Science*, 340(6137):1177–8, 2013.

[29] M. Davidian and D. M. Giltinan. Nonlinear models for repeated measurement data: an overview and update. *J Agr Biol Envir St*, 8(4):387–419, 2003.

[30] A. Gelman, F. Y. Bois, and J. Jiang. Physiological pharmacokinetic analysis using population modeling and informative prior distributions. *J Am Stat Assoc*, 91(436):1400–1412, 1996.

[31] F. Y. Bois, A. Gelman, J. Jiang, D. R. Maszle, L. Zeise, and G. Alexeef. Population toxicokinetics of tetrachloroethylene. *Arch Toxicol*, 70(6):347–55, 1996.

[32] F. Y. Bois, L. Zeise, and T. N. Tozer. Precision and sensitivity of pharmacokinetic models for cancer risk assessment: tetrachloroethylene in mice, rats, and humans. *Toxicol Appl Pharmacol*, 102(2):300–15, 1990.

[33] N. Metropolis, A. W. Rosenbluth, M. N. Rosenbluth, A. H. Teller, and E. Teller. Equation of state calculations by fast computing machines. *J Chem Phys*, 21(6):1087–1092, 1953.

[34] M. Mezzetti, J. G. Ibrahim, F. Y. Bois, L. M. Ryan, L. Ngo, and T. J. Smith. A Bayesian compartmental model for the evaluation of 1,3-butadiene metabolism. *J R Stat Soc Ser C Appl Stat*, 52(3):291–305, 2003.

[35] F. Jonsson, F. Bois, and G. Johanson. Physiologically based pharmacokinetic modeling of inhalation exposure of humans to dichloromethane during moderate to heavy exercise. *Toxicol Sci*, 59(2):209–18, 2001.

[36] F. Jonsson and G. Johanson. A Bayesian analysis of the influence of GSTT1 polymorphism on the cancer risk estimate for dichloromethane. *Toxicol Appl Pharmacol*, 174(2):99–112, 2001.

[37] F. Y. Bois. Analysis of PBPK models for risk characterization. *Ann N Y Acad Sci*, 895:317–37, 1999.

[38] W. A. Chiu, M. S. Okino, and M. V. Evans. Characterizing uncertainty and population variability in the toxicokinetics of trichloroethylene and metabolites in mice, rats, and humans using an updated database, physiologically based pharmacokinetic (PBPK) model, and Bayesian approach. *Toxicol Appl Pharmacol*, 241(1):36–60, 2009.

[39] I. Gueorguieva, L. Aarons, and M. Rowland. Diazepam pharamacokinetics from preclinical to phase I using a Bayesian population physiologically based pharmacokinetic model with informative prior distributions in WinBUGS. *J Pharmacokinet Pharmacodyn*, 33(5):571–94, 2006.

[40] T. A. Leil, S. Kasichayanula, D. W. Boulton, and F. LaCreta. Evaluation of 4beta-Hydroxycholesterol as a Clinical Biomarker of CYP3A4 Drug Interactions Using a Bayesian Mechanism-Based Pharmacometric Model. *CPT Pharmacometrics Syst Pharmacol*, 3:e120, 2014.

[41] T. J. Zurlinden and B. Reisfeld. Physiologically based modeling of the pharmacokinetics of acetaminophen and its major metabolites in humans using a Bayesian population approach. *Eur J Drug Metab Pharmacokinet*, 2015.

[42] N. Tsamandouras, G. Dickinson, Y. Guo, S. Hall, A. Rostami-Hodjegan, A. Galetin, and L. Aarons. Development and Application of a Mechanistic Pharmacokinetic Model for Simvastatin and its Active Metabolite Simvastatin Acid Using an Integrated Population PBPK Approach. *Pharm Res*, 32(6):1864–83, 2015.

[43] M. Girolami and B. Calderhead. Riemann manifold langevin and hamiltonian monte carlo methods. *J R Stat Soc Series B Stat Methodol*, 73(2):123–214, 2011.

[44] H. Haario, E. Saksman, and J. Tamminen. Componentwise adaptation for high dimensional MCMC. *Comput Stat*, 20(2):265–273, 2005.

[45] H. Haario, M. Laine, A. Mira, and E. Saksman. DRAM: efficient adaptive MCMC. *Stat Comput*, 16(4):339–354, 2006.

[46] C. Andrieu, A. Doucet, and R. Holenstein. Particle markov chain monte carlo methods. *J R Stat Soc Series B Stat Methodol*, 72(3):269–342, 2010.

[47] D. Schmidl, C. Czado, S. Hug, and F. J. Theis. A vine-copula based adaptive MCMC sampler for efficient inference of dynamical systems. *Bayesian Anal*, 8(1):1–22, 2013.

[48] S. Hug, A. Raue, J. Hasenauer, J. Bachmann, U. KlingmÃ¼ller, J. Timmer, and F. J. Theis. High-dimensional Bayesian parameter estimation: case study for a model of JAK2/STAT5 signaling. *Math Biosci*, 246(2):293–304, 2013.

[49] A. Raue, C. Kreutz, F. J. Theis, and J. Timmer. Joining forces of Bayesian and frequentist methodology: a study for inference in the presence of non-identifiability. *Philos Trans A Math Phys Eng Sci*, 371(1984):20110544, 2013.

[50] P. G. Georgopoulos, S. Balakrishnan, A. Roy, S. Isukapalli, A. Sasso, YC Chien, and C. P. Weisel. A Comparison of Maximum Likelihood Estimation Methods for Inverse Problem Solutions Employing PBPK Modeling with Biomarker Data: Application to Tetrachloroethylene. CCL, 2008.

[51] H. T. Banks, Y. Ma, and L. K. Potter. A simulation-based comparison between parametric and nonparametric estimation methods in PBPK models. *J Inverse Ill Pose P*, 13(1):1–26, 2005.

[52] S. A. Peters. *Physiologically-based pharmacokinetic (PBPK) modeling and simulations: principles, methods, and applications in the pharmaceutical industry*. John Wiley & Sons, 2012.

[53] L. B. Sheiner, B. Rosenberg, and V. V. Marathe. Estimation of population characteristics of pharmacokinetic parameters from routine clinical data. *J Pharmacokinet Biopharm*, 5(5):445–79, 1977.

[54] L. B. Sheiner. The population approach to pharmacokinetic data analysis: rationale and standard data analysis methods. *Drug Metab Rev*, 15(1-2):153–71, 1984.

[55] S. Brooks, A. Gelman, G. Jones, and XL. Meng. *Handbook of Markov Chain Monte Carlo*. CRC press, 2011.

[56] S. Willmann, J. Lippert, M. Sevestre, J. Solodenko, F. Fois, and W. Schmitt. PK-Sim®: a physiologically based pharmacokinetic 'whole-body' model. *Biosilico*, 1(4):121–124, 2003.

[57] H. Haario, E. Saksman, and J. Tamminen. An adaptive Metropolis algorithm. *Bernoulli*, pages 223–242, 2001.

[58] H. Haario, E. Saksman, and J. Tamminen. Adaptive proposal distribution for random walk Metropolis algorithm. *Comput Stat*, 14(3):375–396, 1999.

[59] M. Rowland, C. Peck, and G. Tucker. Physiologically-based pharmacokinetics in drug development and regulatory science. *Annu Rev Pharmacol Toxicol*, 51:45–73, 2011.

[60] Michaela Meyer. Bayer-Technology-Services GmbH. 2011.

[61] T. Rodgers, D. Leahy, and M. Rowland. Physiologically based pharmacokinetic modeling 1: predicting the tissue distribution of moderate-to-strong bases. *J Pharm Sci*, 94(6):1259–76, 2005.

[62] T. Rodgers and M. Rowland. Physiologically based pharmacokinetic modelling 2: predicting the tissue distribution of acids, very weak bases, neutrals and zwitterions. *J Pharm Sci*, 95(6):1238–57, 2006.

[63] Bayer-Technology-Services GmbH. *SB Model Suite 5.5. - users manual*, 2014.

[64] S. D. Cohen and A. C. Hindmarsh. CVODE, a stiff/nonstiff ODE solver in C. *ComPh*, 10(2):138–143, 1996.

[65] P. Poulin, K. Schoenlein, and F. P. Theil. Prediction of adipose tissue: plasma partition coefficients for structurally unrelated drugs. *J Pharm Sci*, 90(4):436–47, 2001.

[66] S. Willmann, W. Schmitt, J. Keldenich, and J. B. Dressman. A physiologic model for simulating gastrointestinal flow and drug absorption in rats. *Pharm Res*, 20(11):1766–71, 2003.

[67] S. Willmann, W. Schmitt, J. Keldenich, J. Lippert, and J. B. Dressman. A physiological model for the estimation of the fraction dose absorbed in humans. *J Med Chem*, 47(16):4022–31, 2004.

[68] E. I. Ette and P. J. Williams. Population pharmacokinetics I: background, concepts, and models. *Ann Pharmacother*, 38(10):1702–6, 2004.

[69] P. S. Price, R. B. Conolly, C. F. Chaisson, E. A. Gross, J. S. Young, E. T. Mathis, and D. R. Tedder. Modeling interindividual variation in physiological factors used in PBPK models of humans. *Crit Rev Toxicol*, 33(5):469–503, 2003.

[70] W. Huisinga, A. Solms, L. Fronton, and S. Pilari. Modeling interindividual variability in physiologically based pharmacokinetics and its link to mechanistic covariate modeling. *CPT Pharmacometrics Syst Pharmacol*, 1:e4, 2012.

[71] W. M. Bolstad. *Understanding computational Bayesian statistics*, volume 644. John Wiley & Sons, 2010.

[72] T. Bayes. An essay towards solving a problem in the doctrine of chances. 1763. *MD Comput*, 8(3):157–71, 1991.

[73] P. Bernillon and F. Y. Bois. Statistical issues in toxicokinetic modeling: a bayesian perspective. *Environ Health Perspect*, 108 Suppl 5:883–93, 2000.

[74] S. L. Beal. Ways to fit a PK model with some data below the quantification limit. *J Pharmacokinet Pharmacodyn*, 28(5):481–504, 2001.

[75] S. Yang and J. Roger. Evaluations of Bayesian and maximum likelihood methods in PK models with below-quantification-limit data. *Pharm Stat*, 9(4):313–30, 2010.

[76] H. Gebelein and H. J. Heite. Ueber die Unsymmetrie biologischer Haeufigkeitsverteilungen. *Klinische Wochenschrift*, 28(3-4):41–45, 1950.

[77] C. L. Zhang and F. A. Popp. Log-normal distribution of physiological parameters and the coherence of biological systems. *Med Hypotheses*, 43(1):11–16, 1994.

[78] A. Sigal, R. Milo, A. Cohen, N. Geva-Zatorsky, Y. Klein, Y. Liron, N. Rosenfeld, T. Danon, N. Perzov, and U. Alon. Variability and memory of protein levels in human cells. *Nature*, 444(7119):643–6, 2006.

[79] F. Y. Bois. Statistical analysis of Fisher et al. PBPK model of trichloroethylene kinetics. *Environ Health Perspect*, 108 Suppl 2:275–82, 2000.

[80] H. Jeffreys. An invariant form for the prior probability in estimation problems. *Proc R Soc Lond A Math Phys Sci*, 186(1007):453–61, 1946.

[81] C. Andrieu, N. De Freitas, A. Doucet, and M. I. Jordan. An introduction to MCMC for machine learning. *Mach Learn*, 50(1-2):5–43, 2003.

[82] W. K. Hastings. Monte Carlo sampling methods using Markov chains and their applications. *Biometrika*, 57(1):97–109, 1970.

[83] G. O. Roberts, A. Gelman, and W. R. Gilks. Weak convergence and optimal scaling of random walk Metropolis algorithms. *Ann Appl Probab*, 7(1):110–120, 1997.

[84] G. O. Roberts and J. S. Rosenthal. Optimal scaling for various Metropolis-Hastings algorithms. *Stat Sci*, 16(4):351–367, 2001.

[85] G. O. Roberts and J. S. Rosenthal. Coupling and ergodicity of adaptive Markov chain Monte Carlo algorithms. *J Appl Probab*, pages 458–475, 2007.

[86] C. Andrieu and J. Thoms. A tutorial on adaptive MCMC. *Stat Comput*, 18(4):343–373, 2008.

[87] G. O. Roberts and R. L. Tweedie. Exponential convergence of Langevin distributions and their discrete approximations. *Bernoulli*, pages 341–363, 1996.

[88] G. O. Roberts and J. S. Rosenthal. Optimal scaling of discrete approximations to Langevin diffusions. *J R Stat Soc Series B Stat Methodol*, 60(1):255–268, 1998.

[89] Y. F. Atchadé. An adaptive version for the Metropolis adjusted Langevin algorithm with a truncated drift. *Methodol Comput Appl Probab*, 8(2):235–254, 2006.

[90] T. Eissing, L. Kuepfer, C. Becker, M. Block, K. Coboeken, T. Gaub, L. Goerlitz, J. Jaeger, R. Loosen, B. Ludewig, M. Meyer, C. Niederalt, M. Sevestre, H. U. Siegmund, J. Solodenko, K. Thelen, U. Telle, W. Weiss, T. Wendl, S. Willmann, and J. Lippert. A computational systems biology software platform for multiscale modeling and simulation: integrating whole-body physiology, disease biology, and molecular reaction networks. *Front Physiol*, 2:4, 2011.

[91] A. W. Van der Vaart. *Asymptotic statistics*, chapter 10.2. Bernstein–von Mises Theorem, pages 140–146. Cambridge university press, 2000.

[92] C. J. Geyer. Markov chain monte carlo maximum likelihood. In E. M. Keramidas, editor, *Computing Science and Statistics: 23rd Symposium on the Interface*, page 156–163. Interface Foundation, 1991.

[93] B. Sengupta, K. J. Friston, and W. D. Penny. Gradient-based mcmc samplers for dynamic causal modelling. *NeuroImage*, 125:1107–1118, 2016.

[94] B. Sengupta, K. J. Friston, and W. D. Penny. Gradient-free MCMC methods for dynamic causal modelling. *NeuroImage*, 112:375–381, 2015.

[95] D. W. Everett, T. J. Chando, G. C. Didonato, S. M. Singhvi, H. Y. Pan, and S. H. Weinstein. Biotransformation of pravastatin sodium in humans. *Drug Metab Dispos*, 19(4):740–8, 1991.

[96] K. T. Kivisto and M. Niemi. Influence of drug transporter polymorphisms on pravastatin pharmacokinetics in humans. *Pharm Res*, 24(2):239–47, 2007.

[97] A. T. Serajuddin, S. A. Ranadive, and E. M. Mahoney. Relative lipophilicities, solubilities, and structure-pharmacological considerations of 3-hydroxy-3-methylglutaryl-coenzyme A (HMG-CoA) reductase inhibitors pravastatin, lovastatin, mevastatin, and simvastatin. *J Pharm Sci*, 80(9):830–4, 1991.

[98] S. M. Singhvi, H. Y. Pan, R. A. Morrison, and D. A. Willard. Disposition of pravastatin sodium, a tissue-selective HMG-CoA reductase inhibitor, in healthy subjects. *Br J Clin Pharmacol*, 29(2):239–43, 1990.

[99] T. Hatanaka. Clinical pharmacokinetics of pravastatin: mechanisms of pharmacokinetic events. *Clin Pharmacokinet*, 39(6):397–412, 2000.

[100] M. Niemi, M. K. Pasanen, and P. J. Neuvonen. SLCO1B1 polymorphism and sex affect the pharmacokinetics of pravastatin but not fluvastatin. *Clin Pharmacol Ther*, 80(4):356–66, 2006.

[101] M. Meyer, S. Schneckener, B. Ludewig, L. Kuepfer, and J. Lippert. Using expression data for quantification of active processes in physiologically based pharmacokinetic modeling. *Drug Metab Dispos*, 40(5):892–901, 2012.

[102] A. E. Smith, P. B. Ryan, and J. S. Evans. The effect of neglecting correlations when propagating uncertainty and estimating the population distribution of risk. *Risk Anal*, 12(4):467–474, 1992.

[103] S. S. Shaphiro and M. B. Wilk. An analysis of variance test for normality. *Biometrika*, 52(3):591–611, 1965.

[104] S. L. Spencer, S. Gaudet, J. G. Albeck, J. M. Burke, and P. K. Sorger. Non-genetic origins of cell-to-cell variability in TRAIL-induced apoptosis. *Nature*, 459(7245):428–32, 2009.

[105] A. W. Bowman and A. Azzalini. *Applied smoothing techniques for data analysis: the kernel approach with S-Plus illustrations*. Clarendon Press ; Oxford University Press, 1997.

[106] M. K. Cowles and B. P. Carlin. Markov chain Monte Carlo convergence diagnostics: a comparative review. *J Am Stat Assoc*, 91(434):883–904, 1996.

[107] W. R. Gilks, G. O. Roberts, and S. K. Sahu. Adaptive markov chain monte carlo through regeneration. *J Am Stat Assoc*, 93(443):1045–1054, 1998.

[108] G. O. Roberts and J. S. Rosenthal. Examples of adaptive MCMC. *J Comput Graph Stat*, 18(2):349–367, 2009.

[109] E. Link, S. Parish, J. Armitage, L. Bowman, S. Heath, F. Matsuda, I. Gut, M. Lathrop, and R. Collins. SLCO1B1 variants and statin-induced myopathy–a genomewide study. *N Engl J Med*, 359(8):789–99, 2008.

[110] C. W. Tornøe, H. Agerso, E. N. Jonsson, H. Madsen, and H. A. Nielsen. Non-linear mixed-effects pharmacokinetic/pharmacodynamic modelling in NLME using differential equations. *Comput Methods Programs Biomed*, 76(1):31–40, 2004.

[111] J. R. Powell, S. Vozeh, P. Hopewell, J. Costello, L. B. Sheiner, and S. Riegelman. Theophylline disposition in acutely ill hospitalized patients. The effect of smoking, heart failure, severe airway obstruction, and pneumonia. *Am Rev Respir Dis*, 118(2):229–38, 1978.

[112] R. I. Ogilvie. Clinical pharmacokinetics of theophylline. *Clin Pharmacokinet*, 3(4):267–93, 1978.

[113] Y. Obase, T. Shimoda, T. Kawano, S. Saeki, S. Y. Tomari, K. Mitsuta-Izaki, H. Matsuse, M. Kinoshita, and S. Kohno. Polymorphisms in the CYP1A2 gene and theophylline metabolism in patients with asthma. *Clin Pharmacol Ther*, 73(5):468–74, 2003.

[114] A. J. Boeckmann, L. B. Sheiner, and S. L. Beal. *NONMEM Users Guide: Part V*. University of California, San Francisco, 1994.

[115] A. Gelman and D. B. Rubin. Inference from iterative simulation using multiple sequences. *Stat Sci*, pages 457–472, 1992.

[116] M. Bergstrand, A. C. Hooker, J. E. Wallin, and M. O. Karlsson. Prediction-corrected visual predictive checks for diagnosing nonlinear mixed-effects models. *AAPS J*, 13(2):143–51, 2011.

[117] S. Willmann, A. N. Edginton, M. Kleine-Besten, E. Jantratid, K. Thelen, and J. B. Dressman. Whole-body physiologically based pharmacokinetic population modelling of oral drug administration: inter-individual variability of cimetidine absorption. *J Pharm Pharmacol*, 61(7):891–9, 2009.

[118] J. L. Dorne, K. Walton, and A. G. Renwick. Uncertainty factors for chemical risk assessment. human variability in the pharmacokinetics of CYP1A2 probe substrates. *Food Chem Toxicol*, 39(7):681–96, 2001.

[119] K. Tappe. *Ordinary and Lévy Copulas in Finance*. PhD thesis, 2009.

[120] B. Meibohm and H. Derendorf. Basic concepts of pharmacokinetic/pharmacodynamic (PK/PD) modelling. *Int J Clin Pharmacol Ther*, 35(10):401–13, 1997.

[121] G. L. de la Grandmaison, I. Clairand, and M. Durigon. Organ weight in 684 adult autopsies: new tables for a Caucasoid population. *Forensic Sci Int*, 119(2):149–54, 2001.

[122] R. A. Blouin, J. F. Elgert, and L. A. Bauer. Theophylline clearance: effect of marked obesity. *Clin Pharmacol Ther*, 28(5):619–23, 1980.

[123] B. Zahorska-Markiewicz, M. Waluga, M. Zielinski, and M. Klin. Pharmacokinetics of theophylline in obesity. *Int J Clin Pharmacol Ther*, 34(9):393–5, 1996.

[124] L. Kuepfer, R. Kerb, and A. M. Henney. Clinical translation in the virtual liver network. *CPT Pharmacometrics Syst Pharmacol*, 3:e127, 2014.

[125] D. J. Greenblatt, D. R. Abernethy, A. Locniskar, J. S. Harmatz, R. A. Limjuco, and R. I. Shader. Effect of age, gender, and obesity on midazolam kinetics. *Anesthesiology*, 61(1):27–35, 1984.

[126] P. Heizmann, M. Eckert, and W. H. Ziegler. Pharmacokinetics and bioavailability of midazolam in man. *Br J Clin Pharmacol*, 16 Suppl 1:43S–49S, 1983.

[127] R. Mandrioli, L. Mercolini, and M. A. Raggi. Benzodiazepine metabolism: an analytical perspective. *Curr Drug Metab*, 9(8):827–44, 2008.

[128] C. Knox, V. Law, T. Jewison, P. Liu, S. Ly, A. Frolkis, A. Pon, K. Banco, C. Mak, V. Neveu, Y. Djoumbou, R. Eisner, A. C. Guo, and D. S. Wishart. DrugBank 3.0: a comprehensive resource for 'omics' research on drugs. *Nucleic Acids Res*, 39(Database issue):D1035–41, 2011.

[129] M. Vossen, M. Sevestre, C. Niederalt, I. J. Jang, S. Willmann, and A. N. Edginton. Dynamically simulating the interaction of midazolam and the CYP3A4 inhibitor itraconazole using individual coupled whole-body physiologically-based pharmacokinetic (WB-PBPK) models. *Theor Biol Med Model*, 4:13, 2007.

[130] B. Chauve, D. Guillarme, P. Cléon, and JL. Veuthey. Evaluation of various HILIC materials for the fast separation of polar compounds. *J Sep Sci*, 33(6-7):752–64, 2010.

[131] J. O. Miners, D. L. Rees, L. Valente, M. E. Veronese, and D. J. Birkett. Human hepatic cytochrome P450 2C9 catalyzes the rate-limiting pathway of torsemide metabolism. *J Pharmacol Exp Ther*, 272(3):1076–81, 1995.

[132] G. Neugebauer, E. Besenfelder, and E. von Mollendorff. Pharmacokinetics and metabolism of torasemide in man. *Arzneimittelforschung*, 38(1A):164–6, 1988.

[133] H. Knauf and E. Mutschler. Clinical pharmacokinetics and pharmacodynamics of torasemide. *Clin Pharmacokinet*, 34(1):1–24, 1998.

[134] H. Spahn, H. Knauf, and E. Mutschler. Pharmacokinetics of torasemide and its metabolites in healthy controls and in chronic renal failure. *Eur J Clin Pharmacol*, 39(4):345–8, 1990.

[135] O. Kerdpin, D. J. Elliot, S. L. Boye, D. J. Birkett, K. Yoovathaworn, and J. O. Miners. Differential contribution of active site residues in substrate recognition sites 1 and 5 to cytochrome P450 2C8 substrate selectivity and regioselectivity. *Biochemistry*, 43(24):7834–42, 2004.

[136] J. O. Miners, S. Coulter, D. J. Birkett, and J. A. Goldstein. Torsemide metabolism by CYP2C9 variants and other human CYP2C subfamily enzymes. *Pharmacogenetics*, 10(3):267–70, 2000.

[137] FDA professional drug information. http://www.drugs.com/pro/torsemide.html, last access: 27/02/2016.

[138] L. Aarons and K. Ogungbenro. Optimal design of pharmacokinetic studies. *Basic Clin Pharmacol Toxicol*, 106(3):250–255, 2010.

[139] F. Y. Bois, T. J. Smith, A. Gelman, H. Y. Chang, and A. E. Smith. Optimal design for a study of butadiene toxicokinetics in humans. *Toxicol Sci*, 49(2):213–24, 1999.

[140] J. K. Roberts, C. Stockmann, A. Balch, T. Yu, R. M. Ward, M. G. Spigarelli, and C. M. T. Sherwin. Optimal design in pediatric pharmacokinetic and pharmacodynamic clinical studies. *Pediatric Anesthesia*, 25(3):222–230, 2015.

[141] A. N. Kristoffersson, L. E. Friberg, and J. Nyberg. Inter occasion variability in individual optimal design. *J Pharmacokinet Pharmacodyn*, 42(6):735–750, 2015.

[142] E. G. Ryan, C. C. Drovandi, and A. N. Pettitt. Simulation-based fully Bayesian experimental design for mixed effects models. *Comput Stat Data Anal*, 92:26–39, 2015.

Appendix A

Figures

A.1 Figures according to chapter 2

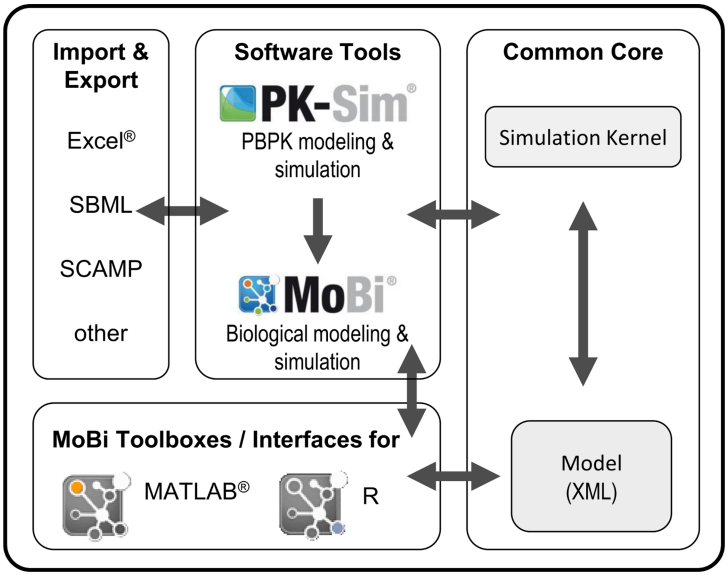

Figure A.1: Overview of the Bayer AG Computational Systems Biology Software Suite (adapted from [90]).

A.2 Figures according to chapter 3

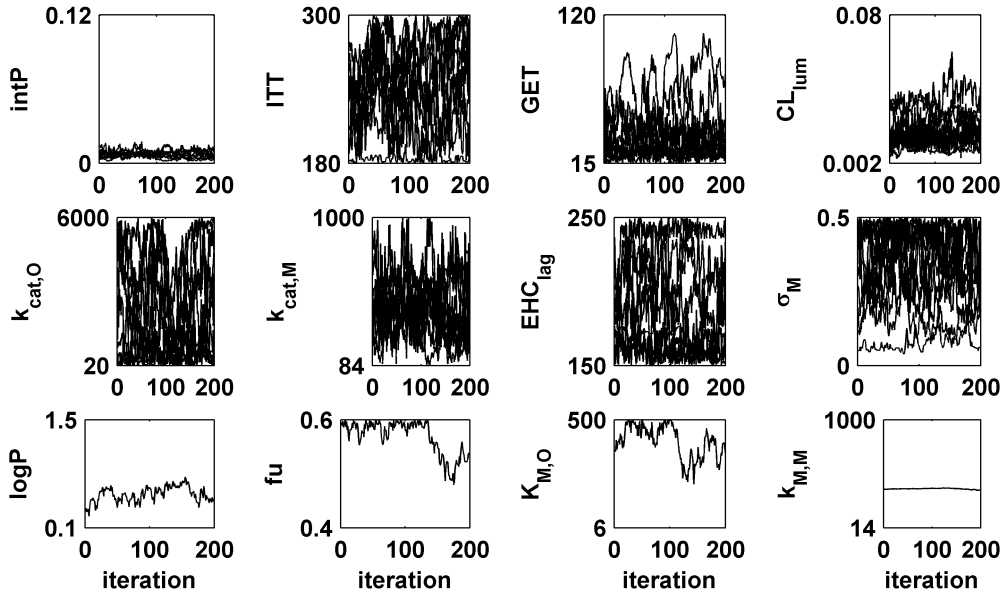

Figure A.2: Exemplary representation of a subsample of the posterior distribution. After a burn-in period of 150000 steps, a subsample of 200 parameter vectors was drawn for each individual. The figure shows the traces for all eight individual parameters for all individuals as well as the four global parameters which were the same for all individuals. The limits on the y-axis represent the physiological constraints (θ_{min}, θ_{max}).

A.3 Figures according to chapter 4

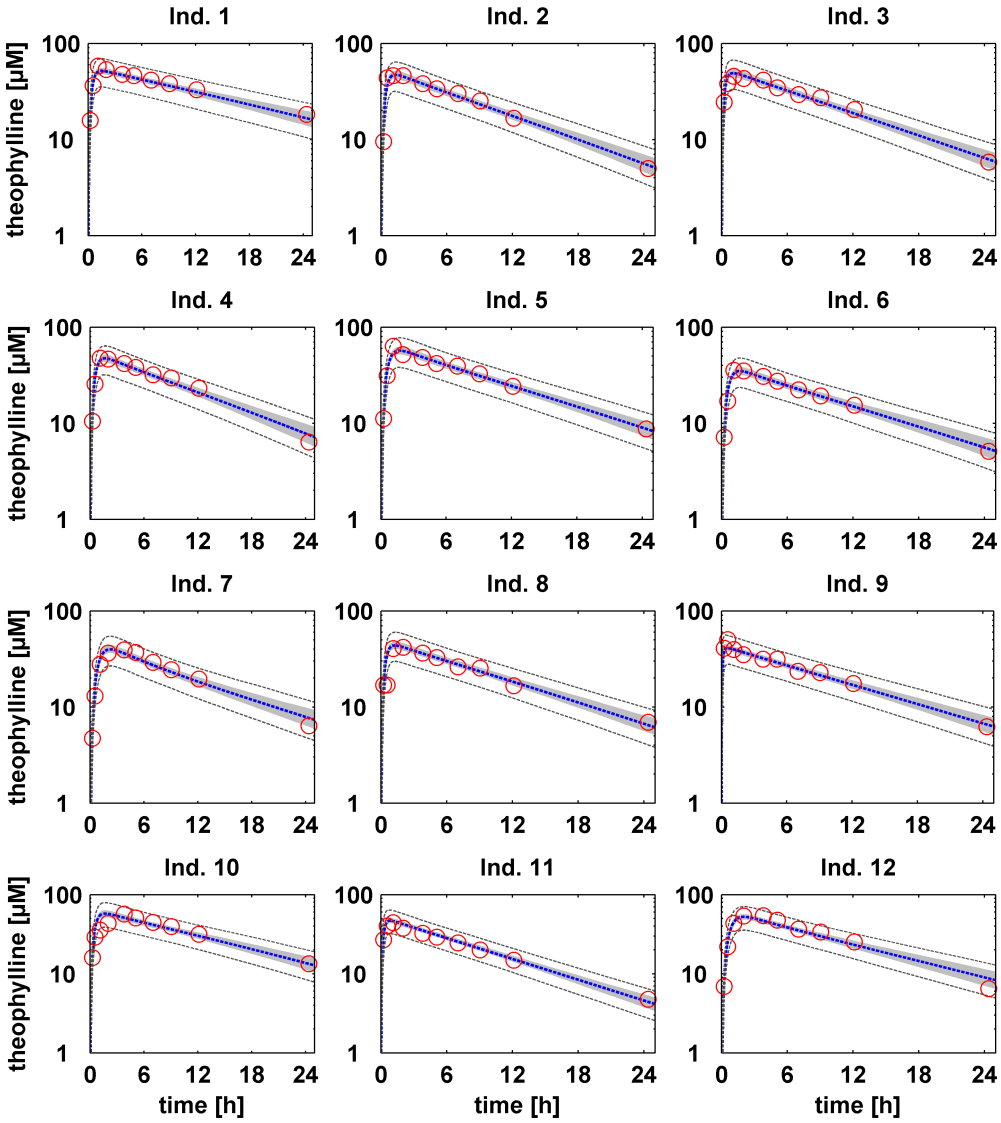

Figure A.3: Individual-specific model simulations of theophylline venous plasma concentrations. The figure shows the same results as depicted in Figure 4.1, but in semi-log scale. For each of the 12 individuals the PBPK model was subsequently parameterized and simulated with each of 500 individual and independent parameter vectors out of the posterior distribution. The 95 % confidence interval of all simulations (grey area) is shown together with the mean value curve (blue dotted line) and the experimental data (red circles). Dark grey dotted lines depict the upper and lower bound of the 95 % confidence interval of all simulations including the inferred measurement error under consideration of the proportional error model as described in equation 2.4.

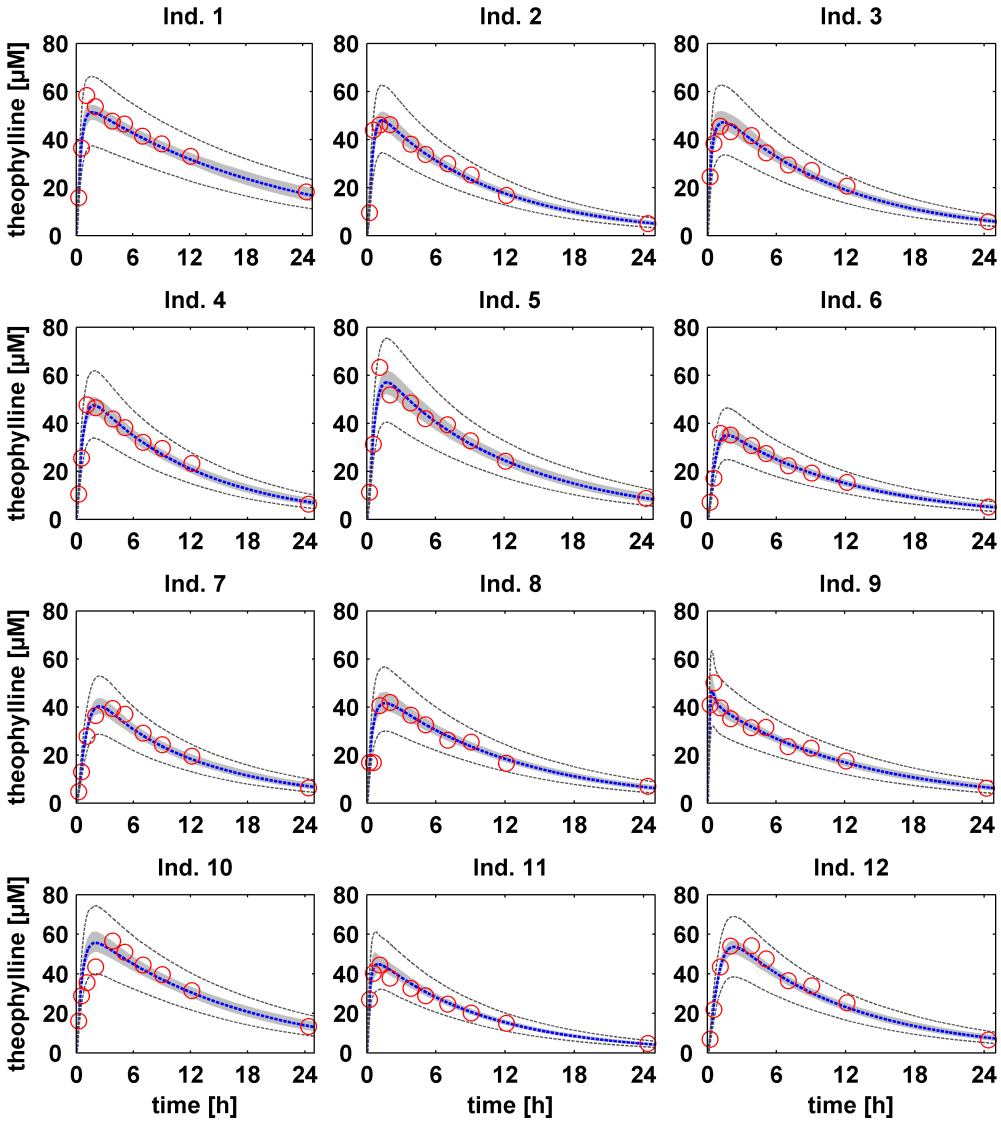

Figure A.4: Individual-specific model simulations of theophylline venous plasma concentrations for the new MH run as described in section 4.4. For each of the 12 individuals the PBPK model was subsequently parameterized and simulated with each of 500 individual and independent parameter vectors out of the posterior distribution. The 95 % confidence interval of all simulations (grey area) is shown together with the mean value curve (blue dotted line) and the experimental data (red circles). Dark grey dotted lines depict the upper and lower bound of the 95 % confidence interval of all simulations including the inferred measurement error under consideration of the proportional error model as described in equation 2.4.

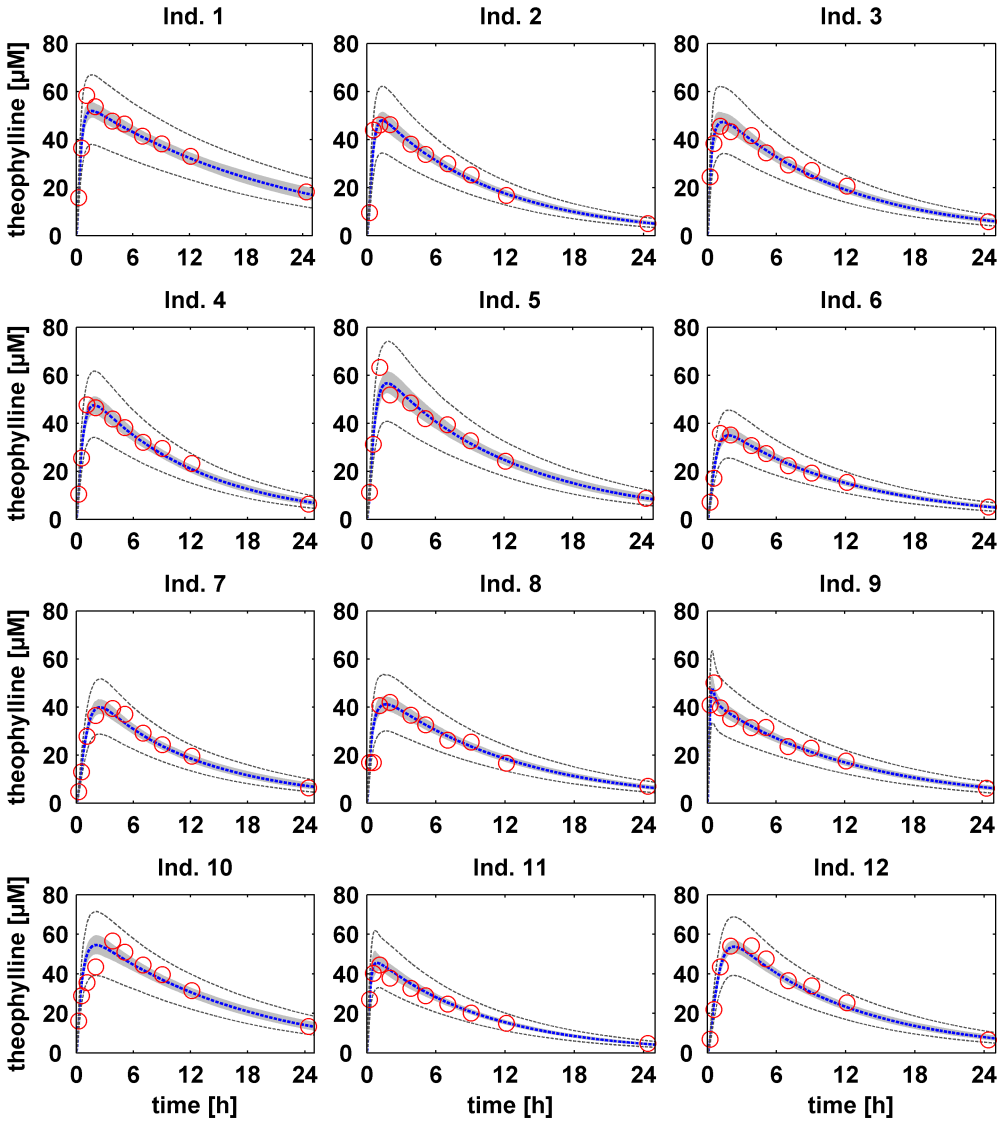

Figure A.5: Individual-specific model simulations of theophylline venous plasma concentrations for the new mMALA/SCAM run as described in section 4.4. For each of the 12 individuals the PBPK model was subsequently parameterized and simulated with each of 500 individual and independent parameter vectors out of the posterior distribution. The 95 % confidence interval of all simulations (grey area) is shown together with the mean value curve (blue dotted line) and the experimental data (red circles). Dark grey dotted lines depict the upper and lower bound of the 95 % confidence interval of all simulations including the inferred measurement error under consideration of the proportional error model as described in equation 2.4.

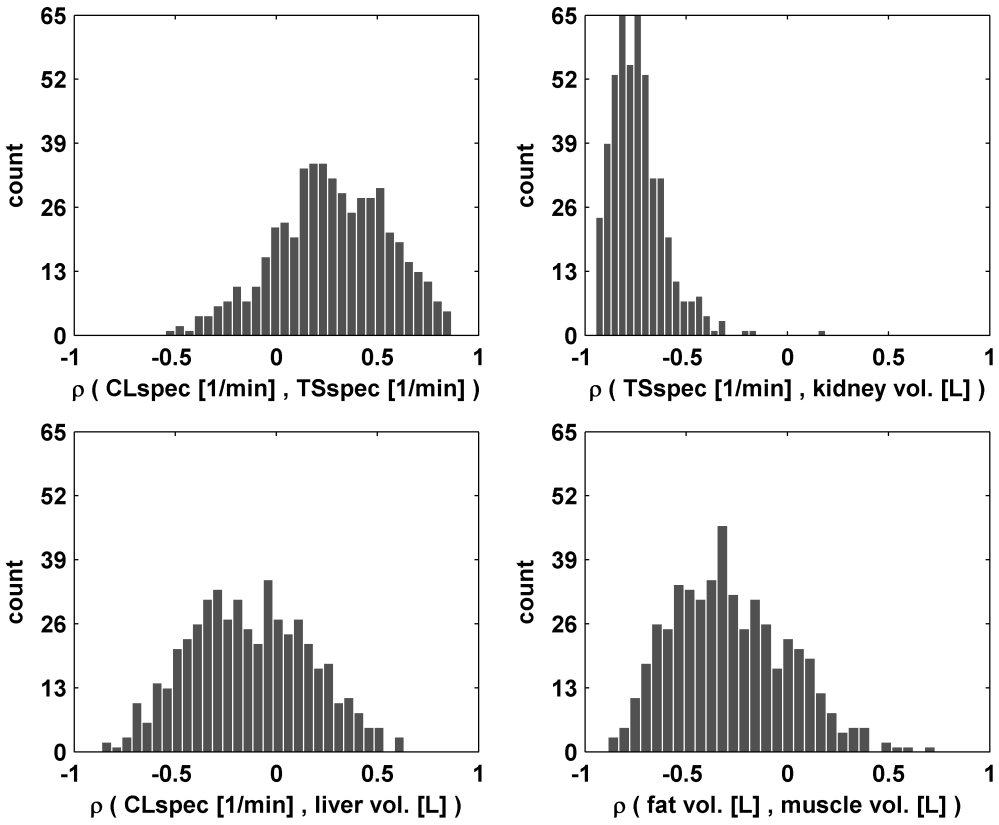

Figure A.6: Exemplary representation of derived distributions of correlation between the population parameters for the new mMALA/SCAM run as described in section 4.4. The correlation of a pair of parameters along all individuals was calculated for each of the 500 subsamples of the posterior distribution. For each pair of parameters the histogram of all correlations is shown, representing the variability of the respective correlation.

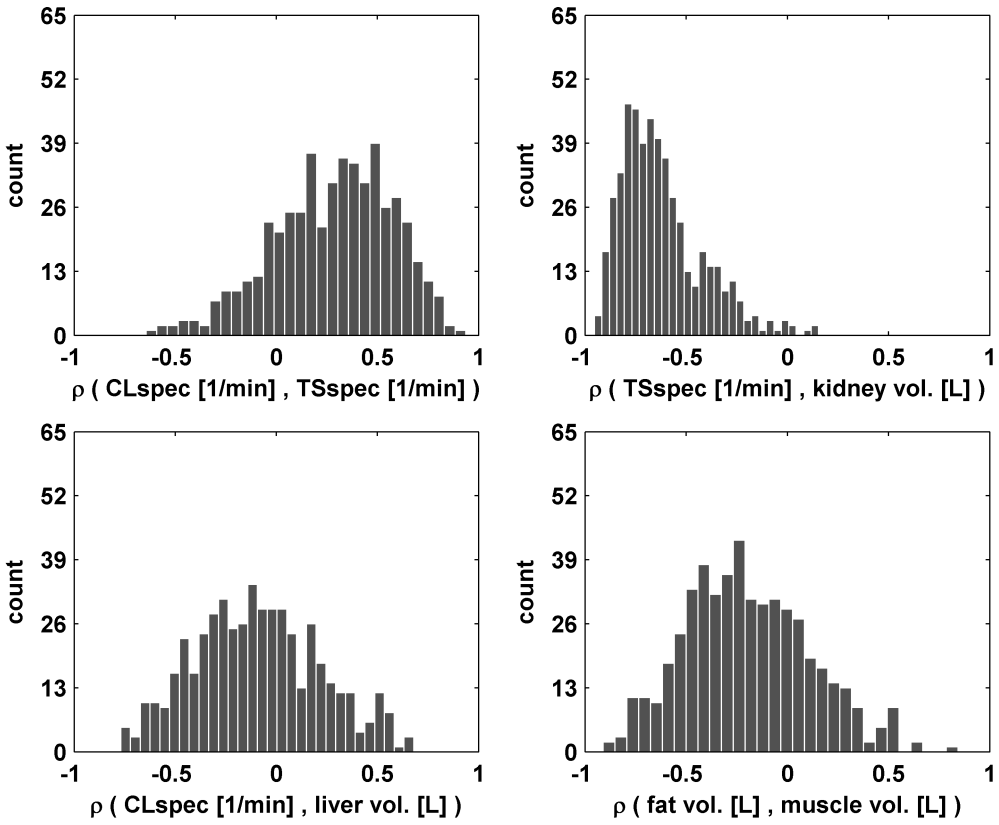

Figure A.7: Exemplary representation of derived distributions of correlation between the population parameters for the new MH run as described in section 4.4. The correlation of a pair of parameters along all individuals was calculated for each of the 500 subsamples of the posterior distribution. For each pair of parameters the histogram of all correlations is shown, representing the variability of the respective correlation.

A.4 Figures according to chapter 5

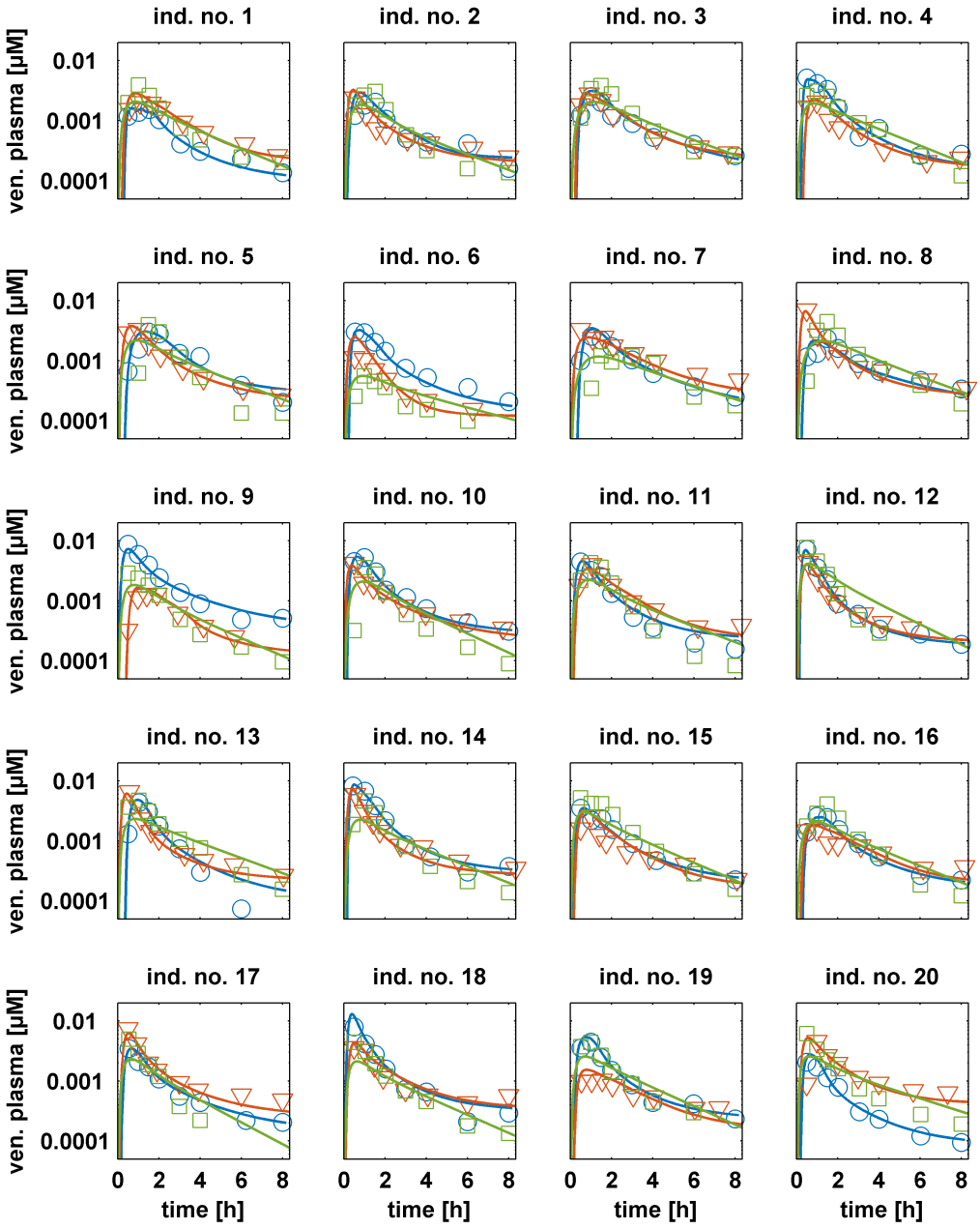

Figure A.8: Individual model simulations of the metabolites OH-midazolam and OH-torsemide.. The simulation of the parameter vector with maximum posterior probability is shown for OH-midazolam in the healthy individuals (blue line and circles), OH-torsemide in healthy individuals (green line and squares) and OH-midazolam in the diseased individuals (red line and triangles)

.

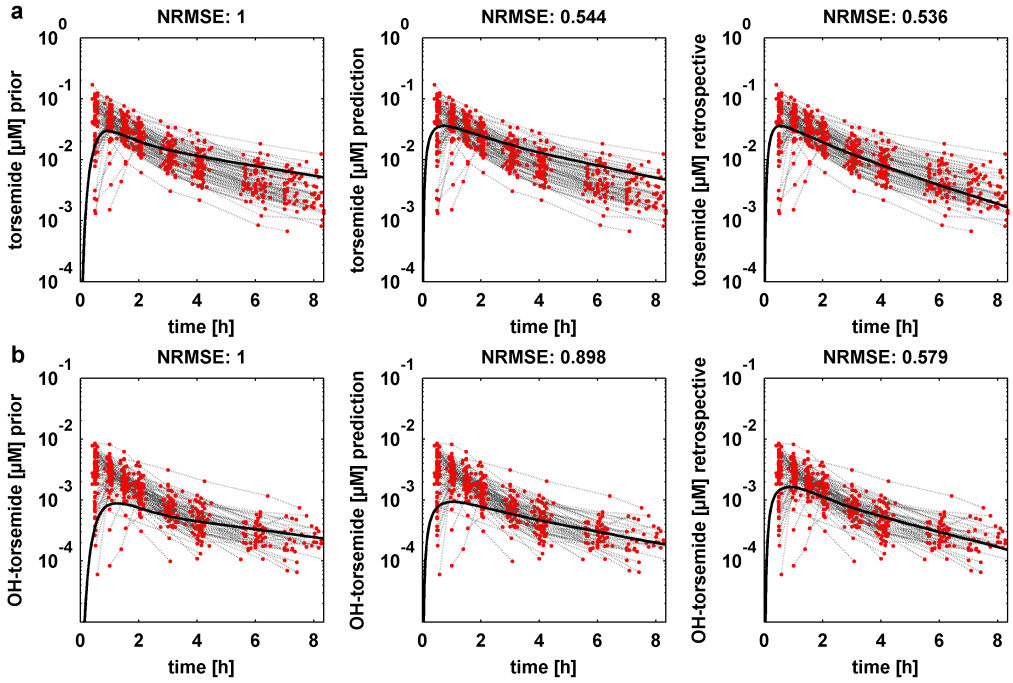

Figure A.9: Quantitative assessment of simulations of PK behavior for torsemide in diseased individuals. Comparison of the experimental data for torsemide in diseased individuals (red dots with grey dotted lines) and the median curve of the population simulation (black line): using a prediction based on prior information (left); the prediction of torsemide based on the results of the systems pharmacology approach (middle); and the retrospective analysis with the Bayesian population PBPK approach under consideration of the experimental data for torsemide in the diseased population (right). The corresponding normalized root-mean-square-error (NRMSE) is provided as figure title. (**a**) Results for torsemide, (**b**) results for OH-torsemide.

Appendix B

Tables

B.1 Tables according to chapter 4

Table B.1: Anthropometric parameters of the considered cohort of individuals. Age was considered to be 30 years for all individuals. Body Height was considered to be different from individual to individual. Dose and body weight are described in the used dataset [114].

ID	**population**	**gender**	**age** [**years**]	**body weight** [**kg**]	**height** [**cm**]	**BMI** [kg/m^2]	**dose** [**mg/kg**]	**total dose** [**mg**]
individual 1	European	male	30	79.6	182	24.03	4.02	319.99
individual 2	European	male	30	72.4	173	24.19	4.4	318.56
individual 3	European	male	30	70.5	189	19.74	4.53	319.37
individual 4	European	male	30	72.7	180	22.44	4.4	319.88
individual 5	European	male	30	54.6	160	21.33	5.86	319.96
individual 6	European	male	30	80	183	23.89	4	320
individual 7	European	male	30	64.6	184	19.08	4.95	319.77
individual 8	European	male	30	70.5	185	20.6	4.53	319.37
individual 9	European	male	30	86.4	190	23.93	3.1	267.84
individual 10	European	male	30	58.2	167	20.87	5.5	320.1
individual 11	European	male	30	65	176	20.98	4.92	319.8
individual 12	European	male	30	60.5	174	19.98	5.3	320.65

Table B.2: Varied ind. parameters together with start value and borders of the final MCMC run. Start values are exemplary for ind. 1, start values for the other ind.s differ slightly.

name	type	unit	start value	min. value	max. value
intP	ind.	dm/min	1.32E-06	3.57E-08	3.57E-04
CLspec	ind.	1/min	9.31E-03	5.00E-03	5.00E-01
TSspec	ind.	1/min	3.17E-02	2.00E-03	2.00E-01
GET	ind.	min	29.333	10	30
ITT	ind.	min	199.07	90	240
plasma protein SV	ind.	-	0.844	0.7	1.3
venous blood vol.	ind.	L	1.02	0.763	1.174
arterial blood vol.	ind.	L	0.462	0.332	0.51
bone Qspec	ind.	L/min/kg org.	0.026	0.023	0.032
bone vol.	ind.	L	12.675	9.443	14.23
brain vol.	ind.	L	1.687	1.282	1.735
brain Qspec	ind.	L/min/kg org.	0.566	0.439	0.594
fat vol.	ind.	L	22.422	3.641	58.48
fat Qspec	ind.	L/min/kg org.	0.02	0.019	0.025
gonads vol.	ind.	L	0.04	0.032	0.049
gonads Qspec	ind.	L/min/kg org.	0.074	0.069	0.093
heart vol.	ind.	L	0.341	0.165	0.696
heart Qspec	ind.	L/min/kg org.	0.594	0.53	0.717
kidney vol.	ind.	L	0.425	0.106	0.806
kidney Qspec	ind.	L/min/kg org.	2.897	2.573	3.481
stomach vol.	ind.	L	0.153	0.086	0.259
stomach Qspec	ind.	L/min/kg org.	0.366	0.328	0.444
small intestine vol.	ind.	L	0.622	0.438	1.036
small intestine Qspec	ind.	L/min/kg org.	0.849	0.763	1.032
large intestine vol.	ind.	L	0.445	0.159	0.693
large intestine Qspec	ind.	L/min/kg org.	0.592	0.536	0.725
liver vol.	ind.	L	0.837	0.655	4.249
liver Qspec	ind.	L/min/kg org.	0.171	0.152	0.206
lung vol.	ind.	L	1.166	0.549	3.012
muscle vol.	ind.	L	31.096	20.08	50.163
muscle Qspec	ind.	L/min/kg org.	0.038	0.029	0.039
pancreas vol.	ind.	L	0.184	0.034	0.364
pancreas Qspec	ind.	L/min/kg org.	0.351	0.291	0.393
portal vein vol.	ind.	L	1.079	0.821	1.263
skin vol.	ind.	L	4.578	2.745	4.889
skin Qspec	ind.	L/min/kg org.	0.079	0.073	0.099
spleen vol.	ind.	L	0.37	0.067	0.87
spleen Qspec	ind.	L/min/kg org.	0.74	0.681	0.921
logP	global	-	1.38	-1	1.5
fu	global	-	0.355	0.33	0.5
σ_M	global	-	0.137	0.01	1

Table B.3: Gelman and Rubin convergence criterion ($\hat{R}$) of the theophylline run. $\hat{R}$ was determined after splitting the Markov chain into two chains with the same length.$\hat{R}$ for individual parameters represents the mean value of all 12 individuals. Overall mean value for $\hat{R}$ is 1.14, when taking all 535 parameters into account. For parameters with a high $\hat{R}$, convergence was calculated in addition for the Markov chain representing the functional relationship (see hepatic clearance x liver volume and kidney clearance x kidney volume).

parameter	**parameter type**	$\hat{\mathbf{R}}$
Intestinal permeability	individual	1
Hepatic clearance constant	individual	1.17
Renal clearance constant	individual	1.74
Stomach gastric emptying time	individual	1
Small intestinal transit time	individual	1
Plasma protein scale factor	individual	1.01
Fat volume	individual	1.03
Kidney volume	individual	1.98
Liver volume	individual	1.22
Muscle volume	individual	1.02
Hepatic clearance constant x liver volume	individual	1.11
Renal clearance constant x kidney volume	individual	1.01
Lipophilicity	global	1.02
Unbound protein fraction	global	1.03
Intestinal permeability	population	1.63
Hepatic clearance constant	population	3.84
Renal clearance constant	population	2.18
Stomach gastric emptying time	population	1
Small intestinal transit time	population	1.01
Plasma protein scale factor	population	1.01
Fat volume	population	1.02
Kidney volume	population	2.33
Liver volume	population	1.54
Muscle volume	population	1.04
Hepatic clearance constant x liver volume	population	1.03
Renal clearance constant x kidney volume	population	1.05